GEL POLYMER ELECTROLYTE BASED ON N-PHTHALOYL CHITOSAN AND ITS APPLICATION IN DYE-SENSITIZED SOLAR CELLS

SITI NOR FARHANA BT YUSUF

THESIS SUBMITTED IN FULFILMENT OF THE REQUIREMENTS FOR THE DEGREE OF DOCTOR OF PHILOSOPHY

DEPARTMENT OF CHEMISTRY
FACULTY OF SCIENCE
UNIVERSITY OF MALAYA
KUALA LUMPUR

2017

UNIVERSITI MALAYA

ORIGINAL LITERARY WORK DECLARATION

Name of Candidate: **SITI NOR FARHANA BT YUSUF** (I.C. No:

Registration/Matric No: **SHC120013**

Name of Degree: **DOCTOR OF PHILOSOPHY CHEMISTRY OF SCIENCE**

Title of Project Paper/Research Report/Dissertation/Thesis ("this Work"):

GEL POLYMER ELECTROLYTE BASED ON N-PHTHALOYL CHITOSAN AND ITS APPLICATION IN DYE-SENSITIZED SOLAR CELLS

Field of Study: **POLYMER CHEMISTRY**

I do solemnly and sincerely declare that:

(1) I am the sole author/writer of this Work;
(2) This Work is original;
(3) Any use of any work in which copyright exists was done by way of fair dealing and for permitted purposes and any excerpt or extract from, or reference to or reproduction of any copyright work has been disclosed expressly and sufficiently and the title of the Work and its authorship have been acknowledged in this Work;
(4) I do not have any actual knowledge nor do I ought reasonably to know that the making of this work constitutes an infringement of any copyright work;
(5) I hereby assign all and every rights in the copyright to this Work to the University of Malaya ("UM"), who henceforth shall be owner of the copyright in this Work and that any reproduction or use in any form or by any means whatsoever is prohibited without the written consent of UM having been first had and obtained;
(6) I am fully aware that if in the course of making this Work I have infringed any copyright whether intentionally or otherwise, I may be subject to legal action or any other action as may be determined by UM.

Candidate's Signature Date

Subscribed and solemnly declared before,

Witness's Signature Date

Name:

Designation:

ABSTRACT

It is widely known that chitosan is not soluble in common organic solvents. Hence there is a need to increase its solubility in a wider range of solvents. To do this, the chitosan biopolymer has been modified by the process of phthaloylation to form N-phthaloyl chitosan (PhCh) by reacting phthalic anhydride with chitosan in dimethylformamide (DMF). The chitosan derivatives, PhCh, can dissolve in DMF, DMSO, DMAc and pyridine. Fourier transform infra-red (FTIR) and proton nuclear magnetic resonance (^{1}H NMR) spectroscopies were used to confirm the PhCh formation and structure. The phthalimido and aromatic peaks of PhCh were seen at 1772, 1708 and 719 cm^{-1}, respectively, and two sets of peaks from ^{1}H NMR centered at 3.0 and 7.5 ppm verified that chitosan has been phthaloylated. The PhCh-based gel polymer electrolytes (GPE) consist of ethylene carbonate (EC), and DMF with different contents of tetrapropylammonium iodide (TPAI) and iodine. X-ray diffraction studies reveal that addition of tetrapropylammonium iodide (TPAI) further reduced the crystallinity of the PhCh. FTIR spectroscopy showed the interaction between polymer, plasticizer and salt. GPE comprising of PhCh : EC : DMF : TPAI : I_2 in wt.% ratio of 12.0 : 36.1 : 36.1 : 14.4 : 1.4 exhibited the highest conductivity of 5.46 mS cm^{-1} at 30 °C. When used in dye-sensitized solar cell (DSSC), it gave the best performance with the efficiency of 5.0 %, J_{SC} of 12.72 mA cm^{-2}, V_{OC} of 0.60 V and fill factor of 0.66. To further improve the efficiency of the solar cell, lithium iodide (LiI) has been added to the PhCh-based electrolyte. The efficiency improved to 6.36 %, with the J_{SC} of 17.29 mA cm^{-2}, V_{OC} of 0.59 V and fill factor of 0.62. Addition of *1*-butyl-*3*-methylimidazolium iodide (BMII) ionic liquid to the electrolyte enhanced the DSSC efficiency to 6.69 % with the J_{SC} of 16.53 mA cm^{-2}, V_{OC} of 0.62 V and fill factor of 0.65.

ABSTRAK

Secara meluas diketahui bahawa kitosan tidak larut dalam pelarut organik. Oleh itu, terdapat keperluan untuk meningkatkan kelarutan dalam julat yang lebih luas. Untuk itu, biopolimer kitosan telah diubah suai dengan proses "phthaloylation" untuk membentuk N-phthaloylchitosan (PhCh) dengan menindakbalaskan kitosan dengan acetic phthalic di dalam dimethylformamide (DMF). Derivatif chitosan, PhCh, boleh larut didalam DMF, DMSO, DMAc dan piridina. Fourier infra-merah (FTIR) dan proton resonans magnetik nuklear (^{1}H NMR) spektroskopi telah digunakan untuk mengesahkan struktur PhCh. Puncak bagi phthalimido dan aromatik PhCh terdapat masing-masing pada 1772, 1708 dan 719 cm^{-1} dan dua set puncak dari ^{1}H NMR berpusat di 3.0 dan 7.5 ppm mengesahkan pembentukkan PhCh. Elektrolit gel polimer (GPE) berdasarkan PhCh terdiri daripada etilena karbonat (EC), DMF, pelbagai kandungan tetrapropylammonium iodida (TPAI) dan iodin. Kajian pembelauan sinar-X menunjukkan bahawa penambahan tetrapropylammonium iodida (TPAI) terus mengurangkan crystallinity dalam PhCh. FTIR spektroskopi menunjukkan interaksi antara polimer, plasticizer dan garam. GPE yang terdiri daripada PhCh: EC: DMF: TPAI: I_2 dalam nisbah wt.% 12.0. 36.1: 36.1: 14.4: 1.4 menunjukkan kekonduksian tertinggi 5.46 mS cm^{-1} pada 30 ℃. Apabila digunakan dalam pewarna peka sel solar (DSSC), ia memberikan persembahan yang terbaik dengan kecekapan sebanyak 5.0%, J_{SC} sebanyak 12.72 mA cm^{-2}, V_{OC} 0.60 V dan isi faktor 0.66. Untuk meningkatkan lagi kecekapan sel solar, lithium iodida (LiI) telah ditambah kepada elektrolit. Kecekapan meningkat kepada 6.36%, dengan J_{SC} 17.29 mA cm^{-2}, V_{OC} 0.59 V dan isi faktor 0.62. Dengan penambahan cecair ionik *1*-butil-*3*-methylimidazolium iodida (BMII) kepada elektrolit, kecekapan DSSC terus meningkat kepada 6.69% dengan J_{SC} sebanyak 16.53 mA cm^{-2}, V_{OC} sebanyak 0.62 V dan isi faktor 0.65.

ACKNOWLEDGMENTS

In the name of Allah, the Most Gracious, the Most Merciful.

I would first like to thank my thesis advisor ***Prof. Dr. Rosiyah Yahya*** and ***Prof Madya Dr. Siti Rohana Majid***. Without their assistance and dedicated involvement in every step throughout the process, this thesis would have never been accomplished. A million thanks also to both of my mentors, ***Prof Dr. Abdul Kariem Arof*** and ***Prof. Dr. Mohamed Abdul Careem***. Your encouragement and advice has led me to places I never thought I would go. Thank you so much for your support, understanding and mentorship throughout these past years.

To my fellow ***labmates***, from both Chemistry (*Vidhya, Danial & polymerlicious kakaks*) and Physics departments (especially my '*Swedish*' crew: *Dr. Bandara, Hazirah & Fareezuan*), seniors and juniors, thank you so much! Thanks for the fun and support! I cannot begin to express my gratitude and appreciation for their friendship. I am lucky to have made such great friends. I greatly look forward to having all of you as colleagues in the years ahead!!

Getting through my dissertation required more than academic support, and I have many, many people to thank for listening to and, at times, having to tolerate me over the past years. Most importantly, none of this could have happened without my family. I must express my very profound gratitude to my parents, ***daddy & mommy***, for giving birth to me in the first place and supporting me spiritually throughout my life. This accomplishment would not have been possible without them. I am also grateful to my siblings, ***Along***, ***Abang*** and especially ***Adik*** who were always keen to know what I was doing and how I was proceeding, although it is likely that they have never grasped what it was all about! Thank you for the countless screams of joy whenever a significant momentous was reached and also just your general impudence. My beloved uncles, aunties and cousins especially ***McD, Kekra, Eppy*** & ***Wana***. Thank you so much!

To my cheerleaders aka my best friends, ***Aqsa, Yomie, Jack, AJ, Yoyong, Kak Ina, Wawan, Kak Dini***, thank you so much! Thank you for knowing exactly when to tell me what I want to hear, when I want to hear it the most. I just don't know how I can say thank you to friends who understand all the things I never say, and never say anything I don't understand. Also, thank you for removing the word EXPECTATION and adding the world HAPPINESS to the dictionary of our friendship!

Thank you so much.

With love,

Farhana

TABLE OF CONTENTS

LIST OF FIGURES

LIST OF TABLES

LIST OF ABBREVIATIONS AND SYMBOLS

ATR	Attenuated Total Reflectance
BMII	1-butyl-3-methylimidazolium iodide
CB	Conduction band
DMAc	N,N-dimetylacetamide
DMF	N,N-dimethylformamide
DMSO	Dimethyl sulfoxide
DSSC	Dye sensitized Solar Cell
E_a	Activation energy
EC	Ethylene carbonate
EIS	Electrical impedance spectroscopy
FF	Fill factor
FTIR	Fourier Transform Infrared Spectroscopy
FTO	Fluorine Tin Oxide
GPE	Gel polymer electrolyte
HOMO	Highest occupied molecular orbital
IL	Ionic liquid
J_{SC}	Short circuit photocurrent density
LUMO	Lowest unoccupied molecular orbital
M_w	Weight average molecular weight
N719 & N3	Ruthenium dye
NMR	Nuclear magnetic resonance spectroscopy
PC	Propylene carbonate
PDI	Polydispersity index

PEO	Polyethylene oxide
PhCh	N-phthaloylchitosan
PP	Polypropylene
PTFE	Polytetrafluoroethylene
PVC	Polyvinyl chloride
SPE	Solid polymer electrolyte
TBP	Tert-butyl pyridine
T_g	Glass transition temperature
TGA	Thermogravimetric analysis
TPAI	Tetrapropylammonium iodide
VB	Valence band
V_{OC}	Open circuit voltage
XRD	X-ray diffraction

LIST OF APPENDICES

CHAPTER 1 : INTRODUCTION

1.1. Motivation

Numerous polymers have been used as the host to ionic conduction. However, most of the polymers are synthetic. Examples are polyethylene oxide (PEO) (Das & Ghosh, 2015; Karan et al., 2008; Karmakar & Ghosh, 2012), polystyrene (PS) (Rohan et al., 2014), polytetrafluoroethylene (PTFE) (Jeong et al., 2016; Mack et al., 2016; Rofaiel et al., 2012) and polyvinylchloride (PVC) (Ramesh & Arof, 2000, Ramesh & Arof, 2001; Ramesh et al., 2007; Ramesh et al., 2002a). Synthetic polymers are detrimental to the environment as it is costly to recycle and has poor degradability, eventually finding its way into the ground soil and as far as the oceans as toxic waste pollutants.

It is these problems that have motivated researchers to turn towards biopolymers. Among many potential biopolymers, chitosan is of particular interest as it exhibits a polyelectrolyte nature due to the protonated NH_2 amino group in its backbone (Klotzbach et al., 2006; Payne & Raghavan, 2007; Wan et al., 2003). Chitosan is derived from hydrolysis of acetamide groups through alkaline treatment of chitin, the second most abundant natural polymer. However, chitosan is soluble only in dilute acidic solutions but not in organic solvents. For the purpose of electrochemical devices with metal components, usage of aqueous media would limit the lifespan and usability of the device due to corrosion of the metal parts. Thus, it has become a necessity for chitosan to be modified to meet the requirements of non-aqueous solvent compatibility.

In this work, chitosan has been modified using phthalic anhydride for *N*-phthaloylchitosan (PhCh) production. N-phthaloylchitosan is soluble in DMF, dimethylacetamide (DMAc), dimethylsulfoxide (DMSO) and pyridine (Kurita et al., 2003; Kurita et al., 2001; Kurita et al., 2005; Yoksan et al., 2001). The ability to dissolve in organic solvents is due to the presence of a new hydrophobic phthaloyl group along

the chitosan backbone that prevents the formation of hydrogen bonding between the solvents and the amino and hydroxyl groups in chitosan.

Chitosan has previously been used as a host for ionic conduction but in the form of solid polymer electrolytes (Khiar et al., 2006; Majid & Arof, 2005; Osman & Arof, 2003). Solid polymer electrolytes have good mechanical strength, electrochemical stability, and ease of fabrication into devices. However its main drawback is that its ionic conductivity is not as high enough to be used in some application such as batteries. Before the emergence of solid polymer electrolytes, liquid electrolytes are used in electrochemical devices. Although liquid electrolytes have the advantage of higher ionic conductivities over solid polymer electrolytes, it does possess some weaknesses: it is prone to leakage, evaporation of the solvents, corrosion and electrochemical instability at high temperatures, all of which does not favour applications in devices and can harm the environment.

Stepping up to the challenge of combining the best properties from both solid and liquid electrolytes and without the weaknesses of either, many researchers have paved the way to arrive at a new class of material: the gel polymer electrolytes (GPE). The GPE can be considered as a liquid electrolyte trapped inside a polymer matrix and has conductivity that is liquid-like ionic (Arof et al., 2014a). Several polymer hosts have been used in the fabrication of GPE based DSSC such as polyaniline (PAN) (Arof et al., 2013; Bandara et al., 2010a; Bandara et al., 2010b; Bandara et al., 2013; Dissanayake et al., 2002; Dissanayake et al., 2012), polyethylene oxide (PEO) (Bandara et al., 2012), polyvinyl acetate (PVA) (Arof et al., 2014b; Aziz et al., 2014), and poly(vinylidene fluoride) (PVdF) (Arof et al., 2014a).

However, this work looks into the potential of PhCh as a host for GPEs. In order to test the strength of the PhCh-based gel polymer electrolytes, it has been used as an electrolyte in DSSC. Why solar cell? This is because energy consumption is increasing

from year to year and with rapid modernization the technology is becoming increasingly sophisticated technology (Maçaira et al., 2013). Energy resources can be divided into two parts, namely non-renewable and renewable as shown in Figure 1.1.

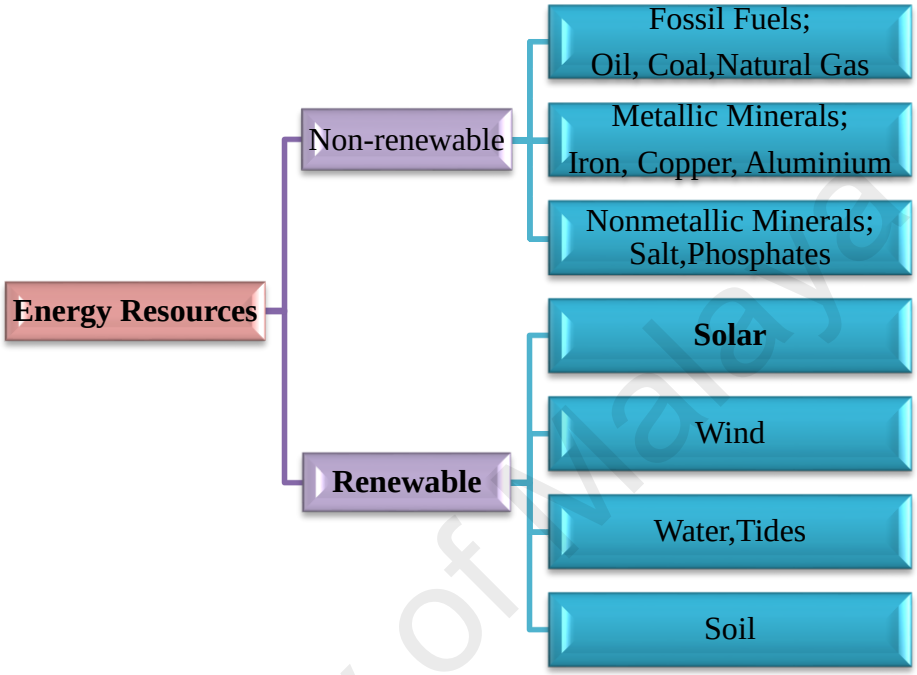

Figure 1.1: Energy resources.

Much of the electricity we currently use is generated from fossil fuels such as coal, oil and natural gas. Many issues arise from this matter, among which is the shortage of this non-renewable resource due to its high demand and usage. In addition, there is no solid guarantee against these resources since they are supplied by limited countries and its price in the market is also volatile. Several of the most well-known harmful gases released into the environment originates from the combustion of fossil fuels. These are nitrogen dioxide (NO_2), sulphur dioxide (SO_2), carbon monoxide (CO) and carbon dioxide (CO_2). NO_2 and SO_2 which are acidic gases will dissolve in the rain to form acid rain that can damage buildings, plants and kill aquatic life. CO will react with haemoglobin in the blood and prevents it from carrying oxygen around the body resulting

in oxygen starvation. Initially, CO_2 is useful to us where it traps heat around the earth. However, earth experiences exceptional warmth due to the excessive CO_2 released into the environment. This leads to climate change, such as the melting of ice at the poles, sea water levels rising and experts predict more storms, drought, floods and famine.

In order to cut back on the amount of CO_2 released and thus slow down global warming, another alternative energy source such as nuclear energy has been introduced. Nuclear energy has two big advantages in that it gives out huge amounts of energy; a pellet of nuclear fuel the size of a pea can give as much energy as a tonne of coal and no CO_2 or other greenhouse gases are produced. However, this energy source is based on nuclear fission which produces dangerous unstable atoms or radioisotopes. An explosion in a nuclear power station could pollute a large area with radiation. Nuclear energy is unfortunately not renewable.

Therefore, much effort is focused on renewable energy resources which mankind will depend more on in the future. Thus, there is a push to switch to a clean, free and extremely reliable source of power i.e. solar energy. A solar cell is a device that directly converts sunlight into electrical energy through the photovoltaic process. There are many types of solar cells, namely, silicon solar cell, perovskite solar cell, cadmium telluride solar cell, organic solar cell, quantum dot solar cell and dye-sensitized solar cell (DSSC). Among many kinds of solar cells, DSSC has been selected for this research because it has several advantages such as it can achieve high sunlight to electrical energy conversion efficiency with low cost and is easy to fabricate. The first DSSC was introduced by O'Regan & Gratzel (1991) and is made up of three main components, namely, the photoactive electrode, electrolytes and a Pt counter electrode.

In this work, the effect of double salts and ionic liquid in the GPEs on the cell parameters was investigated, with the goal to improve the efficiency of the DSSC. Iodide salts with bulky cations will be utilized. The bulky cations are expected to reduce cationic conductivity and thereby enhance the iodide ion conductivity and transference number in the electrolytes. In order to enhance the efficiency of the DSSCs, a mixture of two iodide salts has been applied in the gel polymer electrolytes. The mixed iodide salts one of bulky cation and the other small cation were used to supply the required iodide ion conductivity. The presence of the small cations with high charge density are expected to contribute towards better photo-generation of electrons and their faster transfer across the dye-TiO_2 interface (Arof et al., 2014a). Other efforts that has been done to increase the efficiency of the DSSC is by adding small portions of ionic liquids in the solid polymer electrolytes (Singh et al., 2011). In the present study, the effects of single cation, mixed cations and addition of BMII in PhCh-based GPEs in the improvement of DSSC performance was explored.

1.2. Objectives of the present investigation

1. To improve the solubility of chitosan in polar aprotic solvents by modifying it via phthaloylation process.
2. To produce a highly efficient DSSC by optimizing the PhCh-based gel polymer host using various masses of tetrapropylammonium iodide (TPAI).
3. To investigate the effects of mixed cation salts system in GPEs towards the efficiency of the DSSC.
4. To optimize the weight percentages of BMII ionic liquid to be added in the mixed cation GPEs in order to further enhance the efficiency of the DSSC.

1.3. Scope of research work

The progress on phthaloylchitosan, quasi-solid polymeric ionic conductors and dye-sensitized solar cells are reviewed in Chapter 2. Chapter 3 will discuss the experimental procedures for the (i) modification and verification of chitosan and (ii) characterisation of the PhCh gel polymer electrolytes (GPEs). This chapter ends with the fabrication of DSSCs using the PhCh based electrolytes and cis-bis(4,4'-dicarboxy-2,2'-bipyridine)dithiocyanato ruthenium(II) (N3) dye as the sensitizer. Chapter 4 presents the results obtained from this study. This chapter comprises of four parts. The first one is the verification of the modified chitosan structural and its physical properties including its crystallinity and solubility. The second part discuss the phthaloylchitosan as the polymer host in GPE. The effect of the salts on dye sensitized solar cell efficiency, conductivity behavior and polymer-salt interaction will be discussed in this chapter. The third part includes the effects of mixed cations in the gel polymer electrolyte towards the DSSC. The last part of this chapter discusses the results of introducing small amounts of ionic liquid to the GPE in order to further improve the efficiency of DSSC. The work will be concluded in Chapter 5. The flow chart in Figure 1.2 summarizes the current work.

1.4. Outline of the research

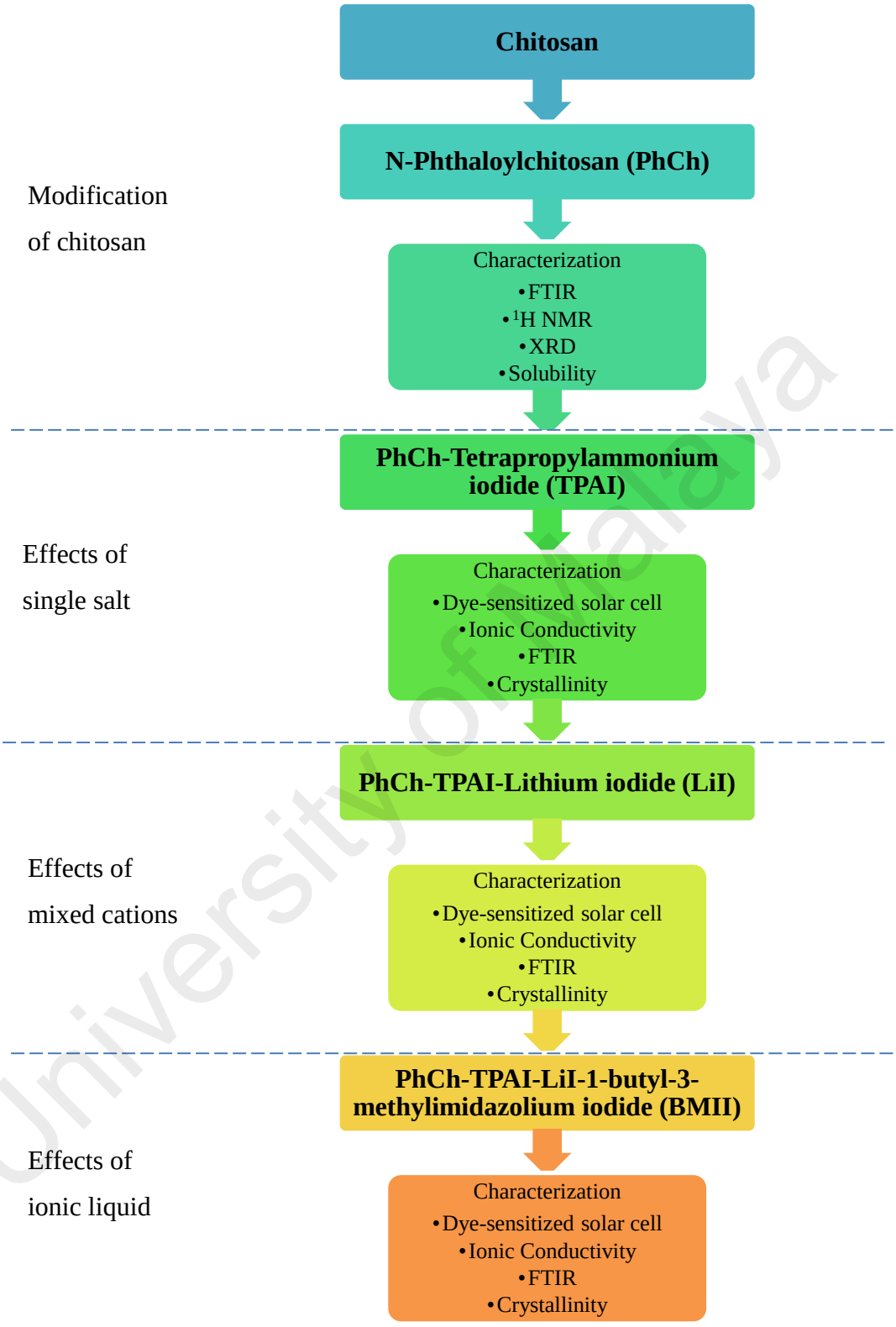

Figure 1.2: Flow chart of current work.

CHAPTER 2 : LITERATURE REVIEW

2.1. Introduction of Biopolymer

A polymer is a substance that contains large molecules that is formed from many small molecules or monomers joined together. There are two types of polymers, natural and synthetic polymers. Examples of synthetic polymers include polyethylene oxide (PEO), polystyrene (PS), polyamide (PA) and polyvinylchloride (PVC). These show some good properties such as being light-weight, strong and can be molded into shape without breaking. However, this type of polymer which is mostly made from chemicals found in the naptha fraction of oil is unreactive as they are not affected by air, water, acids or other chemicals. This matter creates a problem since they do not break down or rot away, thus it will be difficult to decompose and resulting it to be costly to recycle.

Hence, the use of natural polymers especially biopolymers has re-emerged in the industry (Chaisorn et al., 2016; de Léis et al., 2017; Kim et al., 2017). Biopolymers have two significant advantages which are (1) it is a renewable resource and (2) it is biodegradable. Since nature has been busy producing natural polymers for millions of years, it has existed abundantly: carbohydrate is an example. Carbohydrate is an important naturally occurring substances that can be found in plants and animals. Figure 2.1 summarizes the classifies carbohydrates into simple and complex carbohydrates. Simple carbohydrates consist only of monosaccharides, which is single sugar such as glucose, $C_6H_{12}O_6$. By linking together two sugar units, for example, glucose and fructose, $C_6H_{12}O_6$, disaccharide sucrose, $C_{12}H_{22}O_{11}$, is obtained. Polysaccharides contain a large number of monosaccharide units joined together by glycosidic linkages.

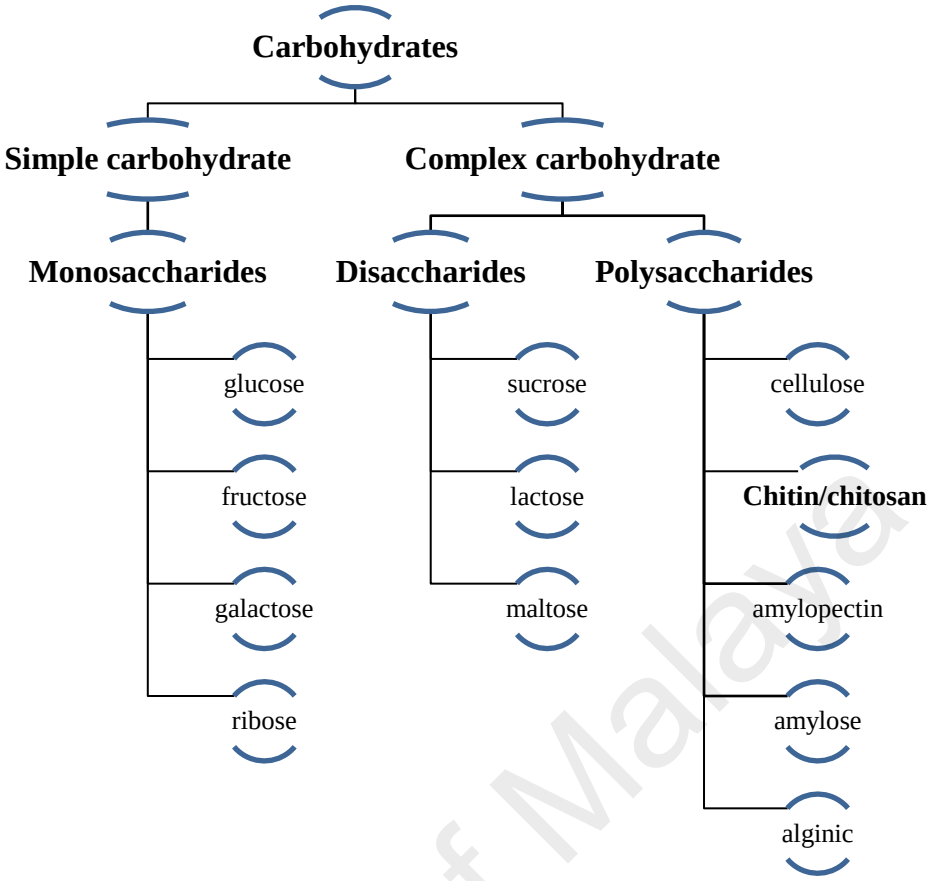

Figure 2.1: Naturally occurring polysaccharides.

2.1.1. Chitosan

Chitosan, a linear amino polysaccharide, has attracted the hearts of many researchers among the multitude of polysaccharides due to it being non-toxic, non-immunogenic, enzymatically biodegradable and biocompatible in animal tissues (Dodane & Vilivalam, 1998; Sashiwa et al., 2002). Chitosan comprises the repeating unit of β-(1-4) linked 2-amino-2-deoxy-*D*-glucopyranose and have no or small amounts of N-acetyl-D-glucosamine units (Badawy et al., 2004; Liu et al., 2005). Chitosan is a product of N-deacetylation of chitin when it is able to dissolve in dilute acids. The changes in the structure of chitin into chitosan can be seen from Figure 2.2. Chitin is the second most abundant natural polymer in the world after cellulose (Binette & Gagnon, 2007). It is widespread in the outer shells of insects (scorpions, ants, cockroaches, spider and beetles) and sea animals (annelid, mollusca coelenterate and crustaceans like crab and shrimp).

Other sources of chitin and chitosan is from microorganisms such as algae, yeast, *mycelia penicillium*, spores and also in the cell wall of certain fungi (Aranaz et al., 2009). Figure 2.3 shows the steps of extraction of chitin and chitosan from the raw materials.

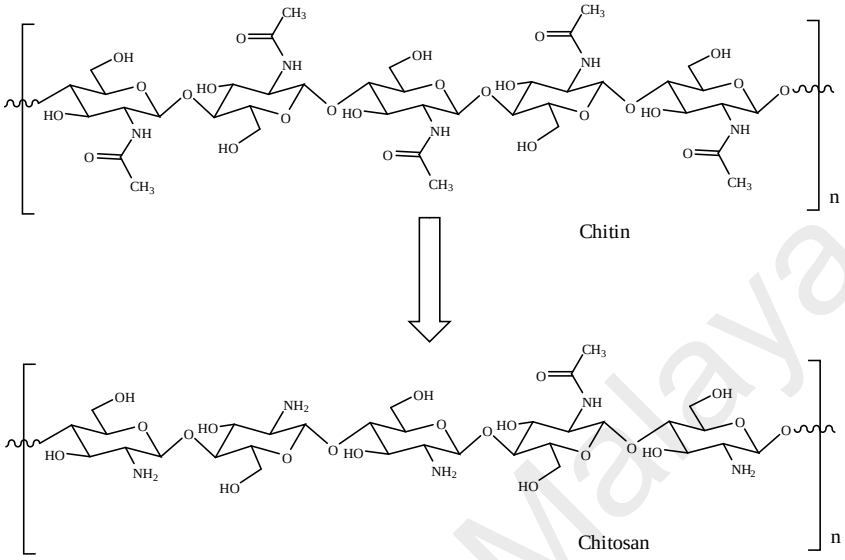

Figure 2.2: Structure of chitin and chitosan.

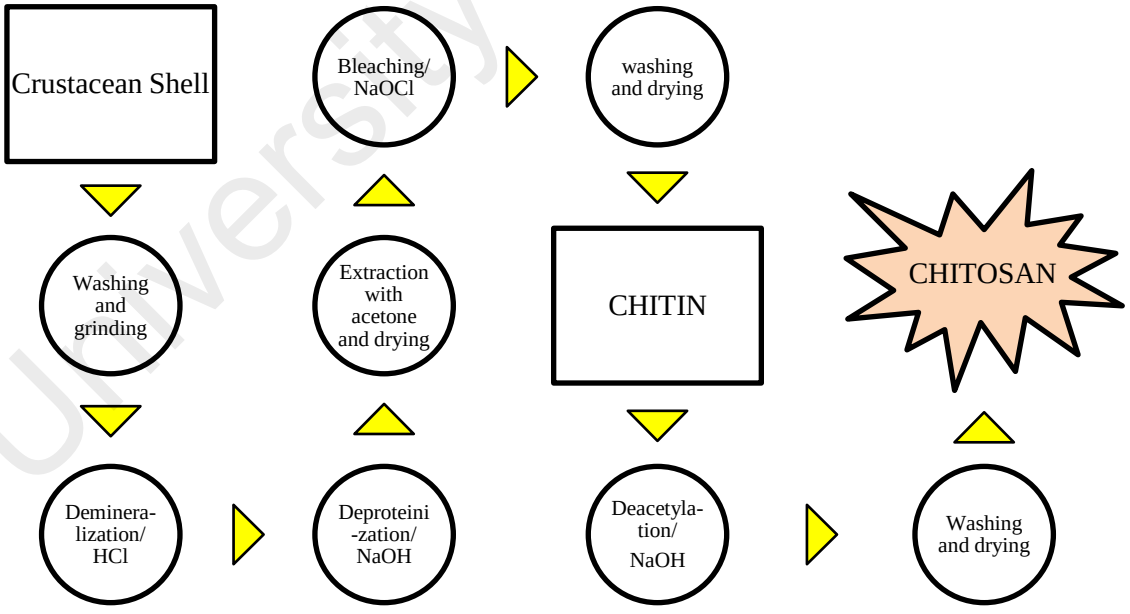

Figure 2.3: Preparation of chitin and chitosan from raw material (Alves & Mano, 2008).

Chitosan is a material with high potential and have been used in various fields such as pharmaceutical, cosmetic, biomedical, environmental, agricultural,

biotechnological, food industries and catalysts. The details have been tabulated in Table 2.1.

Table 2.1: Applications of chitosan in various fields.

Field	Descriptions	References
Pharmaceutical	Chitosan has been used in pharmaceutical and drug delivery applications. Its absorption-enhancing controlled release and bioadhesive properties have made it useful for such applications.	Dodane & Vilivalam (1998)
	It has the potential to significantly improve the transmucosal delivery of macromolecule drugs.	Issa et al. (2005)
Cosmetic	Skin (moisture, treat acne), hair and oral care (toothpaste and chewing gum).	Rinaudo (2006)
Biomedical	Chitosan plays a role in tissue engineering and antimicrobial agents in wound healing applications.	Aranaz et al. (2009)
Environmental	Chitosan flocculation involved in the removal of phytoplankton cells from aquaculture systems to reduce the nitrogenous waste and improves water quality.	Lertsutthiwong et al. (2009)
	Chitosan can remove suspended titanium dioxide particles in water by flocculation in the presence of humic acids.	Divakaran & Pillai (2004)
	Water treatment.	Miretzky & Cirelli (2009)
Agricultural	Chitosan can be used as a growth promoter.	El-Sawy et al. (2010)
Biotechnological	Wool fabric.	Issa et al. (2005)
Food industries	Antimicrobial properties of chitosan blends with gliadin proteins isolated from wheat gluten.	Fernandez-Saiz et al. (2008)
Catalysts	Renewable polymeric supports for catalysts	Macquarrie & Hardy (2005)

Chitosan as Polymer Electrolytes

Chitosan has been used to develop high conducting polymer electrolyte systems as it has polyelectrolyte behaviour, a protonated amino group in its structure (Hu et al., 2007; Klotzbach et al., 2006; Payne & Raghavan, 2007; Wan et al., 2003). Moreover, chitosan attracts more attention with its chelating properties with various substances, such as fats, metals, proteins, and others (Bordenave et al., 2008). Polyelectrolyte complexes

of chitosan with other natural sources such as DNA and proteins have also been reported. Denuziere et al. (1998) had studied the chitosan polyelectrolyte complexes with polysaccharides, including those with glycosaminoglycans (GAG). In the field of chitosan polyelectrolyte complexes with synthetic polyacid anions, the largest numbers of publications were devoted to chitosan polyelectrolyte complexes with polyacrylic acid (PAA) (de la Torre et al., 2003; Shieh & Huang, 1997).

Polyelectrolyte is slightly different from solid or gel electrolyte because in polyelectrolyte, cationic or anionic groups are chemically bonded to a polymer chain, while their counterions are solvated by a high dielectric constant solvent and mobile. In polymer electrolytes, interaction of polymer with the doping salt will lead to the complexation. Chitosan has good complexing ability as the $-NH_2$ groups are involved in specific interactions with metal ions (Rinaudo, 2006).

Table 2.2: Examples of Chitosan-based polymer electrolyte.

Chitosan	Salt/acid	References
Chitosan in acetic acid	Lithium acetate	Yahya & Arof (2002)
Chitosan in acetic acid	Sodium Alginate	Smitha et al. (2005)
Chitosan in acetic acid	Sulfuric acid	Smitha et al. (2008)
Chitosan in acetic acid	Ammonium nitrate	Ng & Mohamad (2006)
Chitosan in acetic acid	Phosphoric acid	Majid & Arof (2007)
Chitosan in acetic acid	Sodium alginate	Sæther et al. (2008)

According to Baril et al. (1997), the four factors for the formation of complexes are (i) high concentration of polar solvating groups (-O-, -OH,-NH, -CN-), (ii) the donor number and polarizability of the solvating groups, (iii) low lattice energy of the doping salt and (iv) low lattice energy of the polymer. Although polyelectrolyte is a bit different from the polymer electrolyte, with all the polyelectrolyte features that exist in chitosan, it helps to fulfil the objective of the work to develop polymer electrolytes. Some examples of chitosan as polymer electrolytes host are shown in Table 2.2.

2.1.2. Modification of Chitosan

Although it has a high potential as a base for polymer electrolyte, there is still a clear weakness in chitosan. Chitosan is reported to be only soluble in dilute aqueous acidic solution (pH 6.5) but insoluble in water and organic solvent (Aranaz et al., 2009; Pillai et al., 2009; Qin et al., 2006; Sashiwa et al., 2002). This is due to the free protonable amino groups present in the *D*-glucosamine units (Aranaz et al., 2009; Holappa et al., 2004). The *β*-1,4'-glycosidic linkages give the biopolymer its rigid and crystalline structure besides promoting formation of intra-molecular hydrogen bonds (Bruice, 2004), involving the hydroxyl groups as shown in Figure 2.4. Solubility of chitosan is a very difficult parameter to control as it is related to the degree of acetylation, the ionic concentration, the pH, the nature of the acid used for protonation and the distribution of acetyl groups along the chain, as well as the conditions of isolation and drying of the polysaccharide (Rinaudo, 2006).

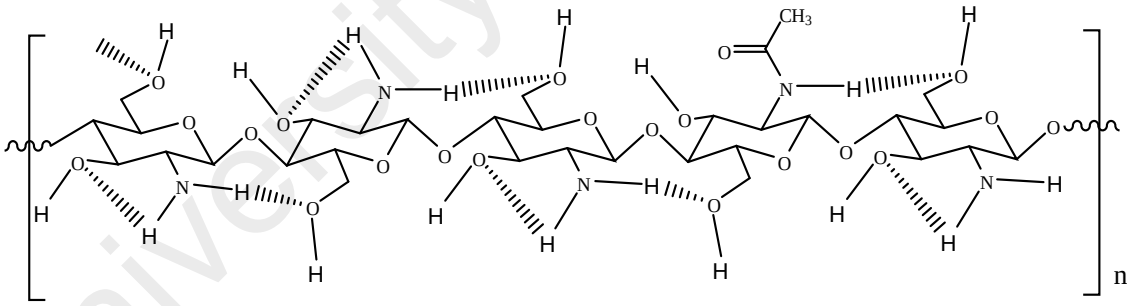

Figure 2.4: Formation of intra-molecular hydrogen bonds between chitosan.

The insolubility of chitosan in many common organic solvents limits its usage and leads to some disadvantages such as poor extent of reaction, structural ambiguity of the products and partial degradation due to harsh reaction conditions (Jančiauskaitė & Makuška, 2008; Kurita, 2006).

With great potential in a variety of applications as well as abundant in existence on this earth, chitosan should be modified to fully explore its ability and development. In

addition, the presence of two functional groups in chitosan's backbone, NH_2 and OH, enables modifications can be done. Many researchers have modified chitosan to fulfil the requirements in their respective fields (Inta et al., 2014; Jeon & Höll, 2003; Mourya & Inamdar, 2008; Sobahi et al., 2014). For example, Sashiwa et al. (2002) reported that chemical modification of chitosan was necessary to improve its adhesion to plastics as well as its organosolubility so as to be able to adhere on the surface of the plastics which is hydrophobic. Roberts & Wood (2001) working in the development of chitosan-based anti-felting treatment for wool, increased the hydrophobic character of the chitosan by introducing long-chain *N*-acyl groups through reaction with hexanoic anhydride or similar long chain acid anhydride.

Various possible methods have been carried out to modify chitosan (Zohuriaan-Mehr, 2005) and some of the potential method is displayed in Figure 2.5 (Prashanth & Tharanathan, 2007). Among the methods are phosphorylation (Ma et al., 2010; Wang et al., 2001), sulfonation (Fredheim & Christensen, 2003; Lv et al., 2014; Wolfrom & Han, 1959), xanthation (Sankararamakrishnan et al., 2006; Sankararamakrishnan & Sanghi, 2006), acylation (Peesan et al., 2006; Peesan et al., 2005; Wu et al., 2004; Zong et al., 2000), cross-linking (Bodnar et al., 2006; Maya et al., 2014), graft copolymerization (Aranaz et al., 2009; Makuška & Gorochovceva, 2006; Wang et al., 2009) and carboxyalkylation (Felicio et al., 2008; He et al., 2011; Liu et al., 2012; Nguyen et al., 2009). Apart from substitution and chain elongation methods, some researchers studied γ-irradiation in order to reduce the molecular weight of chitosan with minor changes to the structure of the chitosan (Yoksan et al., 2001). Among the various modified chitosan, only a few has been applied as the polymer electrolyte base (Rosli et al., 2012; Winie & Arof, 2006; Winie et al., 2009). Hexanoyl chitosan based polymer electrolyte achieved a conductivity value of 4.26×10^{-5} S cm^{-1} with lithium trifluoromethanesulfonate, $LiCF_3SO_3$ (Winie et al. 2009).

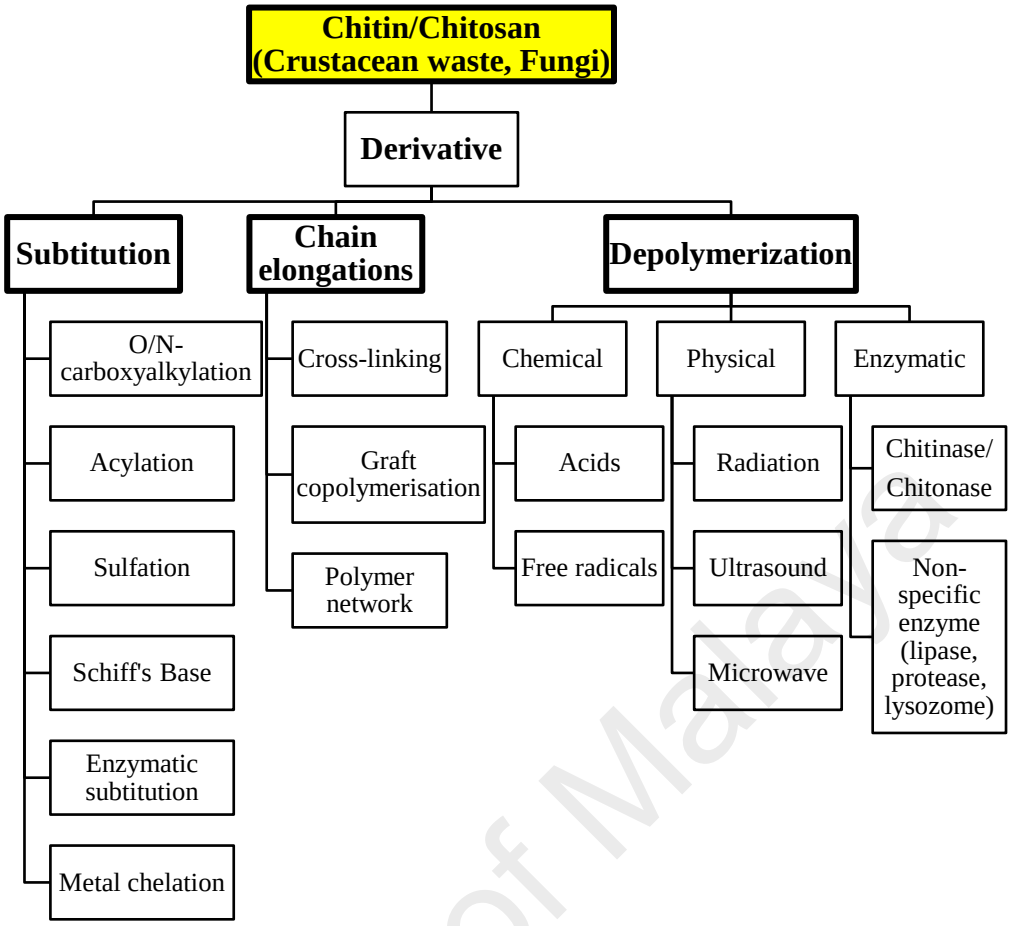

Figure 2.5: Multifaceted derivatization potential of chitin/chitosan (Prashanth & Tharanathan, 2007).

2.1.3. N-phthaloylation of chitosan

In the previous section, we have seen that there are numerous methods to modify chitosan. As discussed before, chitosan is insoluble in organic solvents due to the hydrogen bonds between the amino and hydroxyl groups with the solvents. In this work, the solubility of chitosan in organic solvents has been improved with phthaloylation as shown in Figure 2.6.

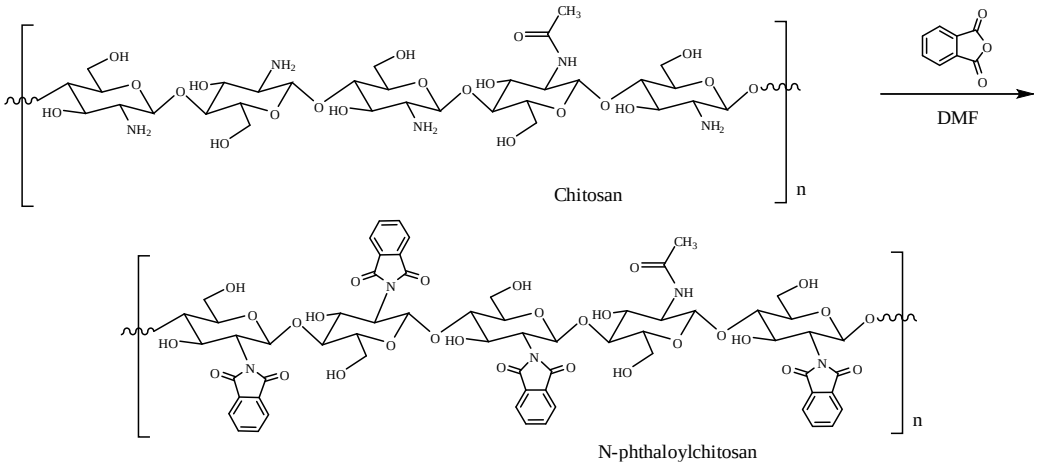

Figure 2.6: Phthaloylation of chitosan

In 1991, Nishimura and colleagues have replaced the two hydrogens of the amino group with a hydrophobic phthaloyl group to destroy the inherent crystalline structure, thereby improving solubility of chitosan in general organic solvents. This site selectivity reaction which introduced side substituent at predetermined positions of the sugar rings, occurs at the primary amino group of the C-2 position, primary hydroxyl at C-6 position and secondary hydroxyl functionalities at C-3 position has distinctly different reactivities (Kurita et al., 2000; Rout et al., 1993; Yoksan et al., 2001). The structure of phthaloylchitosan is shown in Figure 2.6. Phthaloylchitosan shows excellent solubility in organic solvents such as DMF, DMSO, DMAc, and pyridine (Bian et al., 2009; Kurita et al., 2007; Kurita et al., 2000; Kurita et al., 1998; Kurita et al., 1993; Liu et al., 2005; Nishimura et al., 1991).

Phthaloylation can be obtained by refluxing chitosan with phthalic anhydride in a particular solvent for 5-7 hours at temperature greater than 100 ℃ (Kurita et al., 1998; Kurita et al., 1993; Nishimura et al., 1991). Besides, phthaloylchitosan can also be successfully obtained by microwave radiation under nitrogen atmosphere (Liu et al., 2005; Liu et al., 2004). Another method to prepare PhCh is by preparing gel-like chitosan with precipitation of an aqueous acetic acid chitosan solution into aqueous $NaHCO_3$, followed by subsequent multiple solvent replacements with DMF (Rout et al., 1993).

Product for phthaloylation of chitosan will usually produce a little O-phthaloylation other than N-phthaloylation as shown in Figure 2.7 (Kurita et al., 2001; Liu et al., 2004).

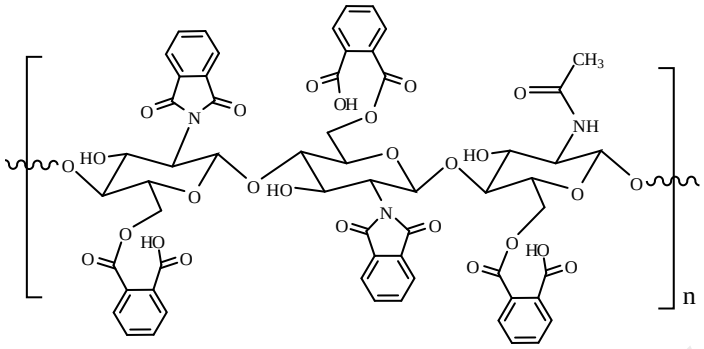

Figure 2.7: Structure of N- and O-phthaloylchitosan.

Another method to avoid O-phthaloylation occurring and thus resulting N-phthaloylation only can be achieved by adding in a small amount of hydroxy-containing compounds such as ethanol, water, ethylene glycol or methyl cellosolve into the solvent for reaction. However, the product exhibits low solubilty in common organic solvents as it swelled in DMF, DMSO and pyridine and high degree of crystallinity as shown in Figure 2.8. The product of this method conflicts with the original purpose of this project and is less suitable as a base polymer electrolyte. Therefore, PhCh was synthesized by the conventional method.

From all of the practical viewpoints of protection, deprotection and solubilisation, phthaloylation is particularly attracted at amino group of chitosan (Kurita et al., 2007). N-Phthaloylation is commonly used in synthesis process as an intermediate step as it can easily be deprotected to generate free amino group (Kurita et al., 2000; Wang et al., 2009; Yoksan et al., 2001; Yoksan et al., 2004). Phthaloylated chitosan (PhCh) is thus a suitable precursor for a variety of site-specific and quantitative modification reactions to construct well-defined molecular environments on chitosan. Some of the synthesis works that involved PhCh as the key precursor are listed in Table 2.3.

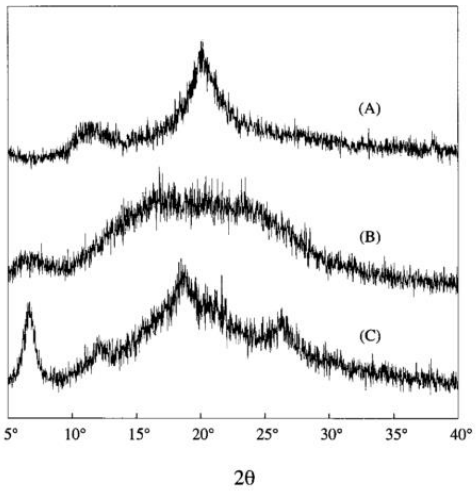

Figure 2.8: X-ray diffraction diagrams of (A) fully deacetylated chitosan, (B) PhCh prepared in DMF and (C) PhCh prepared in DMF/water (95/5) (Kurita et al., 2001).

Table 2.3: Applications of phthaloylchitosan.

Chitosan derivatives	**Structure**	**Ref.**
Regioselective introduction of α-mannoside branches at C-6 of chitin and chitosan.	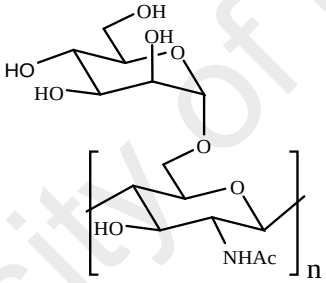	Kurita et al. (1998)
Regioselective introduction of N-acetyl-D-glucosamine and D-glucosamine branches at C-6 of chitin and chitosan	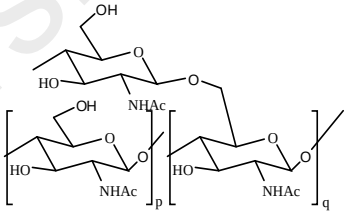	Kurita et al. (2000)
Chain modification of γ-ray irradiated chitosan under the conditions where reaction occurs mainly at hydroxyl groups	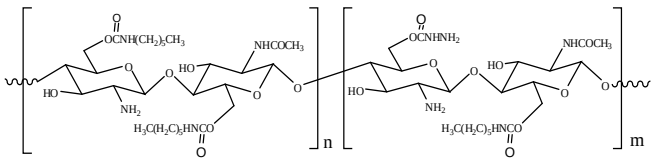	Yoksan et al. (2001)
Introduction of *β*-maltoside branches at the C-6 position of chitin and chitosan.	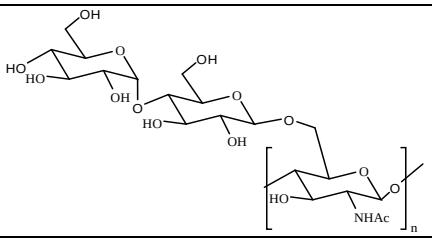	Kurita et al. (2003)

Table 2.3 continued.

Chitosan derivatives	Structure	Ref.
N-acylation of chitosan with the quaternary betaine moiety.	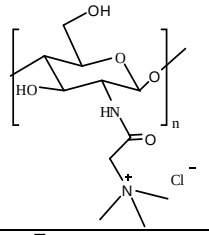	Holappa et al. (2004)
Synthesis of Chitosan-O-PEG-galactose	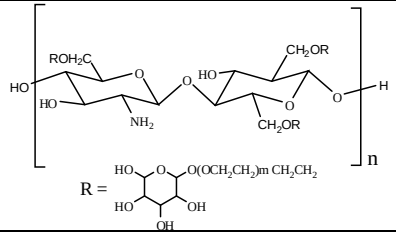	Lin & Chen (2007)
Selective C-6 oxidation of chitosan by 2,2,6,6-tetrameth-ylpiperidine-1-oxy radical	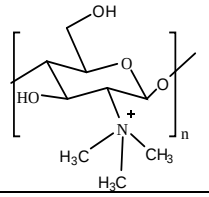	Bordenave et al. (2008)
Synthesis of chitosan-g-poly(N-isopropylacrylamide)	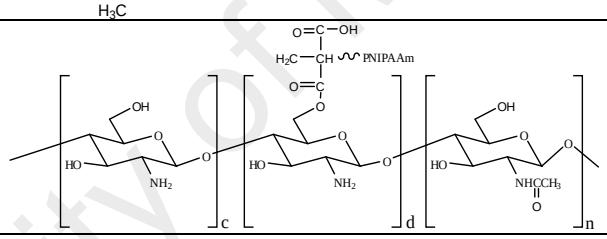	Mu & Fang (2008)
Synthesis of 6-N,N,N-trimethyltriazole chitosan	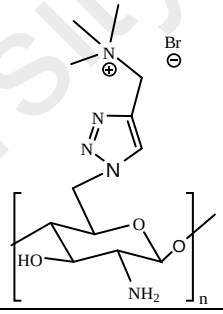	Gao et al. (2009)

The usefulness of the PhCh used as a precursor or intermediate in the synthesis of chitosan derivatives can be observed from Table 2.3. However, PhCh is rarely used as an end product except for self-assembled polymeric micelles (Casettari et al., 2012). Other workers have also used PhCh for the same purpose i.e. N-phthaloyl chitosan-*g*-mPEG (Opanasopit et al., 2006), N-phthaloyl-carboxymethylchitosan (Peng & Zhang, 2007) and N-phthaloylchitosan-g-polyvinylpyrrolidone (Bian et al., 2009). Due to the presence of lone pair electrons on the oxygen of carbonyl (C=O), –N– and hydroxyl (–

OH) groups in the structure of PhCh, it has the potential to become a base for polymer electrolytes. Thus, in this study, the potential of this biopolymer chitosan as an electrolyte in dye-sensitized solar cell is investigated.

2.2. Solar cell

A solar cell is a device that converts light energy directly into electrical energy through the process of photovoltaic. Solar energy conversion is considered the most credible and viable way to face the growing energy demand, both for its high intensity (1000 W m^{-2} at ground level with the sun directly overhead) and equitable geographical distribution (Bella et al., 2014). The general understanding of how solar cells work is that sunlight is composed of photons with a spectrum of energies. Photons can interact with atoms. With enough energy the photons release an electron from the atom. For solar cells to produce electricity, it must be able to "collect" the electron once separated from the atom. The electrons flow is the photocurrent.

Solar cells can be divided into several types. According to their material composition, these can be silicon solar cell, perovskite solar cell, cadmium telluride solar cell, quantum dot solar cell, plasmonic solar cell, multi-junction solar cell and dye sensitized solar cell.

2.2.1. Dye-sensitized Solar Cell (DSSC)

Out of the various kinds of solar cell, DSSC has been widely studied. DSSC have many advantages, namely cheap fabrication without expensive and energy-intensive high-temperature and high vacuum processes and compatibility with flexible substrates. DSSC can be presented in various looks in order to facilitate market entry, both for domestic devices and in architectural or decorative applications (Grätzel, 2005).

A DSSC consists of three main parts as illustrated in Figure 2.9 which are:

a) Photo-active electrode

b) Counter electrode

c) Electrolyte

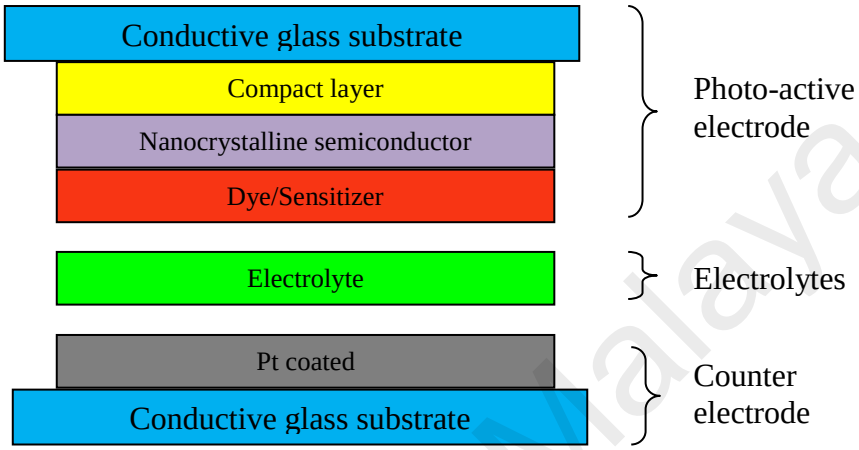

Figure 2.9: Dye-sensitized solar cell configuration

There are three important steps for photocurrent generation (Mohamad et al., 2007; Park, 2010) in DSSCs as shown in Figure 2.10.

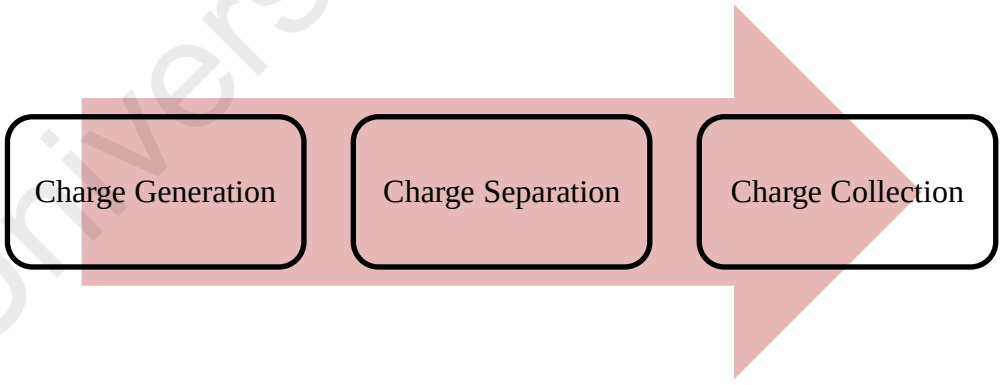

Figure 2.10: Steps for generation of photocurrent in DSSCs

Cations and anions (usually a free iodides) are formed when the salt(s) dissociate. The iodide, I^- will interact with I_2 (also added in the electrolyte) form a triiodide according to the equation 2.0.

$$I^- + I_2 \rightarrow I_3^- \quad (2.0)$$

Charge is generated when the dye (S*) in DSSC absorbs photons that excite the ground state (or Highest Occupied Molecular Orbital, HOMO) electrons of dye to the excited state (Lowest Unoccupied Molecular Orbital, LUMO) as shown in Equation 2.1. The photo-excited electrons are separated from the oxidized dye when they are injected into the mesoporous TiO_2 that occurs within pico- to femto-seconds.

$$S^*(adsorbed\ on\ TiO_2) \rightarrow S^+(adsorbed\ on\ TiO_2) + e^-(injected) \quad (2.1)$$

After electron injection has occurred, the photo-injected electrons percolate through the mesoporous TiO_2 network within micro to milliseconds, reach the conducting substrate and enters the external circuit.

The photo-injected electrons may recombine with the oxidized dye molecule via surface state of TiO_2 as shown in Equation 2.2;

$$S^+(adsorbed\ on\ TiO_2) + e^-(TiO_2) \rightarrow S(adsorbed\ on\ TiO_2) \quad (2.2)$$

Besides that, recombination of the injected electrons may occur with the oxidized redox couple at the TiO_2 surface.

$$I_3^- + 2e^-(TiO_2) \rightarrow 3I^- \quad (2.3)$$

The electrons can also recombine with the triiodide ions within nano-second time scale, Equation 2.4:

$$3I^- \rightarrow I_3^- + 2e^- \quad (2.4)$$

When the electrons reach the counter electrode, the triiodide ions are reduced to iodide ions, which then diffuse towards the photoanode. Here the I^- ions release an electron to the oxidized dye molecule and in turn as reduced to an I_3^- ion. The dye is regenerated and the circuit is completed. These processes are illustrated in Figure 2.11.

The improvement of the solar cell performance is dependable to the charge transport as the electrons pass through the three interfaces; TiO_2/FTO, electrolyte/counter electrode and dye/electrolyte. The matching of the energy level of each component as shown in Figure 2.11 is essential in DSSC. The conduction band of TiO_2 must be below the LUMO edge of the dye. The redox potential energy level should be higher than the HOMO level of the dye. The redox potential of the electrolyte is usually unaffected by the current whether in the dark or under illumination. The photo-injected electrons percolate through the TiO_2 because of the lack of the built-in electric field in the semiconducting TiO_2 layer. The entrance and exit of the photocharge in and out of the TiO_2 layer decreases the Fermi level in the direction of the conductive glass substrate contact at short-circuit.

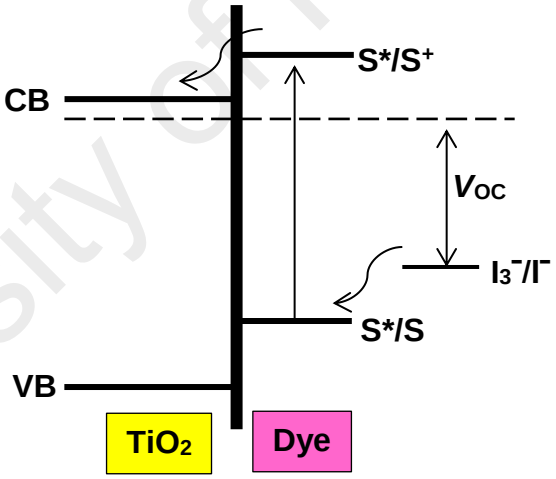

Figure 2.11: Energy position of each component in DSSC.

Open-circuit voltage

The open-circuit voltage (V_{OC}) is determined by the energy difference between the electronic energy of a redox system, I_3^-/I^- and the fermi level of the semiconductor as shown in Figure 2.11. Under working condition of DSSCs, the fermi level of the semiconductor gets close to the energy of the conduction band edge because of the trap sites located below the conduction band are sufficiently occupied by the photo-generated

electrons. Therefore, the choice of semiconductor and redox mediator can affect V_{OC}. However, the V_{OC} value is difficult to presume due to two reasons (Katoh & Furube, 2014). One of the reasons is energy shifts in both conduction band edge and redox system can be influenced by surrounding molecules. The energy level of conduction band is sensitive to some additives. For example, it shifts towards lower energy as Li^+ ions was introduced to the electrolyte due to the surface adsorption and intercalation of Li^+ ions in the lattice of TiO_2 (Bandara et al., 2013). It can also shifts toward higher energy as 4-tert-butylpyridine (TBP) was added since TBP adsorbs on the surface of TiO_2 (Hassan et al., 2016). The second reason is that some conducting electrons can be lost due to the recombination process with the redox mediator during transport in the semiconductor electrode.

Short-circuit current

According to Katoh & Furube (2014), the short-circuit current (J_{SC}) is the photocurrent obtained under short-circuit conditions, that is, without any load. J_{SC} is proportional to the product of generation efficiency of conducting electrons under sunlight irradiation (Φ_G), its charge collection efficiency from the device to the external circuit (Φ_C) and the solar cell's sunlight-harvesting efficiency (Φ_{LH}).

$$J_{SC} = \Phi_G \times \Phi_C \times \Phi_{LH}$$

By improving the generation efficiency of conducting electrons under sunlight irradiation, it can give rise to the higher J_{SC} value as it contributes to the electron conduction. In addition, the properties of sensitizer dye and the structure of nanocrystalline semiconductor films, both located at the photo-active electrode (further discussion on the next section), need to be adjusted to get an excellent solar cell's sunlight-harvesting efficiency. Thus, leading to the high number of dye molecule adsorbed on its surface.

2.2.2. Photo-Active Electrode

In DSSCs, charge carrier generation takes place in a chemisorbed monolayer of photoactive dye that is sandwiched between a semiconducting oxide and an electrolyte (Tétreault et al., 2011). When light penetrates the photosensitized semiconductor "sponge", it crosses hundreds of adsorbed dye layers. The mesoporous structure thus fulfils a function similar to the thylakoid vesicles in green leaves, which are stacked in order to enhance light harvesting by chlorophyll (Grätzel, 2005).

Photo-active electrode comprises two layers coated onto the conducting glass substrate. The layer deposited on the conducting glass is the compact layer. The mesoporous TiO_2 layer is deposited on the compact layer. The conducting glass substrate provides an advantage as it holds the photoanode, absorbs the incident light and sends the photo-injected electrons as current to the external circuit (Katoh & Furube, 2014). The usual conducting glass substrates are:

i. Fluorine doped tin oxide (FTO) (Yusuf et al., 2014; Yusuf et al., 2016)
ii. Indium doped tin oxide (ITO) (Mohamad et al., 2007)
iii. Hartford TEC8 conductive glass substrate (Chatzivasiloglou et al., 2007)

Mesoporous layer

The thin mesoporous nanocrystalline TiO_2 film onto which the dye adsorbs is one of the important parts in DSSCs. Mesoporous semiconductor oxide layer which is placed in contact with the redox electrolyte or an organic hole conductor, is to serve as an electron conductor and also to provide a folded surface to enhance light harvesting by the adsorbed sensitizer (Grätzel, 2005). Certain characteristics are required for the semiconductor electrode to produce an efficient DSSC (Liu et al., 2010) namely; (1) enough surface area to provide sufficient photosensitive dye adsorption, (2) an adequate conduction band edge that matches the LUMO level of the photosensitive dye, and (3)

fast electron transport or long electron lifetime, which guarantees high charge-collection efficiency.

In addition, the performance of the DSSC depends on the type of material, the nanoparticle morphology and the porosity of TiO_2. The advantage of using a semiconductor layer is that such an inorganic oxide is extremely stable and allows for fast electron movement. Some of the metal oxides that have been used are TiO_2 (Kim et al., 2013), ZnO_2 (Wang et al., 2013) , SnO_2 (Lee et al., 2011), Nb_2O_5 (Ghosh et al., 2011) and $SrTiO_3$ (Yang et al., 2010). Although other metal oxides can be used as the semiconductor layers, TiO_2, is frequently used. TiO_2 has shown better performance compared to other oxides (Arof et al., 2014a; Aziz et al., 2014; Bandara et al., 2015; Grätzel, 2005; Hassan et al., 2014; Katoh & Furube, 2014; Noor et al., 2014; Park, 2010; Yusuf et al., 2014). Besides, TiO_2 has been widely used in various devices such as solar cells, sensors, batteries, and photocatalysis (Parussulo et al., 2011). The mesoporous structure and composition of TiO_2 has been attuned to tailor optical, magnetic, photonic, electronic, and catalytic properties (Patel et al., 2008). The dye which is usually a ruthenium complex strongly absorbs light in the visible (Chatzivasiloglou et al., 2007). In addition, TiO_2 has the highest refractive index in the wavelength region from 430 to 1530 nm (Bond, 1965; Devore, 1951; Dodge, 1986; Gao et al., 2012; Pan et al., 2008).

TiO_2 exists in three natural forms namely anatase, rutile and brookite (Tang et al., 1994). Anatase form of TiO_2 is usually used in DSSCs as it exhibits a higher V_{OC} compared to that using the rutile form of TiO_2. This is due to the smaller difference in energy between the conduction band and the redox potential in the rutile TiO_2. Due to its large intrinsic band gap, for rutile 3.0 eV and for anatase 3.2 eV (Tang et al., 1994), the TiO_2 optical absorption is limited to the UV region. According to Zallen & Moret (2006), the absorption spectrum of brookite extends throughout the visible with broad and gradual edge and that the lowest direct gap for brookite is larger than 3.54 eV. However, the

brookite form of TiO_2 is not used in DSSCs as it is thermodynamically less stable and can be transformed into other phases at high temperatures (Koyama et al., 2006).

Blocking layer

DSSC performance can be improved by maximizing photon absorption and minimizing electron recombination. Electron recombination in DSSCs is due to the significant electron loss and performance degradation. During electron injection, certain electron did not contribute to the electron conduction as it undergoes recombination with an oxidized dye from the redox mediator, triiodide ions. In addition, generated electron can migrate in the nanocrystalline film through hopping between nanoparticles can contribute to electron conduction. Thus, this limits the performance of the DSSC. Blocking layer, a thin barrier layer at the conducting substrate/electrolyte interface is introduced in order to prevent electron recombination during the transport and collection process of electrons in DSSCs. TiO_2 is said to be the most effective electrolyte blocker among the many metal oxides and have been frequently used in DSSCs (Cameron & Peter, 2003; Li et al., 2015). It blocks electron recombination to the electrolyte (Barea & Bisquert, 2013).

Dye as sensitizer

Dye is one of the main factors to stress towards the great performance of DSSC. There are certain requirements for an excellent sensitizer to be function in DSSC (Grätzel, 2005; Katoh & Furube, 2014; Nazeeruddin et al., 2004);

1. It should absorb light with wide range of wavelength as it is necessary to obtain high value of sunlight-harvesting efficiency since the specific surface area of the nanoporous structure is very high which lead to the high number of dye molecule adsorbed on its surface.

2. Dye should be able to form a strong coordinative bond with the titanium surface ions as these will influence the free energy change for electron injection that can be evaluated from the energy difference between LUMO of the dye and the conduction band edge of the semiconductor as shown previously in Figure 2.11.
3. The energy difference between HUMO of the dye and the oxidation potential of the redox mediator, also shown in Figure 2.11, should also be optimized so that dye can be regenerated rapidly via electron donation from the electrolyte
4. Contact between dye sensitizer and the semiconductor surface has to be considered in order to achieve high quantum yields of the excited state electron transfer process.

Dye has been divided into two groups; natural dye and synthetic dye. Natural dyes give certain advantages such as no resource limitations, no harm to the environment and are easily prepared. Some of the natural dyes that have been used in the DSSC are listed in the Table 2.4. However, the values of the efficiency observed from the DSSC using natural dye are quite low.

The production process of the ruthenium based dye requires less solvents and eluents. In addition, ruthenium dye also possessed fair photo conversion efficiency and a quite good resistance to degradation. Ruthenium dye also have wide absorption spectrum covering visible and near IR regime (Qin & Peng, 2012). UV–Visible spectra of certain ruthenium based were shown in Figure 2.12. These factors favored the wide use of ruthenium dye which becomes one of the most used dyes in prototype and pre-industrial DSSC production (Parisi et al., 2014).

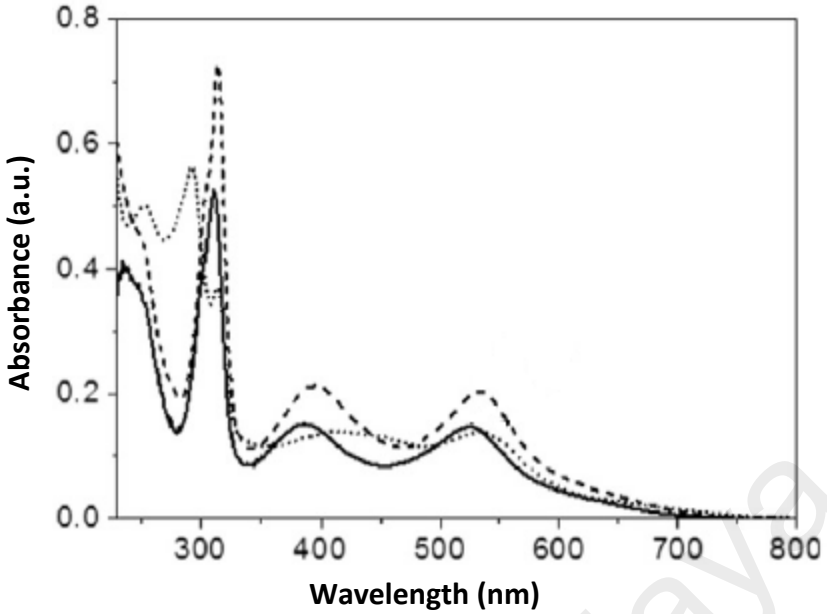

Figure 2.12: UV–Visible spectra of certain ruthenium based dyes; (1) N3 (dash), (2) N719 (solid) and (3) Z907 (dot) (Nosheen et al., 2016).

Therefore, to enhance the efficiency of DSSCs, the exploration of better dye molecules is never stopped. Molecular structure of classical metal-organic dyes, N3 and N719, and black dye are shown in Figure 2.13 (Yang et al., 2013).

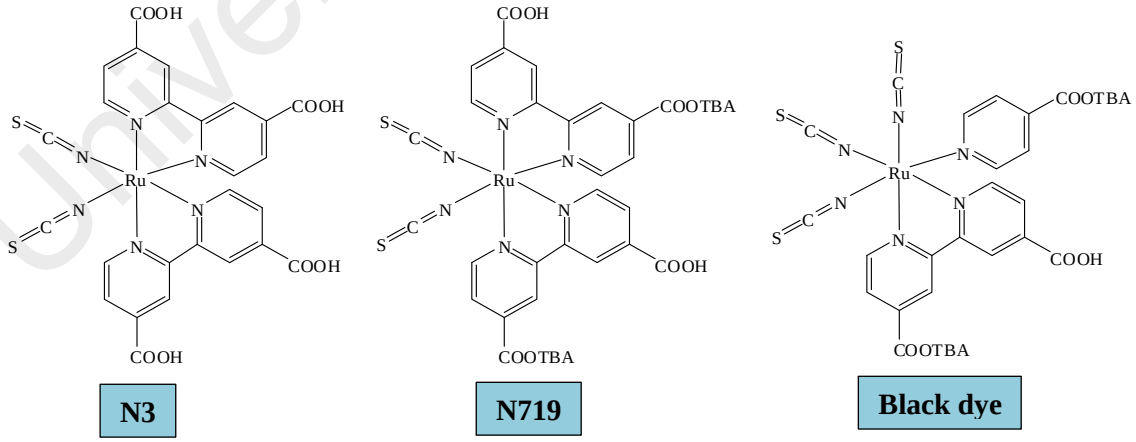

Figure 2.13: Molecular structures of some ruthenium based sensitizer dyes.

Table 2.4: List of the DSSCs using natural dyes.

Natural dyes	**Sources**	J_{SC}/ mA cm^{-2}	V_{OC}/ V	**FF**	**η/ %**	**Ref.**
Anthocyanin	Red seaweeds collected at Kefallinia Greek Island	1.26	0.66	0.63	0.52	Rapsomanikis et al. (2016)
	Malvidin-3-fructoside from grape fruits	4.06	0.43	0.33	0.55	Gokilamani et al. (2014)
	Mulberry fruit	1.89	0.56	0.53	0.55	Chang & Lo (2010)
	Red Sicilian orange juice (Citrus Sinensis)	3.84	0.34	0.50	0.66	Calogero & Marco (2008)
	Eggplant peels (Solanum melongena, L.)	3.40	0.35	0.40	-	
	Canna indica L.	0.82	0.54	0.59	0.29	Luo et al. (2009)
	Salvia splendens	0.7	0.56	0.61	0.26	
	Solanum nigrum L.	1.01	0.54	0.51	0.31	
	Cowberry	0.40	0.56	0.54	0.13	
Chlorophyll	Spinach	0.46	0.55	0.51		Chang et al. (2010)
	Ipomoea	0.91	0.54	0.56		
	Pomegranate leaf	2.05	0.56	0.52	0.60	Chang & Lo (2010)
Carotenoid	Achiote shrub (Bixa orellana L.)	1.10	0.57	0.59	0.37	Gómez-Ortíz et al. (2010)

There are numerous mechanisms on how a dye sensitizer can be attached to the metal oxide substrate surface namely covalent attachment, electrostatic interaction, hydrophobic interaction, physical entrapment, hydrogen bonding or van der waals forces (Kalyanasundaram, 1998). However, the dye and the TiO_2 surface atoms in most DSSC are bound by covalent bonding to achieve strong coupling, a homogeneous dye distribution and stability of the device (Zhang & Cole, 2015).

As previously mentioned, electron injection from dye into the conduction band of semiconductor is one of the most important steps towards high efficient DSSC and it is strongly influenced by the dye sensitizer/semiconducting metal oxide nanoparticles contact. A chemical substituent from the dye sensitizer, or "anchoring group", is capable to attach the dye molecule onto the surface of the metal oxide (Zhang & Cole, 2015).

Carboxylic acid group is one of the most common and the best-performing classical anchoring group of the family of ruthenium-polypyridyl complexes sensitizers to the semiconductor surface (Ellis-Gibbings et al., 2012; Warnan et al., 2013). The six types of possible anchoring modes of carboxylic acid are shown in Figure 2.14. The structures with bidentate chelating and bidentate bridging mode show great stability among all the anchoring modes due to the intimate contact between carboxylate anchor based dye and metal oxide (Zhang & Cole, 2015). As the anchoring groups possess an excellent electron withdrawing capabilities, they typically act as electron acceptor as the intermolecular charge transfer is promoted from the donor region of the dye to the region in the vicinity of TiO_2 substrate (Zhang & Cole, 2015).

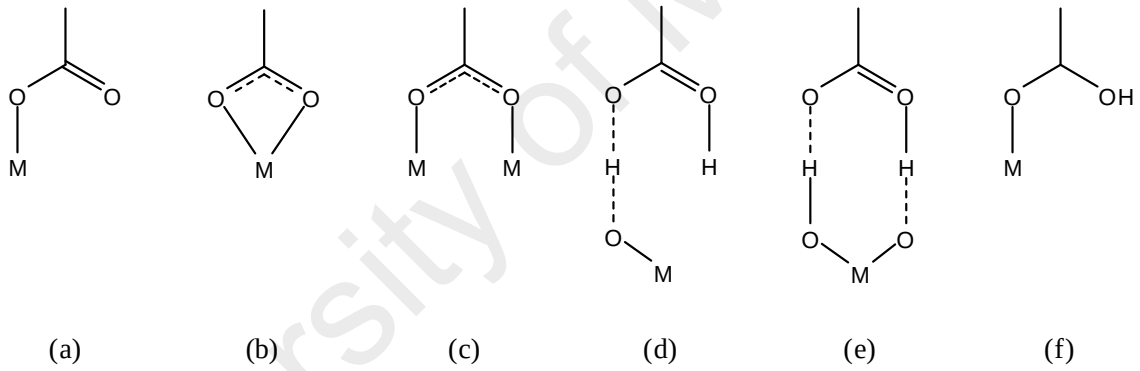

Figure 2.14: Possible binding modes for carboxylic acid anchors onto a metal oxide; (a) monodentate ester, (b) bidentate chelating, (c) bidentate bridging, (d) monodentate H-bonding, (e) bidentate H-bonding and (f) monodentate through C-O (Zhang et al., 2015).

Chemisorption to the surface will only occur in a monolayer, and as such, full coverage of a monolayer, the self-assembled monolayer, is considered and expected to be the most efficient dye interface configuration of a cell. Dye to dye electron transfer is expected to be increased by full dye coverage. In addition, a complete dye sensitizer layer will lessen the recombination losses by physically separating the electrolyte solution and the TiO_2 layer. Further, full coverage can also be expected to maximize the absorption

efficiency, thus enhance the photoelectron injection efficiency. (Ellis-Gibbings et al., 2012).

2.2.3. Counter Electrode

The counter electrode is normally platinum or carbon access material coated on the ITO or FTO substrate. The platinum film catalyses the iodide regeneration. The absence of catalyst results in a slower rate of I_3^- to I^- reduction.

Beside platinum, other materials that have been applied in the compact layer are V_2O_3 (Wu et al., 2012) , ZnO (Wang et al., 2013), SnO_2 (Bu & Zheng, 2015), TiC (Wu et al., 2013), VC (Wu et al., 2012), WC (Vijayakumar et al., 2015), NbN (Cui et al., 2015) and TiN (Li et al., 2010).

2.2.4. Electrolyte for DSSC

Researchers mostly focused more on the electrolytes than the other components in DSSC (Bella et al., 2014) as electrolyte is one of the main components that influences the conversion efficiency (Jin et al., 2012). In DSSCs, an electrolyte assures internal electrical contact between the two electrodes and mainly provides the potential barrier necessary for photovoltaic conversion (Chatzivasiloglou et al., 2007). Bandara et al. (2013) have also stated that electrolyte is an anion conductor and mostly are iodide ion conductor. This can be varied both for the redox couple used (I^-/I_3^-, Co^{2+}/Co^{3+}, Br^-/Br^{3-}, SCN group) and for the nature of the solution (Parisi et al., 2014). However, iodide ions, I^-/I_3^-, has been frequently used as the redox couple (Arof et al., 2014a; Aziz et al., 2014; Bandara et al., 2010b; Buraidah et al., 2011; Dissanayake et al., 2012; Hassan et al., 2014; Noor et al., 2011; Yusuf et al., 2014). The redox system is reduced at the counter electrode. Until very recently, the iodide/triiodide redox system has offered the best

performance in DSSCs. Its fast kinetics of dye regeneration and slow kinetics of unwanted recombination reactions at the photoelectrode surface give efficient cells with relatively low losses (Ellis-Gibbings et al., 2012). Some of the high efficiency DSSCs with ruthenium based dyes contain I^-/I_3^- redox couple (Bandara et al., 2014a). The iodide ion conductivity is a key factor that determines the J_{SC} and efficiency of a DSSC (Bandara et al., 2014a). The iodide ion participates in the I^-/I_3^- reaction that provides an efficient charge transfer at the interfaces enabling current flow in the external circuit (Bandara et al., 2010b; Bandara et al., 2013). During the working of the solar cell, the I^- and I_3^- ions diffuse between the photoanode and counter electrode (Bandara et al., 2010b; Jayaweera et al., 2015). The I^- ions migrate from the Pt counter electrode to the photoanode and the I_3^- diffuse from the photoanode to the counter electrode (Dissanayake et al., 2014).

Ionic liquid

Ionic liquid is a salt comprising ions in the liquid state at room temperature (Bicak, 2005). Prior to the presence of polymer electrolytes, ionic liquid is often used in devices as the electrolyte. High value of energy conversion efficiency has been numerously reported by using liquid electrolyte based DSSCs such as ionic liquid (IL) *5*-mercapto-*1*-methyltetrazole *1*-methyl-*3*-propylimidazolium salt PMIT with di-*5*-(*1*-methyltetrazole) disulfide as the organic redox couple (Wu et al., 2013). Moreover, the highest power conversion efficiency, over 12%, has also been achieved for DSSCs with a volatile organic liquid electrolyte (Yella et al., 2011).

However, fabrication of devices using liquid electrolytes is difficult since it is volatile and may lead to a leakage (Huo et al., 2008; Shi et al., 2009) especially during the long-term out-doors operation (Jin et al., 2012). These problems will lead to electrode corrosion and photodecomposition of the dye in the solvent medium (Bandara et al., 2013; Dissanayake et al., 2014), thus leading to sealing and stability problem (Bandara et al., 2014a; Li et al., 2005).

Solid polymer electrolytes

Polymer electrolyte has received much attention since Wright and coworkers discovered ionic conduction in the seventies (Morni & Arof, 1999). This has led to the development of energy devices such as sensors, fuel cells, rechargeable batteries, super capacitor and photoelectrochemical cells (Göktepe et al., 2008; Rocco et al., 2002). Polymer has been used as the polymer host as because of their advantages such as chemically inert towards electrodes and their mechanical and geometrical flexibility (Bandara et al., 2010b).

Solid polymer electrolyte (SPE) was used in order to overcome problems stemming from the ionic liquid. SPE is said to be excellent compared to liquid electrolyte in terms of stability. Utility of solid polymer electrolytes in power sources is due to its advantages such as wide operating temperature range, high energy density, solvent-free condition, minimize the leakage problem, wide electrochemical stability windows, easy process ability (desirable shape mould ability and flexibility of design) and light weight (Pradhan et al., 2008; Silva et al., 2002).

However, the greatest problem of SPE is the low ionic conductivity due to resistive losses both in the bulk and at the interfaces (Bandara et al., 2014a), thus decrease the energy conversion efficiency. Besides, solid electrolytes in DSSC are poor pore-filling, due to the difficulty for the penetration of the solid material into the pores of the dye-coated, nanocrystalline semiconductor particles. This leads to problems of dye regeneration and, consequently enhancing the recombination and lowering the efficiency (Jayaweera et al., 2015).

Gel polymer electrolytes

Researchers have tried to replace liquid and SPEs with gel polymer electrolyte (GPE) (Huo et al., 2008; Shi et al., 2009). The GPE yields several advantages including high energy density, structural stability and low volatility (Nicotera et al., 2006) thus minimizing the problems associated with electrolyte leakage, sealing and electrode corrosion. The conductivity of GPEs is usually higher compared to that of SPEs and can be improved to be almost comparable to that of liquid electrolyte (Saito et al., 2000).

According to Nicotera et al. (2006), a gel-type membrane is achieved by immobilizing an ionic liquid solution into a polymeric matrix. Leakage can be avoided (Bandara et al., 2014a). The solvent entrapped in the polymer matrix improves the electrolytes conductivity and the contacts between interfaces (Saito et al., 2000; Shi et al., 2009). The advantage expected by replacing liquid electrolytes by gel electrolytes is obviously the difficulty to attain with electrolytes containing such volatile solvents (Bandara et al., 2014a).

Hence, a few organic molecules with low molar mass and high dielectric constant has been introduced to balance the loss of ionic conductivity with a liquid-like environment by providing channels for ion transport within the polymer matrix (Bar et al., 2014). Some of the examples that have been frequently applied are ethylene carbonate (EC) (Muchakayala et al., 2017), propylene carbonate (PC) (Richardson et al., 2016), vinylene carbonate (VC) (Petibon et al., 2015), dimethyl carbonate (DMC) (Mustafa et al., 2012), diethyl carbonate (DEC), ethyl methyl carbonate (EMC) (Pradeepa & Prabhu, 2015) and γ-butyrrolactone (Matsuda et al., 2003). Most of the cases, combination of plasticizers propylene carbonate (PC) and ethylene carbonate (EC) solutions were employed to dissolve the salt (Aziz et al., 2014; Hassan et al., 2014; Noor et al., 2011). The degree of salt dissociation in the electrolyte can be improved by adding plasticizers. Plasticizers will also reduce viscosity and form channel-like pathways for ion-transfer (Li

et al., 2005). Addition of plasticizers also favours the segmental motion of polymer chains above the glass transition temperature, T_g. This enables ionic mobility enhancement and improves salt solvation (Bandara et al., 2009).

GPE research commonly involve synthetic polymers such as polyacrylonitrile (PAN) (Bandara et al., 2013; Dissanayake et al., 2012; Hassan et al., 2014), polyvinyl alcohol (PVA) (Aziz et al., 2014), polyvinylidene fluoride (PVdF) (Arof et al., 2014a) and polymethyl methacrylate (PMMA) (Dissanayake et al., 2014). These polymers have been used as the host matrix for ionic conduction. Biopolymers such as agarose (Singh et al., 2013; Singh et al., 2016), cellulose derivatives (Bella et al., 2013; Salvador et al., 2014), carrageenan derivatives (Rudhziah et al., 2015) and chitosan (Buraidah et al., 2010) have also received attention due to its availability, biocompatibility and biodegradability. The performances of biopolymer electrolytes in DSSC in recent literature have been tabulated in Table 2.5.

Bulky cation

Cations play an important role in the performance of DSSCs in setting up of the Fermi level of the active electrode (Jayaweera et al., 2015). The cation/TiO_2 interactions cause two effects in a DSSC (Dissanayake et al., 2014) such as a positive shift of the flat band potential of the semiconductor. In addition, the interaction also creates deeper electron-trapping states, which is significant in electron transport through TiO_2 to the current collector. Cations can efficiently screen the photo-injected electrons on the TiO_2 film, ensuring that electro-neutrality is maintained throughout the TiO_2 network. Ionic migration is therefore strongly correlated with electron transport in the TiO_2 film.

Table 2.5: Comparison of performance parameters of some biopolymer electrolyte based DSSCs in recent literature.

Polymer electrolytes	J_{SC}/ **mA cm^{-2}**	V_{OC}/ **V**	***FF***	***η*/%**	**Ref.**
Agarose–H_2O–KI/I_2–N719	3.27	0.67	*0.24*	0.54	Singh et al. (2013)
Agarose–DMSO/GuSCN/PC/NMBI–AEII/I_2–N719	11.45	0.76	0.68	5.89	Hsu et al. (2013)
Starch–MPII–NaI/I_2–N719	4.78	0.57	0.77	2.09	Khanmirzaei et al. (2015)
CM-cellulose/PEO–CH_3CN/MPII–NaI/I_2 –TBP/N719	10.03	0.75	0.69	5.18	Bella et al. (2013)
micro-cellulose–H_3CN/EMISCN/ MPII–LiI/I_2–TBP/N719	8.39	0.59	0.67	3.33	Salvador et al. (2014)
CM-κ-carrageenan/CMC–AcOH–NH4I/I_2–N719	0.42	0.50	0.64	0.13	Rudhziah et al. (2015)
CM-κ-carrageenan–EC/AcOH–NaI/I_2–N719	7.60	0.51	0.53	2.06	Bella et al. (2015)
Chitosan–EC/BMII–NH_4I/I_2–anthocyanin	0.07	0.23	0.22	N/A	Buraidah et al. (2010)
PhCh/PEO–DMF/BMII–NH_4I/I_2–tartaric acid/anthocyanin	3.50	0.34	0.39	0.46	Buraidah et al. (2011)
PhCh–EC/PC–TPAI/LiI/I_2–N719	7.25	0.77	0.67	3.71	Yusuf et al. (2014)

Bulky cations generally enhance the iodide ion transport in the electrolyte (Dissanayake et al., 2014). The relatively immobile bulky cations enhance the mobility of iodide and triiodide ions within the quasi-solid, thus enhancing the solar cell performance (Jayaweera et al., 2015). Apart from immobilization of the cation, bulky cations are expected to have higher degree of salt solvation due to reduction of lattice energy of the salt. Lower lattice energy is expected for TPAI ion with the ionic radius of 4.60 Å (Bandara et al., 2009).

PAN based DSSC with TPAI showed the best performance among the six quaternary ammonium iodide salt from the series: ammonium iodide (AI), tetraethylammonium iodide (TEAI), tetrapropylammonium iodide (TPAI), tetrabutylammonium iodide (TBAI), tetrapentylammonium iodide (TNAI) and

tetrahexylammonium iodide (THAI) (Bandara et al., 2013). From Figure 2.15, efficiency is observed to increase from AI to TPAI as the J_{SC} value increases due to the increment of iodide ions conductivity. However, as the cation size increases from TPAI to THAI, the downward shift of the TiO_2 conduction band get smaller, then lower the driving force for electron injection from LUMO of dye to the CB of TiO_2 caused decreasing in efficiency. In this case, we have introduced bulky salt tetrapropylammonium iodide (TPAI) into the gel polymer electrolytes.

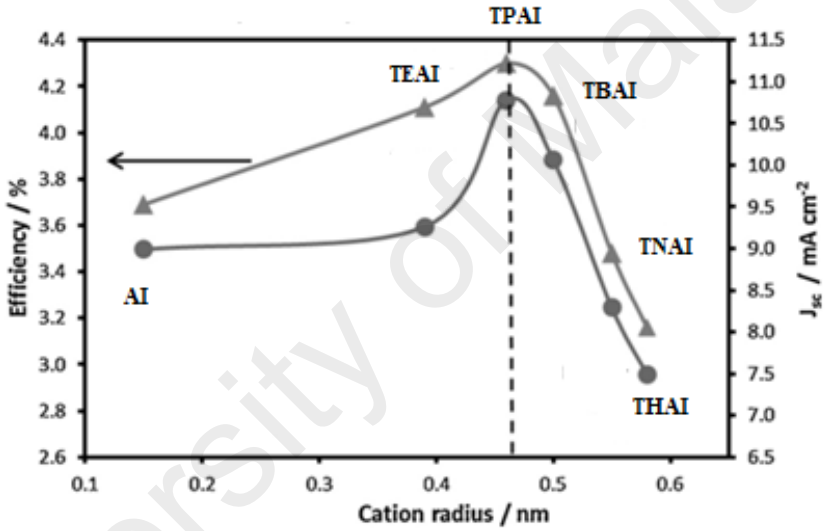

Figure 2.15: Relationship between efficiency and J_{SC} with cation radius of six quaternary ammonium iodide in PAN based gel polymer electrolytes (Bandara et al., 2013).

CHAPTER 3 : RESEARCH METHODOLOGY

3.1. Chemicals

Table 3.1 contains the list of chemicals and the corresponding suppliers used throughout this work. The chemicals have been used as received without further purification.

Table 3.1: List of materials used throughout this work

Chemical / material	**Details**
Chitosan	Aldrich, 75% deacetylation, viscosity: 800-2000 cps
Phthalic Anhydride	AC Chemical Co. Ltd.
Ethanol	Sigma-Aldrich, 95.0%
N,N-dimethylformamide	Merck Sdn Bhd, 99.8%
Ethylene carbonate	Merck Sdn Bhd
Propylene carbonate	Merck Sdn Bhd
Tetrapropylammonium iodide	Friendemann Schmidt Chemicals
Lithium Iodide	Friendemann Schmidt Chemicals

3.2. Synthesis of N-phthaloylchitosan

The method of synthesis was obtained from Nishimura et al. (1991). 1 g of chitosan and 4.39 g of phthalic anhydride was dissolved in DMF between 100 ^{o}C and 120 ^{o}C under nitrogen atmosphere for 6 h. Temperature of the mixture was then lowered to 60 °C and left overnight. The clear yellowish solution was put into ice water to precipitate out the product. The precipitate was collected and washed with distilled ethanol in a soxhlet extractor for 8 h. The product was vacuum dried. Photographs of selected steps in preparation of PhCh are shown in Appendix A.

3.3. Preparation of Gel Polymer Electrolytes

As we mentioned previously, solubility of chitosan is improved by modification with phthalic anhydride to produce PhCh. DMF was chosen as the solvent to prepare the

GPE as it has been involved in the synthesis of phthaloylchitosan. Although ionic compounds could not dissolve in most non-polar solvents, they can be soluble in aprotic polar solvents such as DMF, DMAc and DMSO. DMF (Figure 3.1) is an aprotic solvent and do not form ion-dipole interaction. The surface of aprotic polar solvent molecules have a partial negative charge that enables them to solvate cations (Bruice, 2004). Thus, DMF has been used in the preparation of the GPE.

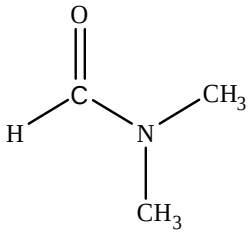

Figure 3.1: Chemical structure of DMF

Besides DMF, another plasticizer is needed in order to prepare a good gel polymer electrolyte as shown in Figure 3.2. Combination of EC-PC has always been chosen as the plasticizers (Aziz et al., 2014; Hassan et al., 2014; Noor et al., 2011). However, in this study, combination of DMF-EC has been chosen as EC showed higher dielectric constant compared to PC.

Figure 3.2: Photograph of the PhCh based gel polymer electrolytes.

3.3.1. Gel polymer electrolytes with single salt

Fixed amounts of 0.3 g of EC and 0.3 g of DMF from Merck Sdn Bhd were stirred well in a closed glass container with the appropriate weights of TPAI as shown in Table 3.2. 0.1 g of PhCh was then added into each salt solution. The mixture was heated to 60 ^{o}C and stirred until the mixture becomes a homogeneous gel. Then, the heater was stopped and the solution was allowed to cool to room temperature. Iodine (10 wt.% of salt) was then added to the GPE and stirred until the solution becomes homogeneous.

Table 3.2: Composition of electrolytes with various mass of TPAI

Designations	PhCh/ g	EC/ g	DMF/ g	TPAI/ g	Wt.%
A0	0.1000	0.3000	0.3000	0.0000	0.0000
A1	0.1000	0.3000	0.3000	0.0200	2.7800
A2	0.1000	0.3000	0.3000	0.0400	5.4100
A3	0.1000	0.3000	0.3000	0.0600	7.8900
A4	0.1000	0.3000	0.3000	0.0800	10.2600
A5	0.1000	0.3000	0.3000	0.1000	12.5000
A6	0.1000	0.3000	0.3000	0.1200	14.6300
A7	0.1000	0.3000	0.3000	0.1400	16.6700

3.3.2. Gel polymer electrolytes with double salt

To the most conducting gel polymer electrolyte, *A6* (also designated as *B0* in this system), lithium iodide, LiI, was added in such a way that the total weight of the iodide salts remained the same (0.12 g) in all the electrolytes. The salt compositions used in the electrolytes are shown in Table 3.3.

Table 3.3: Composition of electrolytes with various ratio of TPAI:LiI

Designation	PhCh/ g	EC/ g	DMF/ g	Mass/ g		Wt.%	
				TPAI	LiI	TPAI	LiI
B0	0.1000	0.3000	0.3000	0.1200	0.0000	14.6300	0.0000
B1	0.1000	0.3000	0.3000	0.1000	0.0200	12.2000	2.4400
B2	0.1000	0.3000	0.3000	0.0800	0.0400	9.7600	4.8800
B3	0.1000	0.3000	0.3000	0.0600	0.0600	7.3200	7.3200
B4	0.1000	0.3000	0.3000	0.0400	0.0800	4.8800	9.7600
B5	0.1000	0.3000	0.3000	0.0200	0.1000	2.4400	12.2000
B6	0.1000	0.3000	0.3000	0.0000	0.1200	0.0000	14.6300

3.3.3. Gel polymer electrolytes with addition of ionic liquid

Various weight percentages of *1*-butyl-*3*-methylimidazolium iodide (BMII) from 1 to 5 wt.% (as shown in Table 3.4) were introduced into the most efficient PhCh-EC-DMF-TPAI-LiI gel polymer electrolyte in DSSC, B3 (also designated as C0 in this system). The mass of the BMII, *x* was measured according to the Equation 3.1:

$$wt.\%\ of\ BMII = \frac{x}{x + mass\ of\ (PhCh + EC + DMF + TPAI + LiI)} \times 100\% \quad (3.1)$$

Table 3.4: Composition of electrolytes with various wt.% of BMII

Designation	PhCh/ g	EC/ g	DMF/ g	TPAI/ g	LiI/ g	BMII	
						Mass/ g	wt.%
C0	0.1000	0.3000	0.3000	0.0600	0.0600	0.0000	0.0000
C1	0.1000	0.3000	0.3000	0.0600	0.0600	0.0100	1.0000
C2	0.1000	0.3000	0.3000	0.0600	0.0600	0.0300	3.0000
C3	0.1000	0.3000	0.3000	0.0600	0.0600	0.0500	5.0000

3.4. Characterisations of Gel Polymer Electrolytes

GPEs that have been prepared will undergo characterisations such as solubility, ^{1}H NMR, FTIR, XRD and EIS.

3.5. Solubility

Solubility test was carried out to find the suitable organic solvent for film forming. 0.05 g of PhCh was put into the test tubes and tested for its solubility in various solvents at room temperature. For comparison, solubility of chitosan in the various solvents was also carried out. The solubility was observed visually.

3.6. Fourier Transformed Infra Red (FTIR)

When an electromagnetic wave passes through a material and its frequency exactly matches the frequency of vibrations of a component group in the material, the component that consists of certain molecules will absorb energy and the rest of the wave is transmitted. By determining experimentally the absorbed wavenumbers by the component group of the material, the kind of functional group can be known as each stretching and bending vibration of the bond in the functional group has a characteristic frequency. FTIR spectrometer has the advantage that it measures all frequencies simultaneously.

Attenuated Total Reflectance-Fourier Transformed Infrared (ATR-FTIR) spectra were recorded with a Spotlight 400 spectrometer (Perkin Elmer, UK). The acquisition parameters were done with a total of 32 accumulations at 4 cm^{-1} resolution with a spectral range from 650–4000 cm^{-1}. The deconvolution analysis with multiple peak fitting was done using Origin Pro 9.1 software with second–order derivatives to determine the hidden peaks. A Gaussian model was used in which maximum error associated with the simulated fits was within ±1%.

3.7. Proton Nuclear Magnetic Resonance (^{1}H NMR)

NMR spectroscopy is another technique to determine a structure of a material. It can identify the carbon-hydrogen framework of e.g. an organic compound and the functionality at a specific carbon and its neighbouring carbons.

Proton nuclear magnetic resonance was taken at 399.65 MHz with JNM–GSX270 spectrometer (JEOL, Japan). DMSO-d_6 is used as the solvent with sample concentration of about 20% w/v.

3.8. X-ray Diffraction (XRD)

X-ray diffraction is a phenomenon when atomic planes of a crystal cause on incident beam of x-rays to interfere with one another as they leave the crystal. Diffraction effects are observed when electromagnetic radiation impinges on periodic structure with geometrical variations on the length scale of the wavelength of the radiation. XRD is a non-destructive analytical technique which is fast and require easy sample preparation. It assists in identification and quantitative determination of various crystalline phases and orientation. XRD also helps to study crystalline and non-crystalline materials by looking at how they diffract x-rays of a known wavelength. The XRD analysis was recorded at room temperature using an Empyrean diffractometer (PANalytical, Netherlands) at 2θ angles between 10º and 60º with a step size of 0.026º, using Cu/Kα_1 irradiation.

3.9. Electrical Impedance Spectroscopy (EIS)

EIS is useful for research and development of new materials and electrode structures, as well as for product verification and quality assurance in manufacturing operations. Impedance is a complex resistance to a current flowing through a circuit made of resistors (R), capacitors (C), inductors (L), or any combination of these, as function of the frequency of the ac source. Resistors represent conductive pathways for ion and

electron transfer. As such, they present the bulk resistance of a material to charge transport such as the resistance of the electrolyte to ion transport or the resistance of a conductor to electron transport. Resistors are also used to represent the resistance to the charge-transfer process at the electrode surface. Capacitors and inductors are associated with space-charge polarization regions, such as the electrochemical double layer, and adsorption/desorption processes at an electrode, respectively. The defining relation and impedance for ideal bulk electrical elements are shown in Table 3.5.

Table 3.5: Relation for ideal bulk electrical elements

	Defining Relation	**Impedance**
Resistor	$V = I \times R$	$Z_R = R$
Capacitor	$I = C\frac{dV}{dt}$	$Z_C = \frac{1}{j\omega C} = -\frac{j}{\omega C}$
Inductor	$V = L\frac{dI}{dt}$	$Z_L = j\omega L$

The impedance of the GPEs were determined using HIOKI 3531 Z HiTester in the frequency range between 50 Hz and 1 MHz. The samples were sandwiched between two stainless steel disc electrodes. The impedance data were presented in Nyquist plots, which showed the imaginary part, Z_i of impedance, against its real part of the cell, Z_r.

The ionic conductivity (σ) of the GPEs can be calculated by using the bulk resistance, R_B values and following Equation 3.2.

$$\sigma = \frac{t}{R_B \times A} \tag{3.2}$$

where t is the thickness of the electrolyte and A is the film-electrode contact area.

3.10. Dye-Sensitized Solar Cell

3.10.1. Preparation of dye solution

0.03 mol dm^{-3} dye solution was prepared by dissolving 10 mg of Ruthenizer 535 also known as N3 dye in 5 mL of ethanol. The solution was then stirred until it is homogenous. The chemical structure of the N3 dye is shown in Figure 3.3.

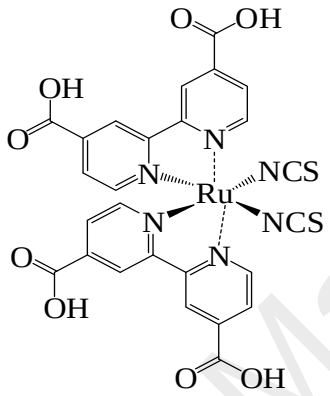

Figure 3.3: Chemical structure of N3 dye.

3.10.2. Preparation of electrodes

The Fluorine Tin Oxide (FTO) glasses (from *Solaronix* SA), that were used as the substrates, were rinsed with distilled water and ethanol before use.

The photo-anode with two layers of TiO_2 was made on a conducting glass substrate using the procedure reported by (Bandara et al. 2013). The paste required for the first dense layer was prepared by grinding 0.5 g of P90 TiO_2 powder for ~30 min with 2 mL of pH 1 nitric acid in a mortar. The resulting slurry was spin-coated on the FTO glass with a multi-speed program: first at 1000 rpm for 2 s and then at 2350 rpm for 60 s. After air drying for 30 min, it was sintered at 450 °C for 30 min.

For the second layer, the TiO_2 colloidal suspension was prepared by grinding 0.5 g of P25 TiO_2 powder with 2 mL of pH 1 HNO_3, 0.1 g of carbon wax and a few drops of Triton X-100 in the agate mortar. The TiO_2 colloidal suspension was spread on the FTO

glass by applying the doctor blade technique. The TiO_2 electrode was sintered in the furnace at 450 ^oC for 45 min (Figure 3.4). The TiO_2 electrode was cooled to 60 °C and dipped in ethanolic N3 dye solution for 24 h.

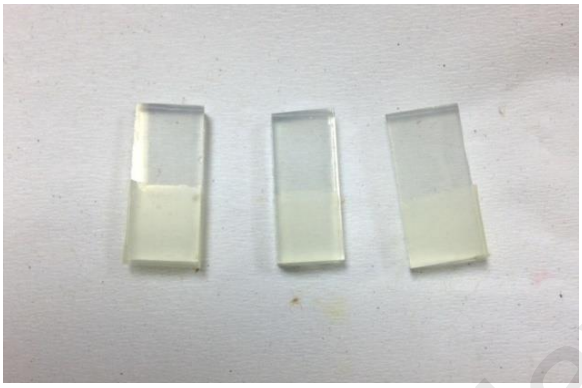

Figure 3.4: FTO glass after mesoporous layer of TiO_2 was deposited.

3.10.3. Fabrication and characterisation of DSSC

The prepared GPE was cast onto the sensitized TiO_2 photoelectrode and then a platinum coated electrode was pressed on top of the photoelectrode to form a DSSC with configuration glass/FTO/dye/TiO_2/electrolyte/Pt/FTO/glass as shown in Figure 3.5. The photovoltaic performance of DSSCs was investigated using AUTOLAB electrometer with active area of 0.196 cm^2. The cell was illuminated through the active photoelectrode, under a solar simulator (1.5 AM, 1000 W m^{-2}) as exhibited in Figure 3.6.

Figure 3.5: Fabricated DSSC with PhCh gel polymer electrolytes

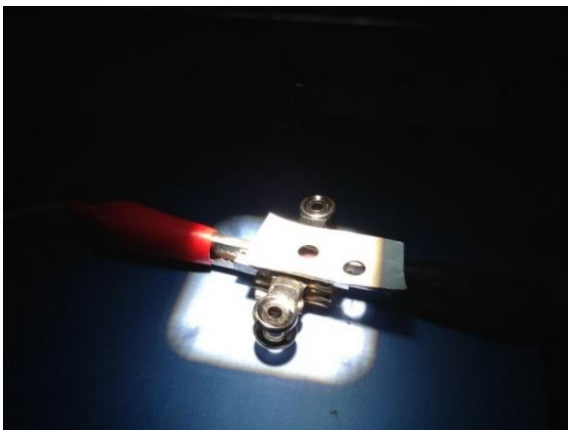

Figure 3.6: Solar cell under illumination of 100 mW lamp.

Results obtained from the measurement were presented in a photocurrent density-voltage curve as shown in Figure 3.7.

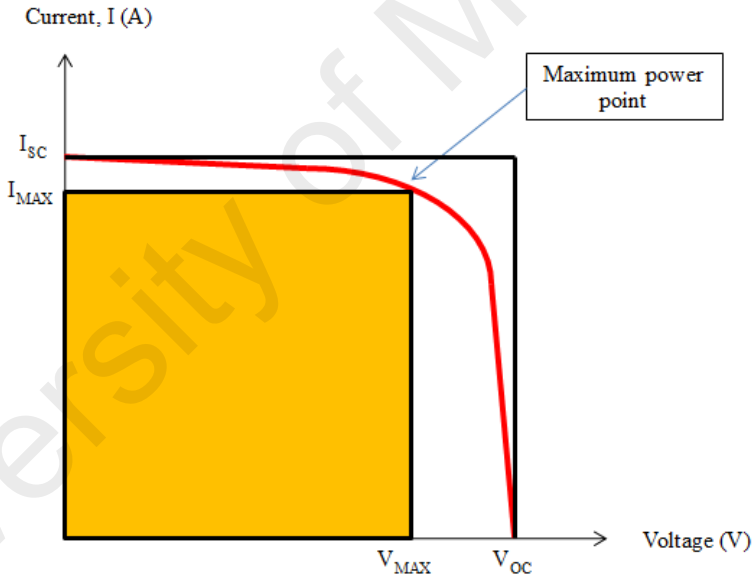

Figure 3.7: Current-voltage curves of DSSCs

The following equation is used in order to determine the overall conversion efficiency of the DSSC, η.

$$\eta = \frac{P_{out}}{P_{in}} \times 100 = \frac{I_{SC} \times V_{OC} \times FF}{P_{in}} \times 100 \qquad (3.3)$$

where P_{in} is the incident light power.

From the Equation 3.3, it can be seen that there are three important parameters in determining the efficiency of a DSSC. The first parameter short circuit current, I_{SC}, can be obtained from the *I-V* curve which is the value of current when the voltage equals to zero. The second parameter, open circuit voltage, V_{OC}, also can be obtained from the curve. V_{OC} is the value of voltage when current equal to zero.

Another parameter, fill factor (*FF*) is the ratio area of the inner rectangle to the outer rectangle (see Figure 3.7). The *FF* value can be calculated according to Equation 3.4. The inner rectangle is product of the maximum current density, I_{max} multiply by the maximum voltage, V_{max}. However, the outer rectangle is given by the $I_{SC} \times V_{OC}$. This quality measurement of the solar cell is described as the "squareness" of the I-V curve.

$$FF = \frac{I_{max} \times V_{max}}{I_{SC} \times V_{OC}} \tag{3.4}$$

CHAPTER 4 : RESULTS AND DISCUSSIONS

4.1. N-PHTHALOYLCHITOSAN OF CHITOSAN

4.1.1. FTIR analysis

In FTIR spectra the position, intensity, and shape of a characteristic transmittance band are helpful in identifying functional groups, thus the chemical structure of the compound. The FTIR spectrum of pure chitosan has been compared with the spectrum of the phthaloylated product, PhCh in Figure 4.1.

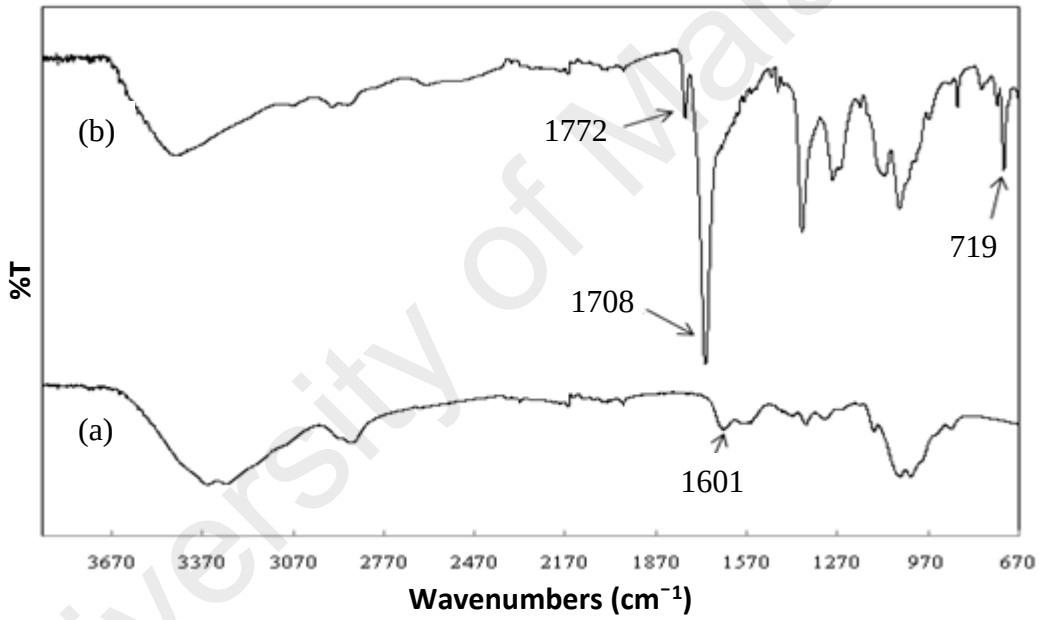

Figure 4.1: FTIR spectra of (a) chitosan, (b) phthaloylchitosan

The NH_2 band appearing around 1601 cm^{-1} in the pure chitosan spectrum (Figure 4.1(a)) has disappeared indicating that the NH_2 group has been stripped of its H atoms and phthaloylation has occurred onto the N atom of chitosan. The spectrum of pure phthaloylchitosan (Figure 4.1(b)) exhibits peaks corresponding to the carbonyl amide at 1772 and 1708 cm^{-1}. There is also a peak at 719 cm^{-1} indicating the presence of aromatic ring. These results verified the synthesis of N-phthaloylchitosan. Previous works have

reported that three main peaks appeared after phthaloylation took place onto the amino group of chitosan (Bian et al., 2009; Liu et al., 2004; Rout et al., 1993; Yoksan et al., 2001). Two of the peaks that belong to phthalimido group arise at 1711-1715 cm^{-1} and 1772-1777 cm^{-1}. The third band is dedicated to aromatic group which appeared at 721 cm^{-1} wavenumber. The details are presented in Table 4.1.

Table 4.1: Significant wavenumbers exhibited by N-phthaloylated chitosan

Vibrational mode	**Wavenumbers/ cm^{-1}**		**References**
	Current study	**Literature review**	
N-Phthalimido group	1772, 1708	1710, 1770	Nishimura et al. (1991)
		1712, 1777	Liu et al. (2004)
		1712, 1776	Kurita et al. (1998), Bian et al. (2009),
		1714, 1777	Rout et al. (1993),
		1714, 1776	Yoksan et al. (2001)
		1711, 1777	Jančiauskaitė & Makuška (2008)
		1713, 1779	Holappa et al. (2004)
		1713, 1777	Opanasopit et al. (2006)
		1713,1777	Peng & Zhang (2007)
O-phthaloylation		~2630	Rout et al. (1993)
		2928	Peng & Zhang (2007)
Amide I band		1655	Yoksan et al. (2001)
Hydroxyl group		3582	Yoksan et al. (2001)
		3600-3100	Holappa et al. (2004)
		3474	Opanasopit et al. (2006)
		3435	Peng & Zhang (2007)
Aromatic group	719	721	Liu et al. (2004), Bian et al. (2009), Rout et al. (1993), Yoksan et al. (2001), Jančiauskaitė & Makuška (2008), Kurita et al. (2003)
		722	Peng & Zhang (2007)
C-O pyranose		1150-950	Holappa et al. (2004)

Treatment of chitosan with phthalic anhydride generally results in partial O-phthaloylation in addition to the N-subtitution as shown in Figure 4.2. From the FTIR spectra in Figure 4.1(b), small extent of O-phthaloylation has also occurred in addition to N-phthaloylation as the peaks at 1240-1300 cm^{-1} were observed. Previous work by Kurita et al. (2001), showed the similar observation of O-phthaloylation.

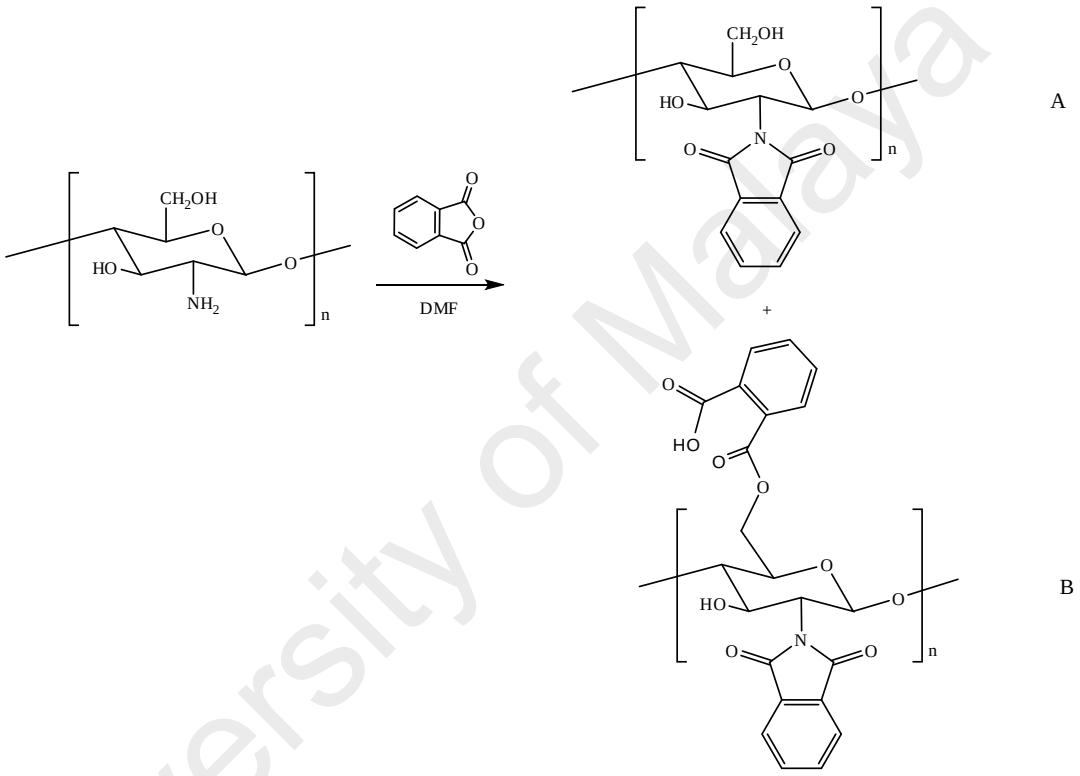

Figure 4.2: Structure of (A) N-phthaloylated chitosan and (B) O,N-phthaloylated chitosan.

Sometimes, O-phthaloyl group is an obstacle in most cases for quantitative and regioselective substitution (Kurita et al., 2001). However, in this study, since we used PhCh as the end product, small extent O-phthaloylation will not be a problem. Chemoselective of N-phthaloylation is possible by using mixture of DMF and hydroxyl-bearing co-solvent as the medium for refluxing. Although O-phthaloylation occurs in the

initial stage under these conditions, the ester linkage would be eventually cleaved by the water formed in the N-phthaloylation process (Kurita et al., 2007).

Co-solvents that have been studied by Kurita et al. (2001) include ethanol, ethylene glycol, *2*-methoxyethanol and water in order to control the N-phthaloylation. Of the four co-solvents examined, water proved to be the most appropriate, whereby the product was much lighter in color and furthermore, the degree of substitution was confirmed to be 1.0.

4.1.2. ^{1}H NMR Analysis

Confirmation of the structure of the synthesized PhCh via ^{1}H NMR is presented in Figure 4.2. ^{1}H NMR spectrum exhibits two distinct sets of signals. One set consists of peaks centering at 7.5, 7.7 and 7.9 ppm assigned to phthaloyl group. The signal peaks for the aromatic ring protons in PhCh occur in the 7.0 to 8.0 ppm region as other kinds of protons usually do not resonate in this region. Yoksan et al. (2001) also observed peak at 7.6 ppm belonging to protons of the phenyl rings for successful phthaloylation. Peaks that exist between 2.0 and 5.0 ppm are dedicated to the chitosan backbone hydrogen atoms. Small extent of O-phthaloylation has also occurred in addition to N-phthaloylation as peaks attributed to O-phthaloyl group appear at 7.3-7.5 ppm (Kurita et al., 2007; Torii et al., 2009). This is supported by the FTIR results where bands at region 1240 - 1300 cm^{-1} due to the O-phthalimido group were observed (Kurita et al., 2001). FTIR and ^{1}H NMR results imply that phthaloylation has occurred onto chitosan to produce N-phthaloylchitosan and to a lesser extent O,N-phthaloylchitosan.

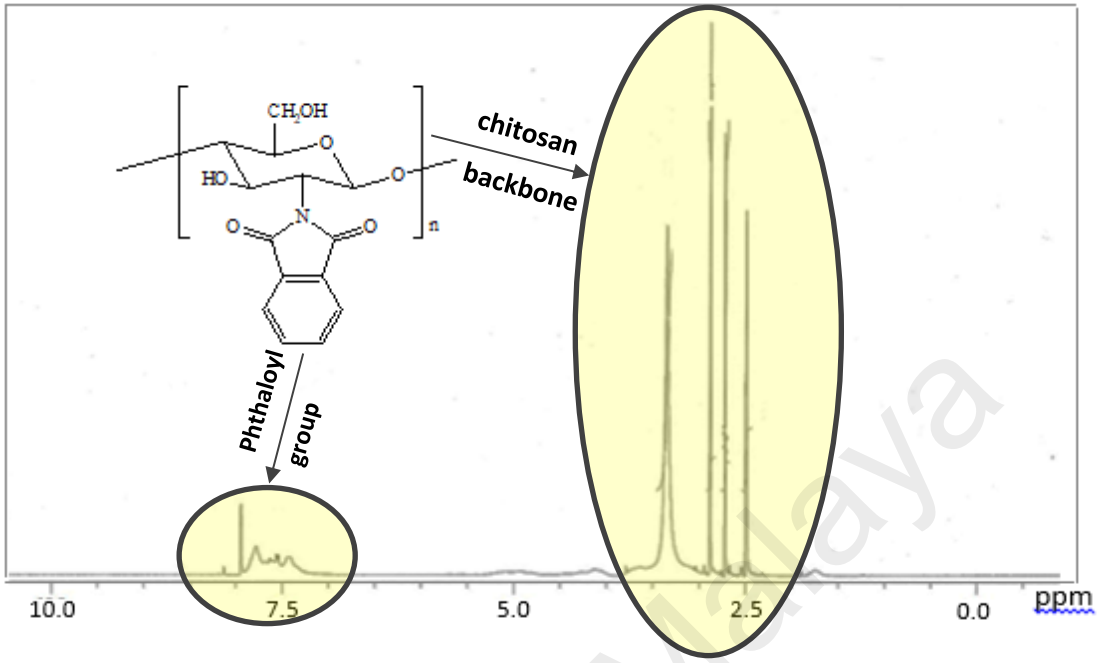

Figure 4.3: ^{1}H NMR spectra of phthaloylated chitosan

4.1.3. XRD Analysis

XRD patterns of pure chitosan and modified chitosan are shown in Figure 4.4. Two characteristic peaks of the pure chitosan can be observed at $2\theta = 15.1^{o}$ and $2\theta = 20.6^{o}$ due to the crystal form I and crystal form II, respectively (Aziz et al., 2012). Both of the peaks merged into a broad peak centred at $2\theta = 21.7^{o}$ after phthaloylation occur. This shows that PhCh is more amorphous than the pure chitosan since the phthalimido groups reduce the inter- and intramolecular H-bonds of the chitosan. Therefore, its crystallinity has been distrupted (Yoksan et al., 2001).

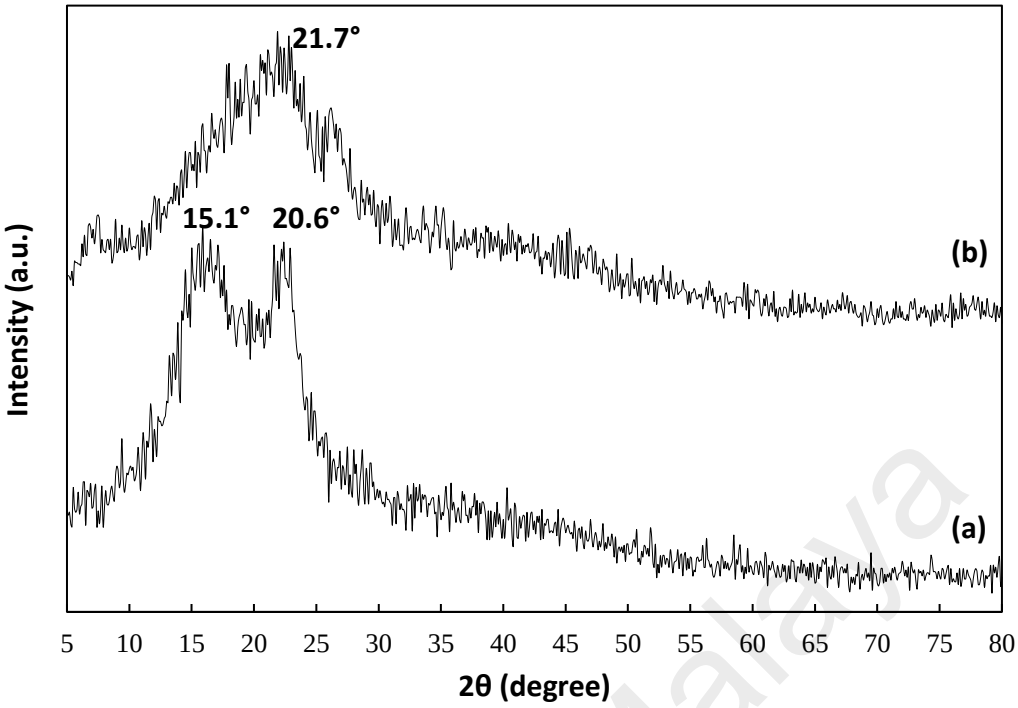

Figure 4.4: XRD pattern for (a) chitosan and (b) phthaloylated chitosan

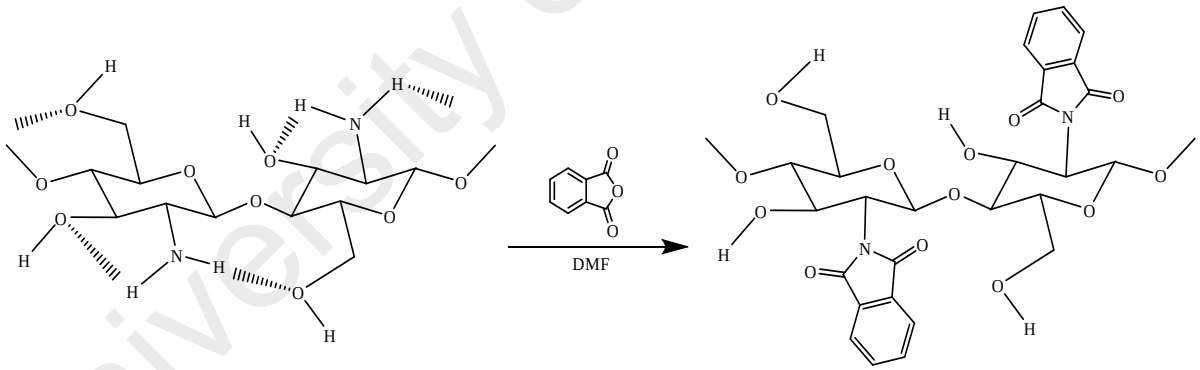

Figure 4.5: Disruption of hydrogen bonds after phthaloylation.

In addition, the heterogeneous structure of PhCh owing to the partial O-substitution also contributes to the amorphous nature. Kurita et al. (2001) had prepared N-phthaloylchitosan (without O-substitution) in DMF/water and obtained certain crystallinity as shown in Figure 4.6. Thus, PhCh with addition of O-phthaloylation is preferable as it fulfil the criteria of an electrolyte. Polymer electrolyte has to be in an

amorphous state as crystallinity prevents mobile species from migrating under AC signal due to the rigid polymer chains (Finkenstadt, 2005).

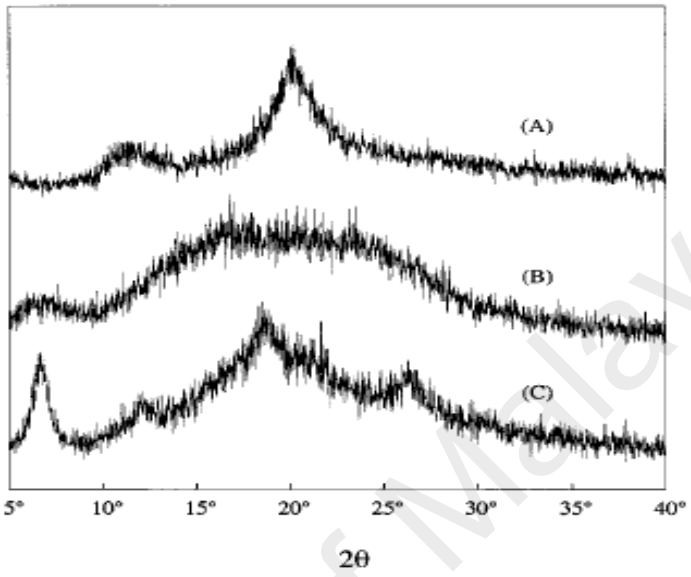

Figure 4.6: XRD analysis of (A) fully deacetylated chitosan, (B) PhCh prepared in DMF, and (C) PhCh prepared in DMF:water (95:5) (Kurita et al., 2001).

4.1.4. Solubility

An amorphous polymer contains a network of entangled, flexible chains in a continuous motion. In the presence of solvent, the polymer network will swell from the osmotic activity of the solvent and the segmental motion will finally increase. The polymer will continue to expand with excess of solvent and increase its freedom to move sufficiently to allow transitional movement to the chains thereafter the substances will separate out to form a solution. Further dilution will result in the intermolecular forces that exist between the polymers chains will become less and finally the solution properties will only exhibit polymer-solvent interaction forces.

In this work, solubility test was carried out using various solvents in order to compare the solubility of the product after chitosan has been phthaloylated. The three classes of solvents identified (Bruice, 2004) were;

I. *Polar aprotic solvents*: This type of solvent does not contribute to H-bond since no hydrogen attached to the -O- or to –N- group. Thus, in the absence of positively charged hydrogens, no formation of ion-dipole interactions will occur.

II. *Polar protic solvents*: On the other hand, protic solvents contribute to the H-bond. The δ^+ hydrogens points toward the negatively charged species.

III. *Non-polar solvents*. Non-polar solvent has low dielectric constant and are poor insulator.

Table 4.2 shows the solubility of PhCh in various solvents at room temperature. The results show that phthaloylated chitosan is soluble in most polar aprotic solvents. Complete dissolution was obtained in DMF, DMSO, DMAc and pyridine giving clear solutions compared to pure chitosan.

N,O-phthaloylchitosan was shown to be more soluble in organic solvents compared to N-phthaloylchitosan as it swells in DMF and pyridine (Kurita et al., 2007). The N-substituted derivative was soluble in some solvents such as dichloroacetic acid, *m*-cresol, N,N-dimethylacetamide/LiCl and methanol/$CaCl_2$•$2H_2O$ while N,O-substituted derivative showed much higher solubility because of the bulky structure and amorphous nature in contrast to the crystalline structure of N-phthaloyled chitosan (Kurita et al., 2001).

Clearly, acetamido or primary amino groups of chitosan have an important role in the formation of peculiar conformational features through intra/inter molecular hydrogen bonding. Therefore, removal of the two hydrogen atoms of amino groups of chitosan and

introduction of some hydrophobic nature by chemical modifications will cause destruction of its inherent crystalline structure, resulting in the improvement of solubility in general organic solvents (Nishimura et al., 1991). Evidence of the phthaloyl group being attached to the amino group is further shown due to it being insoluble in acetic acid, an acidic solvent. This solubility of phthaloylated chitosan may be partly attributable to the less crystallinity as confirmed by XRD results in *Section 4.1.3.1* (Kurita et al., 2001).

Table 4.2: Solubility of PhCh in various solvents

Solvents	Chitosan	PhCh
Polar solvents		
DMF	-	√
THF	-	-
DMAc	-	√
Pyridine	-	√
DMSO	-	√
Acetone	-	-
Ethyl Acetate	-	-
Acetic acid	√	-
Methanol	-	-
Cyclohexanone	-	-
Acetonitrile	-	-
Non-polar solvents		
Chloroform	-	-
Hexane	-	-
Toluene	-	-

√**:** soluble -: insoluble

4.2. GEL POLYMER ELECTROLYTE WITH SINGLE SALT

4.2.1. EIS Analysis

Various mass contents of TPAI have been introduced to the gel polymer electrolytes from 0.02 g to 0.14 g TPAI. The effects of the TPAI salts to the gel electrolytes can be observed in the Figure 4.7. The ionic conductivity values of the PhCh/EC/DMF/TPAI/I_2 system are tabulated in Table 4.3. The ionic conductivity value of 0.75×10^{-3} S cm^{-1} was obtained by GPE without TPAI (Table 4.3). The value was observed to increase as the mass of TPAI increased up to 5.46×10^{-3} S cm^{-1} with the addition of 0.12 g. This is due to the increment of the mobile ions number in the electrolyte (Yahya & Arof, 2002). As the salt dissociation increases with the increasing of salt content in the electrolyte, thus the amount of mobile ions also increases. Consequently, the conductivity increases. The conductivity is expected to be dominated by the mobility of I^- ions since TPA^+ ions are bigger compared to I^- ions, thus assumed to be entangled in the polymer matrix. However, the ionic conductivity value decreased to 5.07×10^{-3} S cm^{-1} after more than 0.12 g TPAI added. The reason is the formation of ion pair and/or ion aggregates interrupt the ions mobility thus lowering the ionic conductivity (Yusuf et al., 2014).

The variation of ionic conductivity value vs temperature in the range between 30º C and 100º C of the PhCh-EC-DMF-TPAI gel polymer electrolytes is shown in Figure 4.8. The Arrhenius model was employed based on the following equation:

$$log\ \sigma = log\sigma_o - \frac{0.4342\ E_a}{kT} \tag{4.1}$$

where σ_o is the pre-exponential factor, E_a, is the activation energy of ionic conduction, k is the Boltzmann constant and T is temperature in Kelvin. The ionic conductivity variation

with temperature for the GPEs follows the Arrhenius law since all of the points from the experimental results fit to a straight line, with $R^2 > 0.95$ for each sample. This suggests that the conductivity is thermally activated.

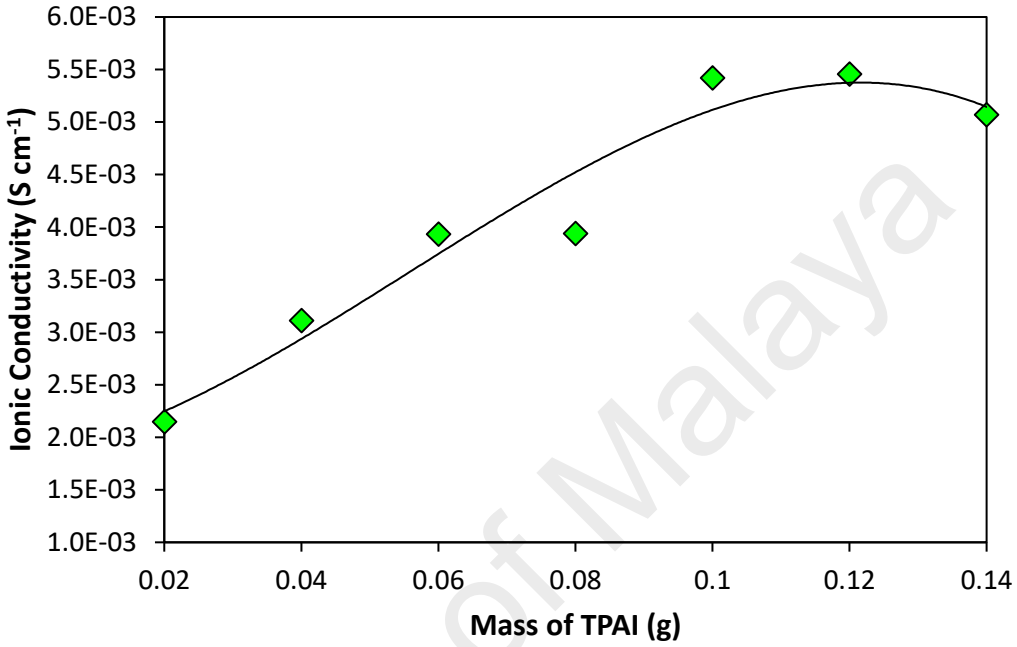

Figure 4.7: Effects of TPAI on the ionic conductivity of PhCh-EC-DMF based gel polymer electrolyte.

Table 4.3: Ionic conductivity value of gel polymer electrolytes with various content of TPAI at room temperature

Designations	**TPAI/ g**	**Conductivity × 10^{-3}/ S cm^{-1}**	**E_a/ eV**
A0	0.00	0.75	0.137
A1	0.02	2.15	0.122
A2	0.04	3.11	0.119
A3	0.06	3.93	0.115
A4	0.08	3.94	0.128
A5	0.10	5.42	0.132
A6	0.12	5.46	0.107
A7	0.14	5.07	0.121

Even though the lowest E_a values were shown by the most conducting GPE sample (A6), the E_a values can be considered to be negligible since the E_a values for rest of the GPEs showed not much difference (see Table 4.3). Other researchers have been reported the similar observations and explanations using PVA and PAN systems (Aziz et al., 2014; Dissanayake et al., 2012). In SPE case, the E_a is dependent on salt concentration (Majid & Arof, 2005). The ion transport with an energy barrier equals to E_a, has been suggested to be thermally activated hopping from an occupied site to a vacant site.

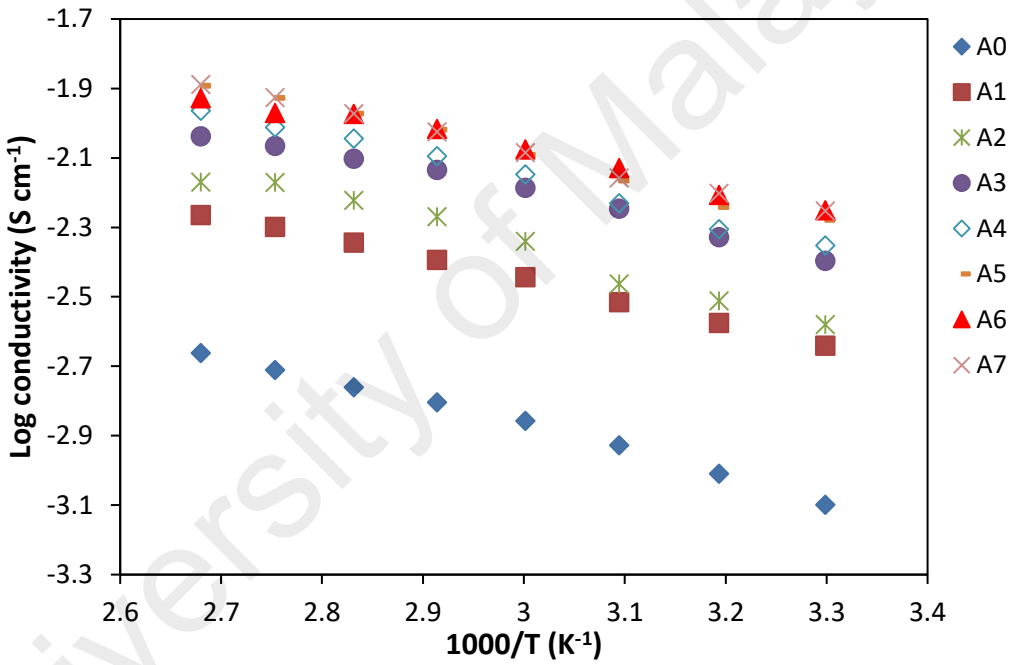

Figure 4.8: Temperature dependence of the ionic conductivity of the PhCh-EC-DMF-TPAI gel polymer electrolytes.

However, that is not the same with organic liquid electrolytes where the E_a does not depend on the salt concentration especially at moderate and low salt contents, or the type of salt used. The E_a value is suggested to be depended only on the type of solvent heteroatom used which influences the dipole re-orientation (Arof et al., 2014a; Bandara et al., 2013). Therefore since the environment of the gel electrolytes is where the PhCh matrix entrapped the ionic salt dissolved in an organic polar co-solvent EC/DMF, GPE is

suggested to behave more to liquid-like behaviour. This explains the similar range of E_a value seen in Table 4.3.

4.2.2. FTIR Analysis

In previous *Section* 4.1.1, FTIR studies have verified the chemical structure of PhCh, indicating that phthaloylation has been successfully occurred onto the chitosan. However, besides polymer host PhCh, the GPEs are also composed of a large portion of the EC and DMF plasticizers. Therefore, detailed analyses on these two materials are necessary.

FTIR spectra of the EC and DMF in the wavenumber range between 600 and 4000 cm^{-1} was shown in Figure 4.9. At 1770 and 1796 cm^{-1}, the strong doublet peaks due to C=O stretching are observed in the EC spectrum (Figure 4.9(a)). The presence of the peak at 1796 cm^{-1} which is assigned to the ring breathing mode can also overlap the overtone from the peak at 889 cm^{-1} (Ikezawa & Nishi, 2008). Peaks due to the scissoring and wagging vibrations of CH_2 and stretching vibration of C–O appeared at 1067, 1155, 1390 and 1481 cm^{-1}, respectively.

In the DMF spectrum, a strong peak attributed to the C=O stretching was present at 1656 cm^{-1} (Jacob & Arof, 2000). Three intense peaks are assigned to O–C–N, CH_3 rocking mode and N–C–H bending modes observed at 657, 1089 and 1385 cm^{-1}, respectively. A peak seen at 865 is attributed to the C–N symmetric mode while peak at 1256 cm^{-1} is attributed to asymmetric stretching mode of the same functional group. The minor peaks observed at 1501 and 2928 cm^{-1} are assigned to N–H bending mode and CH_3 symmetric stretching mode, respectively. While DMF is not a strong hydrogen bonding donor, according to Zhang et al. (2011) the C=O is expected to be the main acceptors and the hydrogen atom coordinated to C=O can theoretically be considered as one possible

donor. Since both of the plasticizers, EC and DMF are aprotic solvents, they are not H-bond donors. Therefore, no ion–dipole interaction formation as no positively charged hydrogens are present (Bruice, 2004). The two plasticizers have only weak interactions where the autoprotolysis is extremely weak (Zhang et al., 2014).

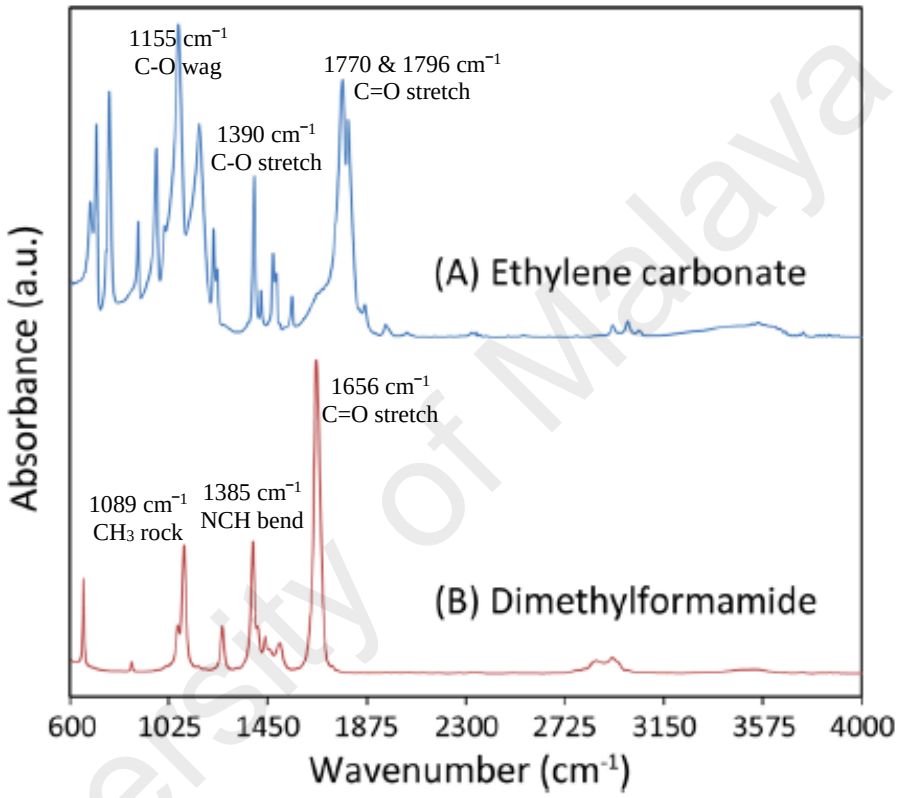

Figure 4.9: FTIR spectra of (A) ethylene carbonate and (B) dimethylformamide.

The FTIR spectrum of the PhCh based GPE with various contents of TPAI are shown in Figure 4.10. The changes in intensity, bandwidth and position from the FTIR spectral indicate that there is interaction behaviour of the components in the electrolytes (Huang et al., 2013). FTIR is one of the effective methods in order to determine the changes due to the cation–polymer binding sites and crystalline–amorphous domain ratios. Besides, FTIR also has been used to examine the extent of hydrogen bonding since

the polymer chains composed of heteroatoms undergo ion complexation through Lewis acid–base interactions forming the basis of an electrolyte medium.

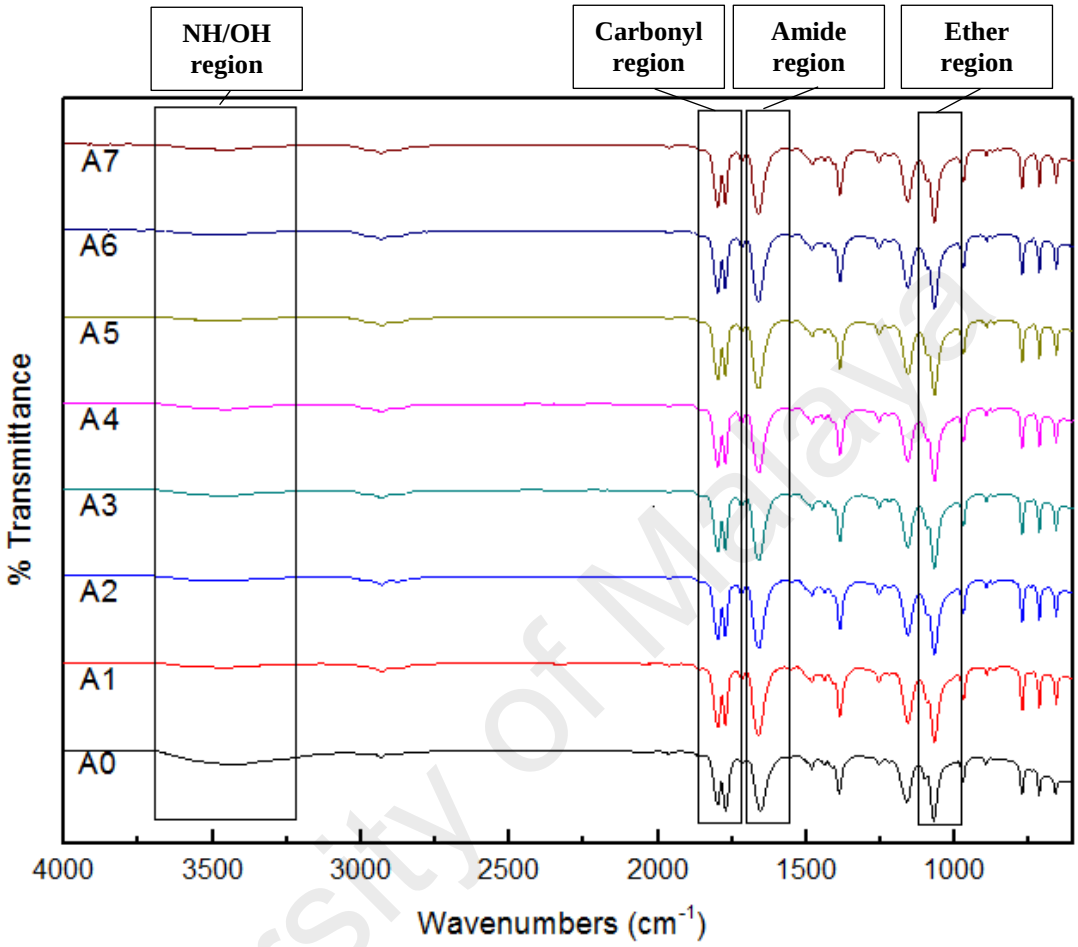

Figure 4.10: FTIR spectra of PhCh–EC–DMF–TPAI based gel polymer electrolytes.

The method of FTIR deconvolution of main peaks has proven itself to be useful as it can detect the hidden peaks of certain ionic species and polymer segments that contribute to the relationships of all the components in the electrolytes (Bar & Basak, 2014). In this work, there are four possible coordination environments that have been identified from the spectrum as depicted in Figure 4.11. There are (1) ether region; 1000–1200 cm^{-1}, (2) amide region; 1580–1700 cm^{-1}, (3) carbonyl region; 1700–1840 cm^{-1} and (4) amine/hydroxyl region; 3130–3700 cm^{-1}.

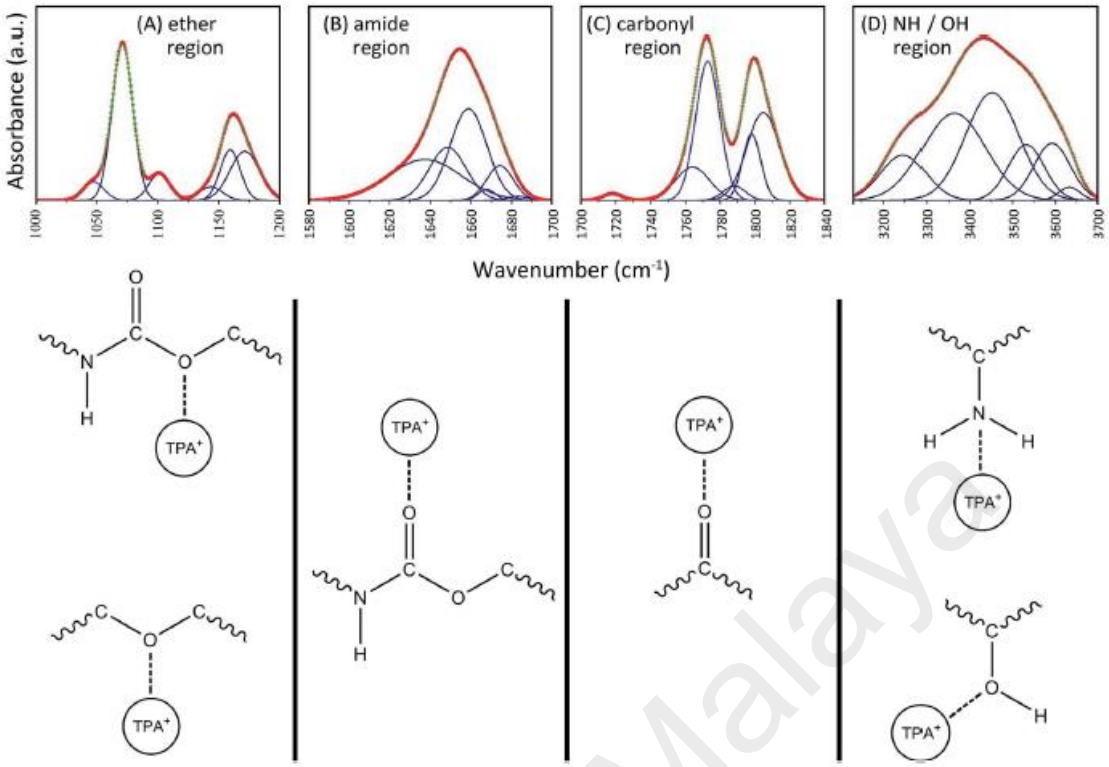

Figure 4.11: Deconvolution of individual FTIR regions: (A) ether (1000–1200 cm^{-1}); (B) amide (1580–1700 cm^{-1}); (C) carbonyl (1700–1840 cm^{-1}); and (D) amine/hydroxyl groups (3130–3700 cm^{-1}).

FTIR spectra of ether group in the range from 1000 to 1200 cm^{-1}.

Deconvolution of the ether (C–O–C) region (Figure 4.11(A)) has been done at the wavenumber range between 1000 and 1200 cm^{-1} (Appendix D1). Seven peaks were resolved from this region and the percentage area for each contributing peak was shown in the histogram in Figure 4.12. The interaction of the C–O–C group of PhCh and/or EC with the salts can be observed from the changes of the peak intensity. The peak due to the hydrogen bonded C–O–C stretching from PhCh appeared at 1047 cm^{-1}. The CH_3 rocking mode from the combination of EC and DMF is dominant at 1069 cm^{-1}. The peak arise at 1079 cm^{-1} is assigned to the coordination of TPA^+ cations with C–O–C sites since this peak was absent in the GPE without TPAI. The presence of the crystalline complexes can be observed from the peak centred at 1094 cm^{-1}. However, the peak due to the free C–O–C stretching mode which most likely took place in the amorphous region can be observed

at 1143 cm^{-1} (Bar & Basak, 2014). The intensity of the peak at 1156 cm^{-1} was higher for the gel electrolytes with TPAI content whereas the opposite effects was true at 1171 cm^{-1}. It can be seen from the histogram that after TPAI was introduced to the gel electrolytes, the changes in all the peak intensity were negligible. This suggests that the complexation between polymer and/or plasticizer with TPAI in these regions does not depend on the salt concentration.

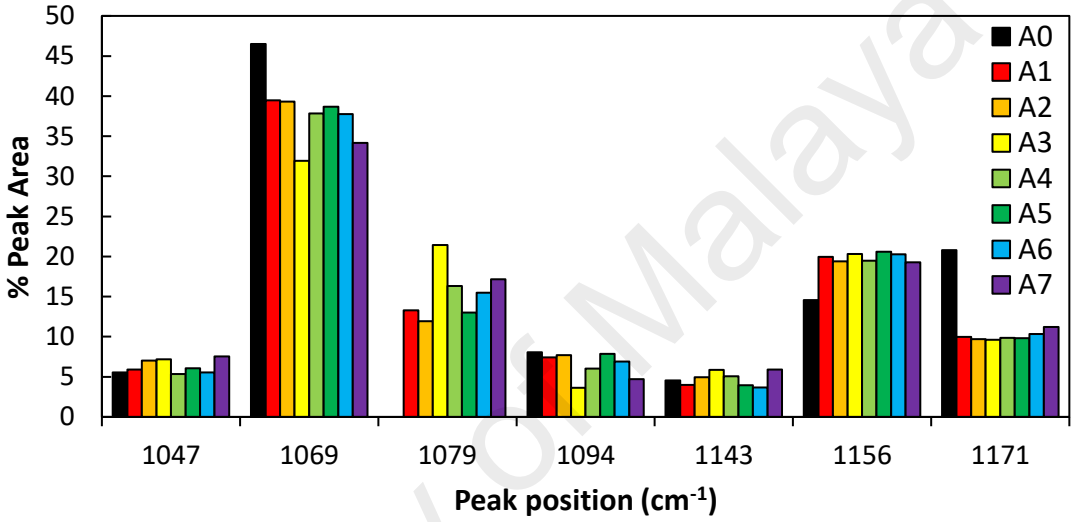

Figure 4.12: Relative FTIR band percentage area in the range of 1000 to 1200 cm^{-1}.

FTIR spectra of amide/carbonyl group in the range from 1580 to 1840 cm^{-1}.

The absorption of the carbonyl functional group is highly sensitive to the interaction behavior such as H-bonding. There are two types of C=O absorption which are; the free uncoordinated carbonyl and the bonded carbonyl where the other proton donating groups (e.g. O–H and N–H) interacts with the electron rich group. The H-bonded carbonyl absorption normally arises at a relatively lower wavenumber compared to that of the free carbonyl. This is because as the interaction occurred at the C=O group, the electron density will be reduced, hence it will decrease the vibrational energy and the

peak shifts its position. Besides H^+, the same observations was reported by Huang et al. (2013) for absorption formation of Li^+ ions bonded to carbonyl group.

The deconvolution of carbonyl (C=O) group absorption is divided into two parts which are; region I (1580-1700 cm^{-1}) and region II (1700-1840 cm^{-1}) (Appendix D2). Region I corresponds to the deconvolution specific to the amide group, $R(C=O)NR_2$, region in between wavenumber 1580 and 1700 cm^{-1} (Figure 4.11(B)). The histogram in Figure 4.13 presents the percentage area of each of the deconvoluted peak. The first peak in the amide region arises at wavenumber 1637 cm^{-1}. After addition of salt, the peak intensity takes a plunge but generally increases with varying salt content.

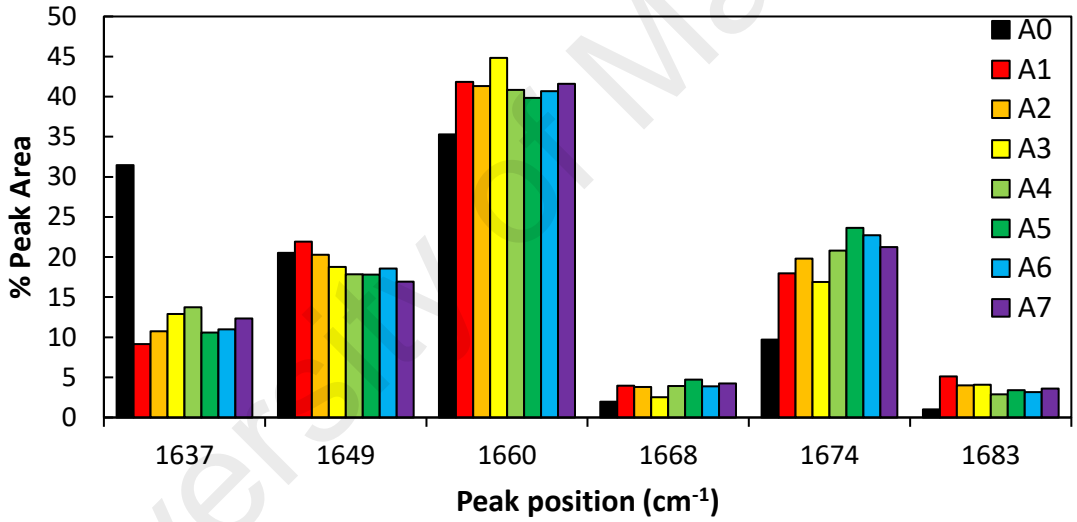

Figure 4.13: Relative FTIR band percentage area in the range of 1580 to 1700 cm^{-1}.

However, the intensity of the peak due to the ordered or disordered interfacial domains in the polymer structure at 1649 cm^{-1} (Bar & Basak, 2014), decreases as salt content increases. Similar pattern can be seen for these two peaks with electrolytes containing single or double salts. The peak at 1660 cm^{-1}, which is the highest peak intensity, is attributed to the carboxamide group from the chitosan. The peak attributed to the amide peak belonging to DMF appears at 1674 cm^{-1}. The intensity of these peaks

mostly increases as the salt content increase especially for the peak at 1674 cm^{-1}. This is due to the better mobility of DMF that provides great access to coordination sites of the C=O region.

Deconvolution on region II was done to the FTIR spectrum of the GPE in a range between 1700 and 1840 cm^{-1} as shown in Figure 4.11(C). This region corresponds to the second part of the carbonyl (C=O) group. Figure 4.14 presents the relative percentage areas of the each of the six deconvoluted peaks. The peaks in this region II are seen to be less sensitive compared to the C=O group peaks in region I. The intensities of the peaks generally show insignificant difference with the variation of TPAI content. However, the intensity of all peaks increase when compared to the blank GPE (A0).

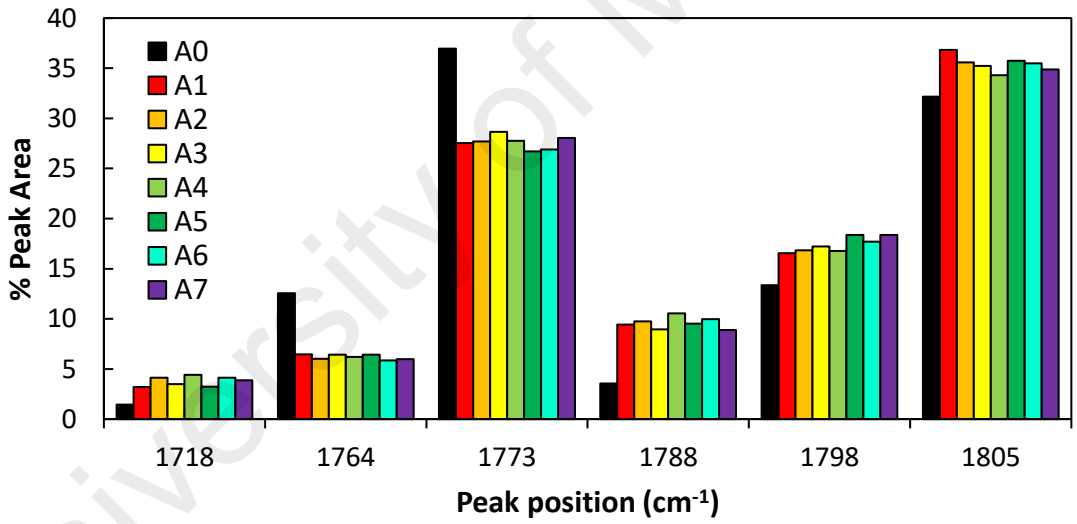

Figure 4.14: Relative FTIR band percentage area in the range of 1700 to 1840 cm^{-1}.

The peak intensities for all A1 until A7 gel polymer electrolytes at 1764 and 1773 cm^{-1} decreases with increasing of TPAI content. The peak which was originally due to a characteristic feature of the pure PhCh at 1708 cm^{-1} has shifted to 1718 cm^{-1} suggesting a strong interaction between polymer host PhCh and the TPAI salt. The peaks dedicating to the carbonyl group of EC can be seen at 1773 and 1805 cm^{-1} (Osman & Arof, 2003).

A strong peak present at 1798 cm^{-1} was attributed to the EC is observed to increase as the TPAI content increase. Since the C=O stretching vibration mode is strongly affected by interactions with other molecules, thus it is evident that there may be interaction occurred between EC and TPAI salt (Ikezawa & Nishi, 2008).

FTIR spectra of amine/hydroxyl group in the range from 3130 to 3700 cm^{-1}.

Figure 4.15 depicts the deconvolution plot in the 3130 and 3700 cm^{-1} region (Appendix D3) corresponding to the O–H and N–H group of the GPE (see Figure 4.11(D)). The peak at 3247 cm^{-1} is assigned to the hydrogen coordination of N–H band to the ether oxygen from PhCh backbone (Bar & Basak, 2014). In the presence of TPAI, these sites instead coordinate to the salt cations hence the sudden drop in peak intensities for GPE of A1 to A7. In contrast, the peak at 3535 cm^{-1} saw its peak intensities increased when compared against the blank GPE, A0, which indicates the possibility of the peak being dedicated to the N–H band coordinated with TPA^+ ions. The peak at 3363 cm^{-1} was attributed to the H-coordination from N–H with C=O. Similarly, a definite decreasing trend was observed in the intensity of peak as the TPAI content increased. The C=O sites no longer being H-coordinated to the N–H and O–H group is now most likely coordinated to TPA^+, as discussed earlier. The peak assigned to the O–H band from pure PhCh at 3442 cm^{-1} has shifted to 3451 cm^{-1}. The lone-pair of the electrons were delocalized due to the strong metal-ions-mediated coordination that reduces the O–H bond length effectively as the vibrational energy increase at higher frequency. The band at 3593 cm^{-1} may also be attributed to the O–H coordinated with the TPA^+ cations.

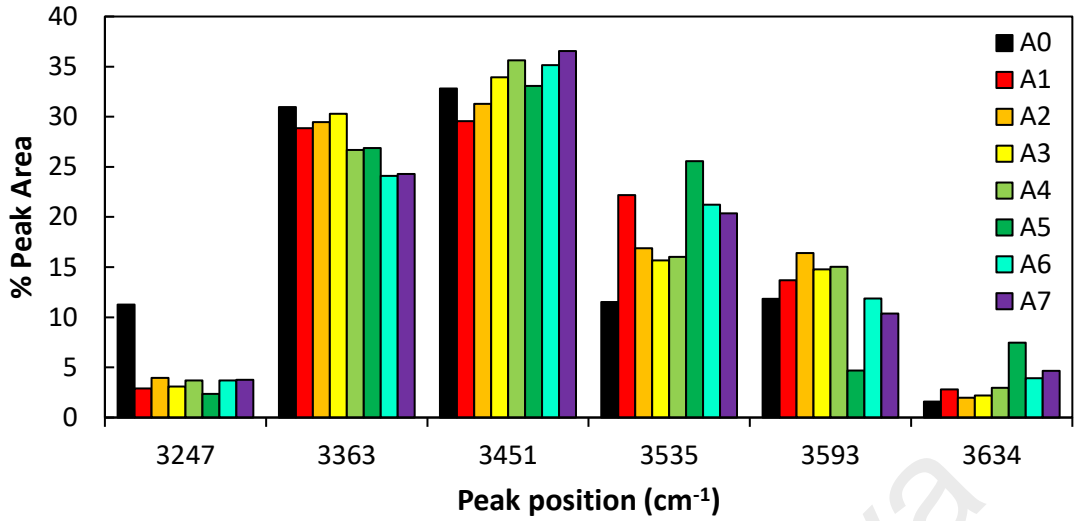

Figure 4.15: Relative FTIR band percentage area in the range of 3130 to 3700 cm^{-1}.

4.2.3. XRD Analysis

The XRD patterns in a range between 2θ = 10° and 2θ = 60° are shown in Figure 4.16 and the details have been tabulated in Appendix B. The area and also height of the broad peak for samples A0 to A6 can be seen to generally decrease with the content of TPAI; from an area and height of 121 913 a.u. and 14 458 a.u. to 22 727 a.u. and 2874 a.u., respectively. This might be due to the decreasing of crystallinity of the gel electrolytes (Aziz et al., 2012). High intensity peaks in XRD occur as the X-rays scatter only in certain directions when they hit the lattice planes formed by atoms which are arranged in periodic crystalline. As the crystallinity in gel electrolyte gets more disrupted, periodicity of the atoms decreases and gets more randomly distributed in 3D space. The X-rays will be scattered in various directions leading to abroad peak distributed in a wide 2θ range instead of high intensity narrower peaks as is shown for every pattern in Figure 4.16. This is parallel with the FTIR analyses where the interactions of gel electrolytes with TPAI leads to further disrupting the crystallinity. The most conducting GPE, sample A6 with 0.12 g of TPAI content, also showed the most amorphous sample among all the

electrolytes in the system. This indicates that conductivity favours the amorphous phase and this results corroborate with the trend seen in the ionic conductivity and DSSC studies. The area and height increased to 24 896 and 3324 a.u., respectively at higher content of TPAI (sample A7) which is beyond the optimum salt concentration point. This is possibly corresponds to the re-association of TPAI ions to form salt aggregates.

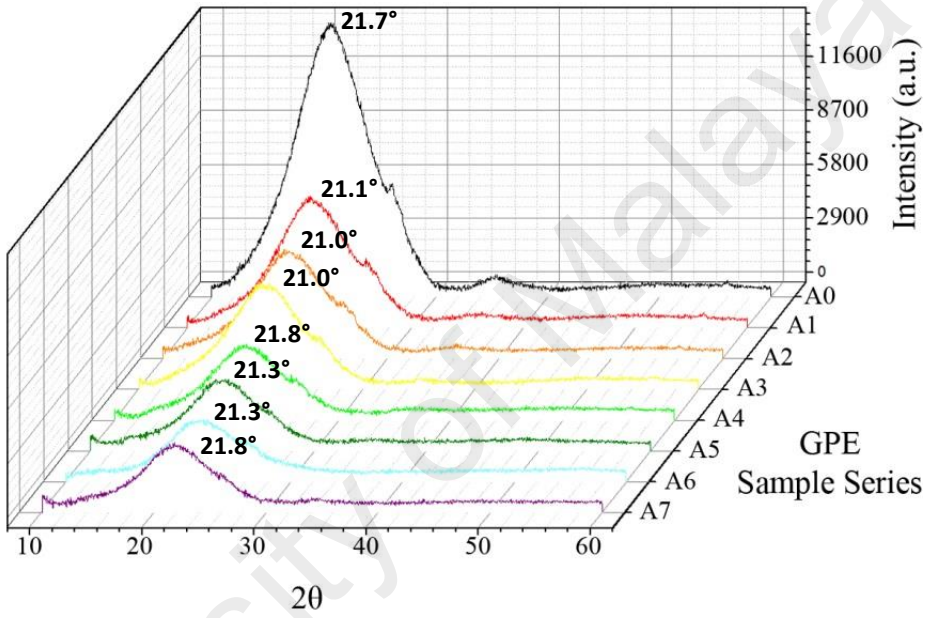

Figure 4.16: XRD patterns of PhCh based GPE with various content of TPAI.

4.2.4. DSSC Analysis

Figure 4.17 shows the *J–V* curves for the DSSCs fabricated with various TPAI contents of GPEs. The photocurrent density-voltage characteristic parameters are tabulated in Table 4.4. DSSC using the GPE with the lowest TPAI content of 0.02 g has produced an efficiency, J_{SC}, V_{OC} and fill factor of 2.86%, 7.70 mA cm^{-2}, 0.64 V and 0.58, respectively. As the TPAI content in the GPE increases, the efficiency of the DSSCs is observed to increase. It should be noted that the η variation follows the same variation as $J_{SC.}$ Thus it is the dominant contributor to the solar cell efficiency. The DSSC fabricated

with A6 (the most conducting and also the most amorphous GPE in the system) gave the best energy conversion η of 5.00 % with parameters J_{SC} of 12.72 mA cm^{-2}, V_{OC} of 0.60 V, fill factor of 0.66. This pattern is observed to be parallel to the conductivity characterizations observed earlier, therefore its behavior could be attributed to the amount of free I^- ions in the GPE. The efficiency at 0.14 g TPAI dropped to 3.58 % after the optimum point at 0.12 g TPAI. This can be explained due to the dissociation of the salt to form free ions, which compete with the occurrence of formation of ion pair and/or ion aggregates. This will hinder the mobility of the ions and also do not assist the ionic conductivity, consequently the conductivity value decreases.

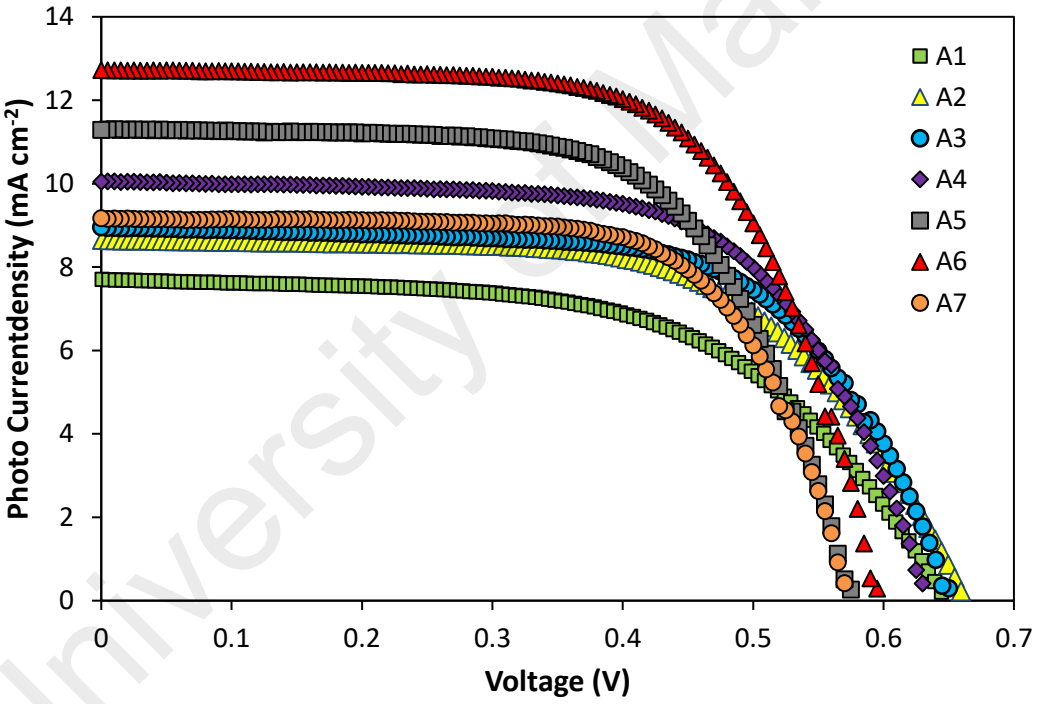

Figure 4.17: Current–voltage curves for DSSCs based on PhCh–EC–DMF–TPAI gel polymer electrolytes with varying amounts of TPAI.

It can be seen from Table 4.4 that the V_{OC} values do not influence by the TPAI content in the GPE. However, the *FF* shows a monotonic increase in values. Generally, V_{OC} is determined by the difference between the quasi Fermi level of the TiO_2 and the redox level of I^-/I_3^- couple. Therefore, the V_{OC} value depends on the cations size in the

electrolyte, as smaller ones can adsorb well to the TiO_2 surface and also alter Fermi level position to some extent. No such changes can be expected since the present electrolyte used larger TPA^+ cations. Thus the V_{OC} value does not show any significant trend of changes as the salt concentration changes in the electrolyte. The value of the *FF*, however depends on many factors which include the charge accumulation within the DSSC due to unbalanced mobility of the charged species and slower the electrons transfer at interfaces and dye regeneration (Qi & Wang, 2013). As the content of TPAI salt increases, the concentration of I^- ions in the electrolyte also increases giving rise to more currents. This corresponds to the improvement in conductivity and *FF* value from the lowering of charge accumulation caused by increased charge transfer at the counter electrode and accelerated dye regeneration.

Table 4.4: *J-V* parameters of DSSC with various content of TPAI.

Designations	J_{SC}/ mA cm^{-2}	V_{OC}/ V	***FF***	***η*/ %**
A1	7.70	0.64	0.58	2.86
A2	8.65	0.66	0.62	3.51
A3	8.95	0.65	0.64	3.75
A4	10.05	0.63	0.65	4.09
A5	11.29	0.58	0.65	4.19
A6	**12.72**	**0.60**	**0.66**	**5.00**
A7	9.17	0.57	0.69	3.58

Relationship between ionic conductivity and DSSC performance with the various mass of TPAI are presented in Figure 4.18. Beyond the optimum amount of TPAI as in sample A7, the photocurrent density drops since the number of I^- ions are reduced due to the formation of ion pairs and aggregates. However, it appears that the charge accumulation has not yet increased to the extent to reduce the *FF* value. The *J–V* curves deviate very much from the ideal rectangular shape when the charge accumulation occurs as can be seen in Figure 4.17. With the increase of the TPAI content, the shape of the *J–V* curves progressively becomes closer to the ideal rectangular shape suggesting that the

charge accumulation is becoming lesser. However, to better explain the observed *FF* value changes is quite difficult as *FF* is controlled by several more factors such as poor contacts that lead to current leakages and also electron recombination. Moreover, these factors influence each other as well.

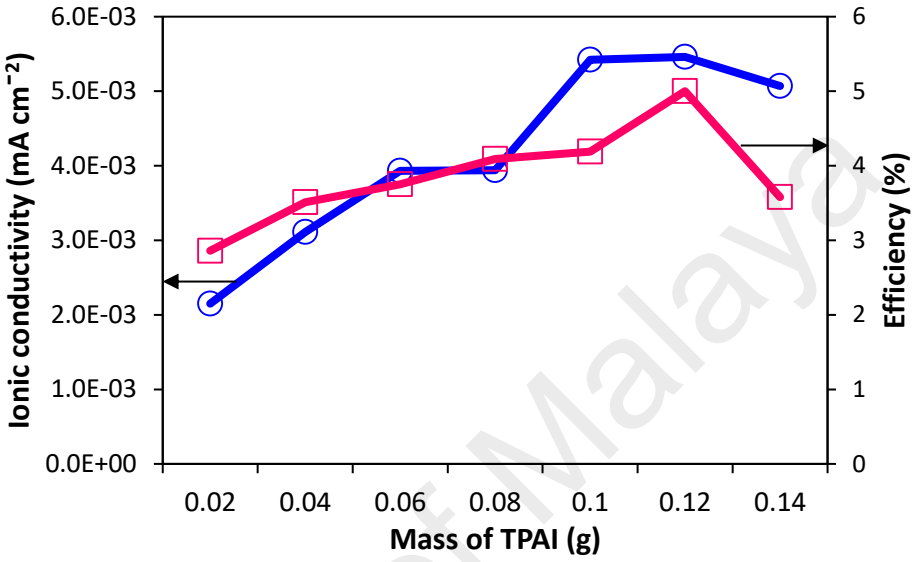

Figure 4.18: Relationship between ionic conductivity and DSSC efficiency with the various mass of TPAI.

The comparison of the DSSCs performance in recent literature has been presented in Table 2.5 (Chapter 2). Values of the performance parameters are from the best electrolyte of the system in each authors' work. From our own work, it has been shown that significant improvements have been achieved in improving the efficiency of the electrolytes based on chitosan and its derivatives. The solar cell parameters are also on par or even better than GPEs using other types of biopolymers. It is also comparable to the best values found in GPEs with synthetic polymer host matrices.

4.3. GEL POLYMER ELECTROLYTE WITH DOUBLE SALTS

In our previous study, a large quaternary ammonium iodide salt was employed since it was expected to reduce the conductivity of the cation while enhancing the conductivity of the iodide anionic in the GPEs (Yusuf et al., 2016). However, recently it has been reported that by including small cations such as Li^+, K^+ or Mg^{2+} into the gel polymer electrolytes along with the bulky cations, the efficiency of solar cells can be significantly improved (Dissanayake et al., 2012; Ileperuma et al., 2004; Yu et al., 2010). Cations with the small size and also high charge density will improve the photogeneration of electrons at the dye. Small size cations will also result in faster diffusion dynamics at the interface between dye and semiconductor (Dissanayake et al., 2014). While the large cations boost iodide ion conductivity, the small cations enhance electron injection yields from dye to TiO_2 film which in turn increases the photocurrent density, J_{SC} value. Therefore, the combination of the two dissimilar cations will positively impact the solar cell performance through their respective roles and this method has been practised by many researchers to improve the efficiency of DSSCs (Dissanayake et al., 2012; Kou et al., 2013; Ozawa et al., 2013; Shi et al., 2011). For example, the binary mixture of potassium iodide (KI) and TPAI in PVdF gel polymer electrolytes produced an efficiency of 3.92 % which was higher than the efficiency of the respective individual salt which only recorded 2.37 % and 2.90 % (Arof et al., 2014a). Similar results were reported for DSSC fabricated using PAN based gel polymer electrolyte with LiI/TPAI salt combination (Wanninayake et al., 2016).

By using binary iodide mixture, enhancement can be observed to the efficiency of the DSSC about 18% compared to the efficiency of DSSC with single iodide. Li^+ with small cation radius of 0.60Å (Bandara et al., 2009), is chosen since KI, RbI and CsI with large cation are hardly employed in a liquid electrolyte for DSSC because of their poor solubility in organic solution (Shen et al., 2008). Bandara et al. (2014a) have also stated

the positive influence of small cations addition on solar cell performance such as enhancement of the electron injection yields from dye to TiO_2 film, electron diffusion through the TiO_2 layer, dye regeneration and effects imposed to the semiconductor band positions with increasing amount of small cation, in this case, the presence of LiI would tend to improve the J_{SC}.

Table 4.5: Comparison of performance parameters of some DSSCs in recent literature for electrolytes consisting of single and double salt systems

Salt system type	Electrolyte system (polymer–co-solvents–salt–dye)	J_{SC} (mA cm^{-2})	V_{OC} (V)	*FF*	η (%)	References
Single	PAN - EC/PC - TPAI/I_2 - N719	10.78	0.75	0.53	4.30	Bandara et al. (2013)
Single	PAN - EC/PC - TPAI/I_2 - N719	9.84	0.72	0.63	4.47	Dissanayake et al. (2012)
Single	PAN - EC/PC - KI/I_2 - N719	13.05	0.64	0.60	4.98	
Double	**PAN - EC/PC - KI/TPAI/I_2 - N719**	**13.79**	**0.68**	**0.57**	**5.36**	
Single	PAN - EC/PC- THAI/I_2 - N719	9.08	0.70	0.47	3.00	Bandara et al. (2014a)
Single	PAN - EC/PC- LiI/I_2 - N719	12.32	0.57	0.57	3.90	
Double	**PAN - EC/PC- THAI/LiI/I_2 - N719**	**13.12**	**0.58**	**0.56**	**4.20**	
Single	PAN - EC/PC - LiI/I_2 - N719	10.90	0.56	0.60	3.60	Bandara et al. (2014b)
Single	PAN - EC/PC- CsI/I_2 - N719	10.3	0.70	0.54	3.90	
Double	**PAN - EC/PC- CsI/LiI/I_2 - N719**	**13.20**	**0.61**	**0.59**	**4.80**	
Single	PVA - EC/PC/DMSO - KI/I_2 – N719	5.08	0.68	0.78	2.74	Aziz et al. (2014)
Single	PVA - EC/PC/DMSO – KI/I_2 - N3	11.03	0.51	0.68	3.83	Aziz et al. (2015)
Single	PVA - EC/PC/DMSO -TBAI/I_2 - N3	11.13	0.67	0.63	4.70	
Double	**PVA - EC/PC/DMSO - KI/TBAI/I_2 - N3**	**12.56**	**0.65**	**0.71**	**5.80**	
Single	PVdF - EC/ PC - KI/I_2 - N719	4.61	0.75	0.68	2.37	Arof et al. (2014a)
Single	PVdF - EC/ PC - TPAI/I_2 - N719	6.15	0.68	0.69	2.90	
Double	**PVdF - EC/ PC - KI/TPAI/I_2 - N719**	**9.16**	**0.67**	**0.63**	**3.92**	
Single	PMMA - EC/PC - TPAI/I_2 - N719	7.42	0.71	0.60	3.21	Dissanayake et al. (2014)
Single	PMMA - EC/PC - KI/I_2 - N719	7.55	0.70	0.64	3.39	
Double	**PMMA - EC/PC - KI/TPAI/I_2 - N719**	**10.70**	**0.66**	**0.57**	**3.99**	
Single	PhCh – EC/PC – TPAI/I_2 – N719	7.38	0.72	0.66	3.50	Yusuf et al. (2014)
Double	**PhCh – EC/PC – TPAI/LiI/I_2 – N719**	**7.25**	**0.77**	**0.67**	**3.71**	
Double	**PAN - EC/PC – TPAI/LiI/I_2 - N719**	**16.10**	**0.61**	**0.65**	**6.40**	Wanninayake et al. (2016)

Thus, in order to improve the efficiency of PhCh based DSSCs, EC and DMF with a binary iodide salt system consisting of TPAI as the bulky cation salt and LiI as the small alkali cation salt were used to prepare the GPE (shown in Figure 4.19).

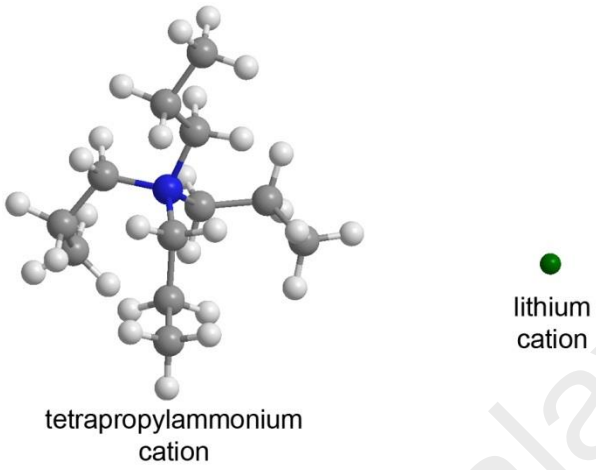

Figure 4.19: The two types of cations present in the PhCh–EC–DMF–TPAI-Li GPE system.

4.3.1. EIS Analysis

Figure 4.20 shows the effects of ionic conductivity at room temperature and activation energy with the concentration of LiI. All of the values are tabulated in Table 4.6. It is obvious that the conductivity value is not significantly influenced by the different combinations of small and large cations used. In general, the conductivity value of an electrolyte is governed by two main factors namely number density of mobile ions, *n* and mobility of the charge carriers, μ. In this study, these transport parameters were evaluated using the Rice and Roth model (Rice & Roth, 1972) which relates ionic conductivity with *n* value through the equation:

$$\sigma = \frac{2}{3}\left[\frac{(Ze)^2}{kTm}\right] nE_a\tau_o e^{\frac{-E_a}{kT}} \qquad (4.2)$$

where *Z* is the valency of the ions, *k* is the Boltzmann constant, *m* is the mass of charge carrier, *n* is the number density of mobile ions, τ_o is the free ion lifetime and E_a is the activation energy. By substituting the *n* value into the general equation of conductivity, $\sigma = n\mu e$, the mobility factor, μ is then evaluated.

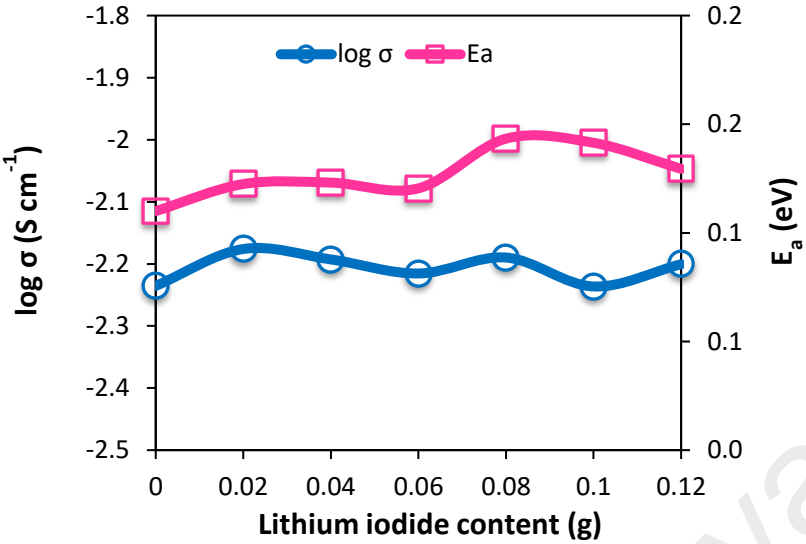

Figure 4.20: Variation of activation energy values and conductivity values as a function of LiI content.

Table 4.6: σ and E_a of GPEs with various mass ratios of TPAI and LiI

Samples	Ionic conductivity, σ/ S cm^{-1}	Activation energy, E_a/ eV
B0	5.46×10^{-3}	0.11
B1	6.67×10^{-3}	0.12
B2	6.41×10^{-3}	0.12
B3	6.09×10^{-3}	0.12
B4	6.46×10^{-3}	0.14
B5	5.80×10^{-3}	0.14
B6	6.30×10^{-3}	0.13

The effect of the LiI composition on the n and μ values is depicted in Figure 4.21 (values in Table 4.7) and the trend in the plot can be dissected into two regions namely, TPAI dominant region (0.00-0.06 g LiI) and LiI dominant region (0.06-0.12 g LiI). The number density of mobile ions is observed to be higher in the LiI dominant regions whereas high mobility is favoured in the TPAI dominant region. Being the salt with lower molecular weight, LiI is expected to dissociate into higher density of mobile ions compared to the higher molecular weight TPAI. However, large concentrations of LiI results in the reduction of polymer flexibility due to inter and intra molecular cross links

by lithium ions induced by its high charge density. The reduction of polymer flexibility can increase the local viscosity of electrolyte medium hindering mobility of the charge carriers. Thus in a system comprising both the salts, high mobile ion concentration is achieved at the expense of mobility at one end and the converse occurs at the other end, therefore resulting in a net ionic conductivity within the same range.

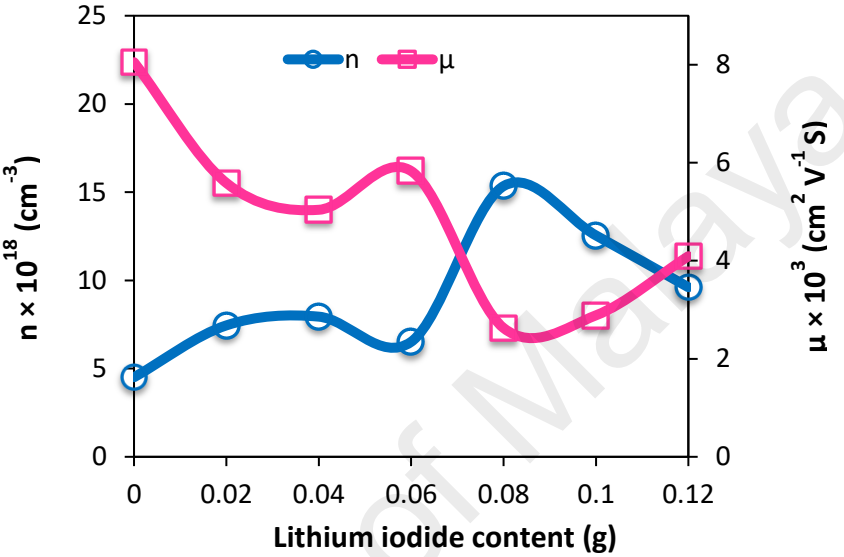

Figure 4.21: Number density and ionic mobility of GPEs with different ratios of LiI:TPAI.

Table 4.7: *n*, μ and *D* values for the GPEs with different ratios of of LiI:TPAI

Samples	$n/\ cm^{-3}$	$\mu/\ cm^2\ V^{-1}\ S$	D
B0	4.509×10^{-18}	7.567×10^{-3}	1.975×10^{-4}
B1	7.450×10^{-18}	5.587×10^{-3}	1.458×10^{-4}
B2	7.944×10^{-18}	5.040×10^{-3}	1.316×10^{-4}
B3	6.519×10^{-18}	5.830×10^{-3}	1.522×10^{-4}
B4	1.534×10^{-18}	2.628×10^{-3}	6.859×10^{-5}
B5	1.255×10^{-18}	2.887×10^{-3}	7.536×10^{-5}
B6	9.611×10^{-18}	4.093×10^{-3}	1.068×10^{-4}

It should be noted for now that although the highest conductivity was achieved for the sample B1, it will be discussed later that the optimum DSSC power conversion efficiency, η was obtained for the sample B3 instead. According to Cha et al. (2010), the

ionic conductivity may not be the rate controlling step among various transport processes in determining the cell efficiency, nonetheless electron recombination might play a significant role in the solid-state DSSCs employing polymer electrolyte.

The electrolytes were also subjected to temperature dependent conductivity studies from 303 K to 363 K and all the samples exhibited Arrhenius behavior within the measured temperature range. The activation energy, E_a, was calculated by fitting the data (Table 4.6) to the Arrhenius equation and the activation energies of electrolytes were also found to be between 0.10-0.14 eV. The observed pattern in the activation energy can be justified by comprehending the nature of the gel formation. In this study, the gel electrolytes are fabricated by the entrapment of the DMF, EC and iodide salt based electrolyte in the phthaloyl chitosan matrix. Thus, the conductivity trend is essentially governed by the electrolytic solution and the system could be viewed in the perspective of a liquid electrolyte in which the E_a is largely independent of the salt concentrations but rather depends on the type of solvent (Petrowsky & Frech, 2010). The binary iodide studies on PAN and PMMA based quasi-solid DSSC also report similar trend as in this study (Bandara et al., 2014a; Dissanayake et al., 2014).

4.3.2. FTIR Analysis

The FTIR spectrum which is typical of the phthaloylchitosan based GPE with various ratio of TPAI:LiI are shown in Figure 4.22. Assignments of the common peaks have been discussed in detail in *Section* 4.2.2. Deconvolution of the peaks were made to study the influence of having LiI in addition to TPAI in this binary GPE salt system towards the ratios of the crystalline-amorphous domain and to the extent of cation-polymer/plasticizer binding sites.

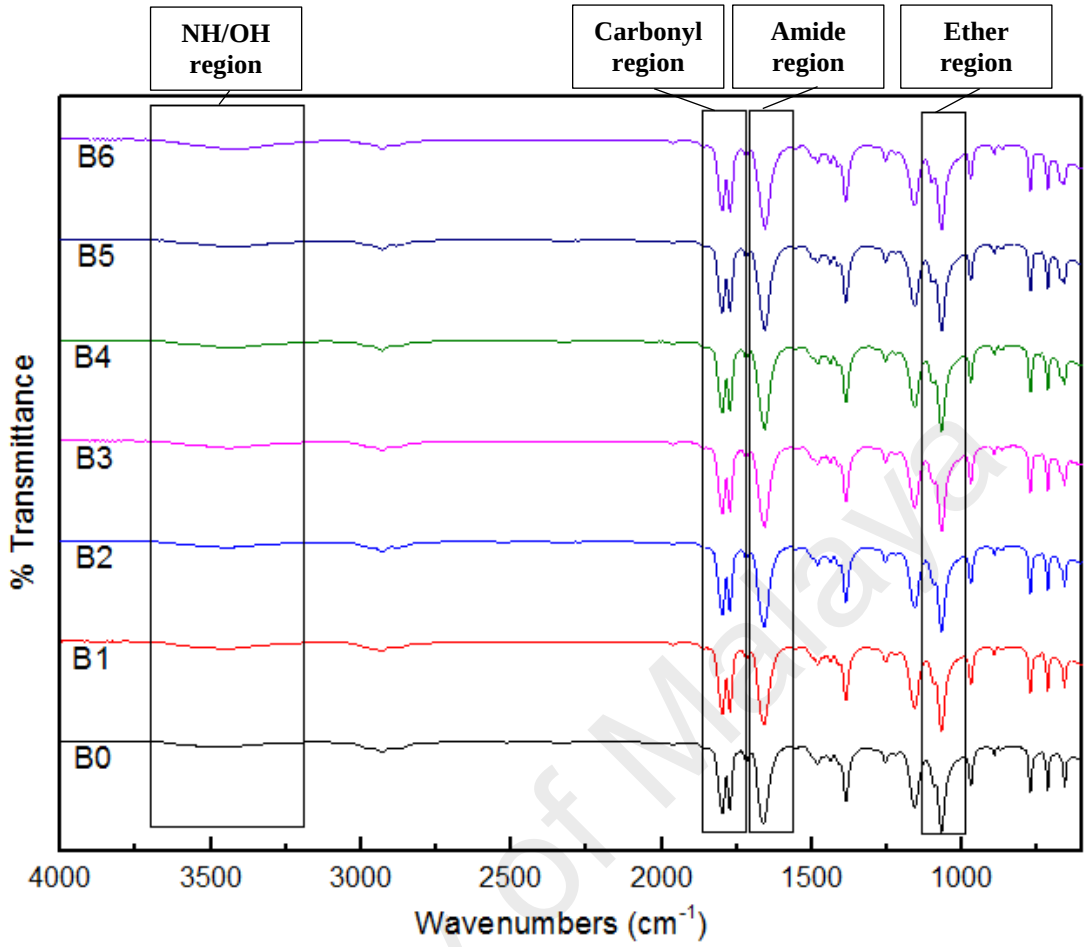

Figure 4.22: FTIR spectra for PhCh based gel polymer electrolytes containing various ratio of TPAI:LiI.

The four possible coordination regions which were scrutinized are: ether, C-O-C (1000-1200 cm^{-1}), amide $R(C=O)NR_2$ (1580-1700 cm^{-1}), carbonyl C=O (1700-1840 cm^{-1}), and amine/hydroxyl groups N-H/O-H (3130-3700 cm^{-1}). These analyses seem to indicate the cause for the perceived drop in ionic mobility, μ when the ratio of LiI is increased against TPAI: it is due to the stronger affinity of the LiI towards forming coordination complexes with the polymer/plasticizer matrix. The reason for this behavior would be that LiI, which has a smaller effective cation size of 0.76 Å (Shannon, 1976) has greater accessibility to the coordination sites when compared against the much larger TPAI which has a cation size of 4.60 Å (Gregor, 1968) as previously shown in Figure 4.19.

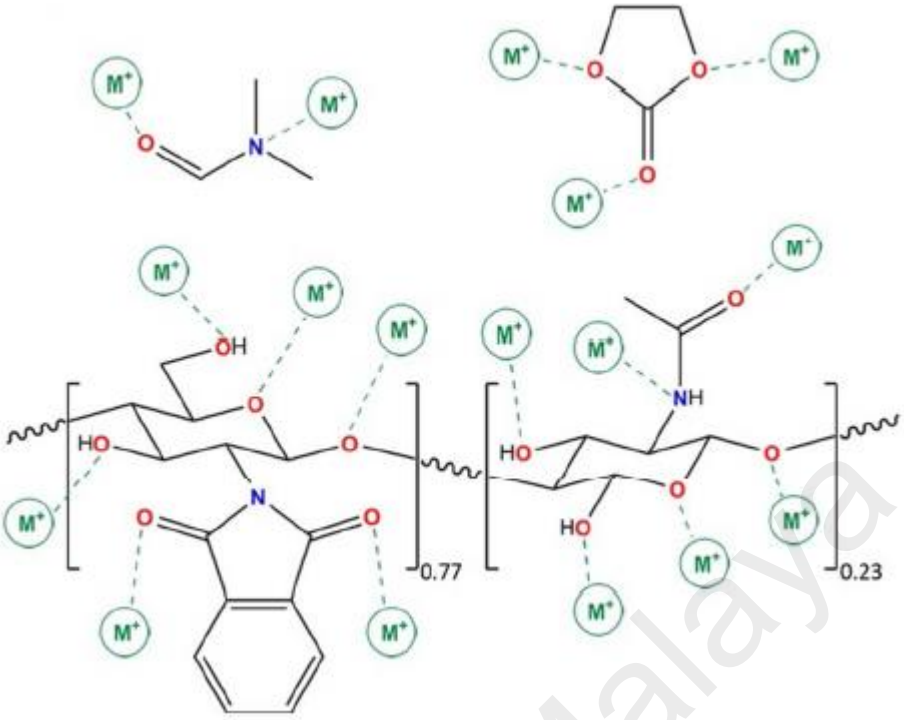

Figure 4.23: A graphical representation of the cation coordination to the electron rich moieties in the GPE system.

FTIR spectra of ether group in the range from 1000 to 1200 cm^{-1}

Deconvolution in this region has resolved up to as many as eight separate major peaks (Appendix E1), each of its relative contribution is shown by the histogram in Figure 4.24. In our previous subtopic (*Section* 4.2.2), the peak intensity at 1047 cm^{-1} which was assigned as the cation-bonded C-O-C stretching from PhCh showed little sensitivity towards changes in salt concentration. In this current work, the total salt concentration was fixed to a constant amount, however it was observed that as the ratio of LiI increases over the TPAI amount, the peak intensity also increases which suggests that the Li^+ cations tends to have better coordination capabilities towards the GPE matrix. The peak at 1069 cm^{-1} which belongs to the $-CH_3$ rocking mode of both uncoordinated EC and DMF also shows negligible changes except when the intensity drops at very high LiI concentrations. A much more prominent change was seen at 1079 cm^{-1} which is dedicated

to the complexation of both Li^+ and TPA^+ to the C-O-C site: when the ratio of LiI was more dominant over TPAI, the peak intensity became significantly higher.

Another point of interest is the relationship of the peak intensities at 1094 cm^{-1} and 1104 cm^{-1}. The degree of amorphousness in the GPE samples is held back by the formation of crystalline complexes (Bar & Basak, 2014) and is the most likely cause for the appearance of the peak at 1094 cm^{-1}, whereas the peak at 1104 cm^{-1} is attributed solely due to coordination of Li^+ ions with C-O-C sites which in turn stifles the crystallinity of the GPE matrix especially at higher LiI concentrations (this observation also tallies with the XRD analysis discussed later where increasing the amount of LiI leads to reduced crystallinity). Also in the amorphous region there is a peak assigned to the stretching mode of unbound C-O-C arise at 1143 cm^{-1}, however this site does not have significant sensitivity towards changes in the LiI/TPAI ratio. Similar indifferences were seen for the peaks at 1156 and 1171 cm^{-1} except when LiI concentration was very high, which suggests peaks in this region are not heavily influenced by the complexation of the salt with the polymer/plasticizer matrix.

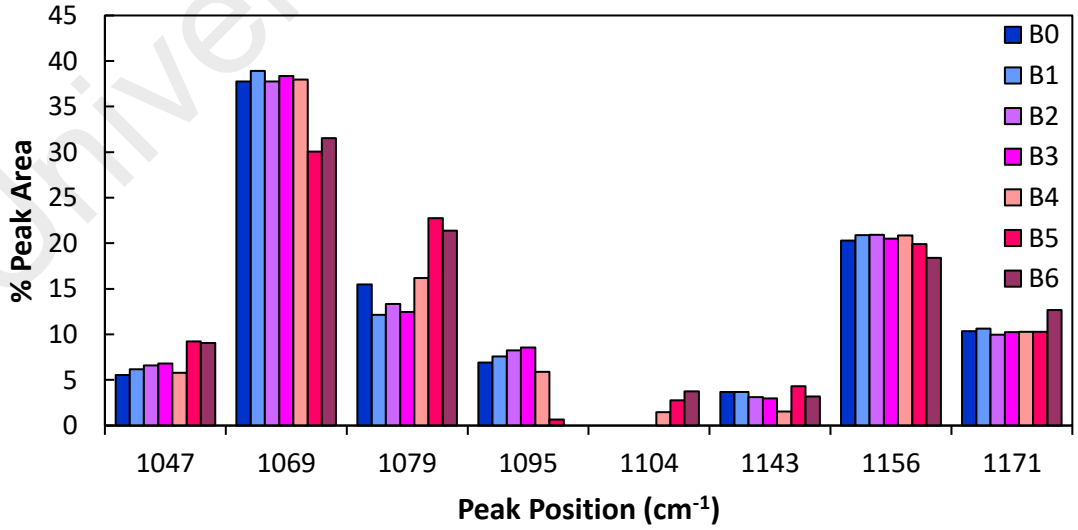

Figure 4.24: Relative FTIR peak area for each deconvoluted peak in the ether region.

FTIR spectra of amide/carbonyl group in the range from 1580 to 1840 cm^{-1}

The presence of carbonyl moieties within the GPE matrix also allows possible bonding sites for the Li^+ and TPA^+ cations. Upon coordination, the electron density of the C=O group is reduced, and because this causes the vibrational energy to decrease, it results in the shifting of peak positions towards lower wavenumbers in the FTIR spectrum (Huang et al., 2013).

To simplify the deconvolution computation, the carbonyl region was split into two parts (Appendix E2), with the first half being dedicated for carbonyl belonging to amide groups present in the GPE system (1580 to 1700 cm^{-1}) and the second half belonging to carbonyls not associated with amide (1700 to 1840 cm^{-1}) as shown in Figure 4.25 and Figure 4.26, respectively.

The peaks at 1637 and 1649 cm^{-1} can be associated to the ordered or disordered interfacial domains in the structure of the polymer, respectively (Bar & Basak, 2014). The two peaks show a clear inverse relationship trend towards changes in LiI/TPAI ratio. This behavior was less noticeable in our previous work for a single TPAI salt system (Yusuf et al., 2016). However, the clear trend seen in Figure 4.25 corroborates with the observation for the C-O-C region discussed earlier whereby the Li^+ attaches itself much easier to negative moieties probably due to it having a smaller cationic size compared to TPA^+.

The carboxamide group belonging to chitosan shows the most intense peak at 1660 cm^{-1} which increases further when LiI is more dominant. The peak at 1668 cm^{-1} is much less noticeable but it does show complete suppression at very high LiI ratios. Also of interest is the peak at 1674 cm^{-1} belonging to the DMF component in the GPE matrix. For a unitary salt system, it has been shown that the intensities generally increases along with TPAI concentration (Yusuf et al., 2016), but in this current work, the total concentration of the binary LiI/TPAI salt system was held constant and yet as the ratio of

LiI over TPAI is increased, the peak intensities decreased steadily. This may suggest that coordination of TPA^+ towards DMF is preferred over the chitosan backbone, probably due to DMF being more mobile and accessible, but in the presence of competition with Li^+, this ability is hindered.

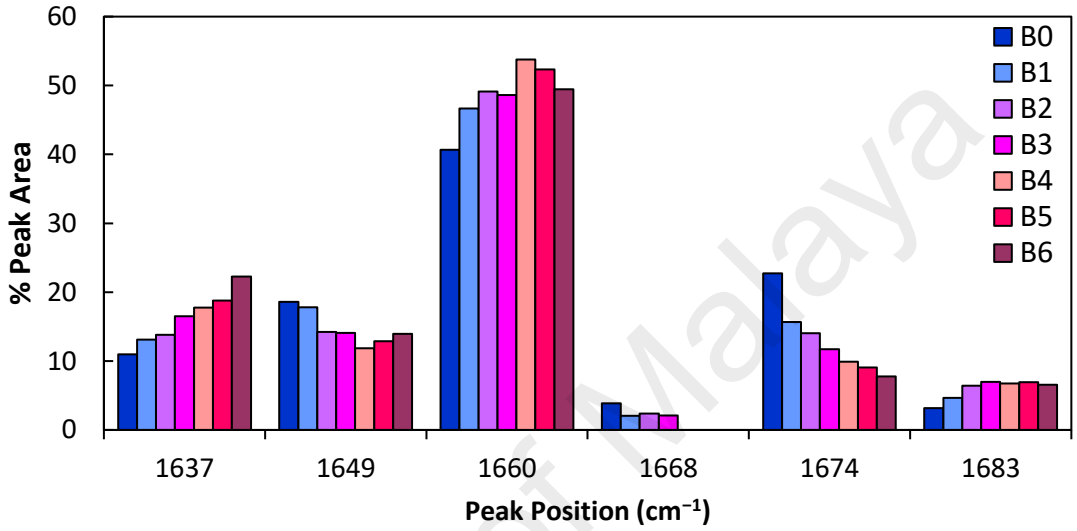

Figure 4.25: Relative FTIR band percentage area in the range of 1580-1700 cm^{-1}.

Deconvolution analyses in the region between 1700 and 1840 cm^{-1} showed negligible sensitivity response intensities towards changes in LiI/TPAI ratio (Figure 4.26) for most of the resolved peaks. The peak at 1718 cm^{-1} is assigned to the coordination of salt cations to the carbonyl anhydride from the phthalimido group of PhCh. The peak resolved at 1788 cm^{-1} was attributed to the unbonded C=O (Barth, 2000). The two strong peaks due to carbonyl group of from EC has appeared at 1773 and 1805 cm^{-1} (Ikezawa & Nishi, 2008; Osman & Arof, 2003). These are the only peaks in this region that show appreciable change with varying amount of LiI/TPAI ratio to indicate salt−EC interaction. The peak at 1798 cm^{-1} is also associated with EC but it shows only a slight downward trend with increasing LiI.

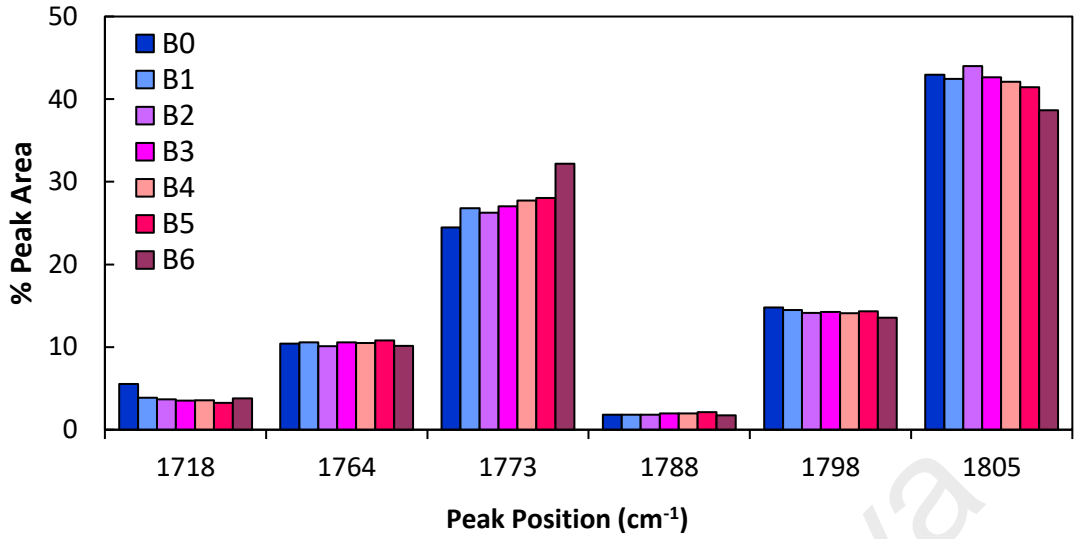

Figure 4.26: Relative area percentage of the deconvoluted peaks in the amide region.

FTIR spectra of amine/hydroxyl group in the range from 3130 to 3700 cm^{-1}

The O-H and N-H groups of the GPE overlap in the region of 3130-3700 cm^{-1} and results from the deconvolution analyses are shown in Figure 4.27. Previously, for the unitary system, the peak at 3247 cm^{-1} was attributed to the coordination of N-H to C-O-C (Bar & Basak, 2014; Yusuf et al., 2016). In the presence of TPAI, the bond favors TPA^{+} to N-H instead. In this current work, additional presence of Li^{+} competes with TPA^{+} as can be seen by the rising peak intensities with increment of LiI content. A similar observation was seen at 3363 cm^{-1}, but this peak was assigned to N-H or O-H coordination with carbonyl. There are no more hydrogen coordinated to the O-H and N-H group at the carbonyl sites. This might be due to the disruption by the contributing factors of TPA^{+} and Li^{+}. Changes in the peak intensities at 3451 and 3593 cm^{-1} however, showed no obvious trends. On the other hand, coordination with TPA^{+} gave peaks at 3535 and 3634 cm^{-1} but competition with Li^{+} may have caused the peak intensities to drop with incremental dominance of LiI.

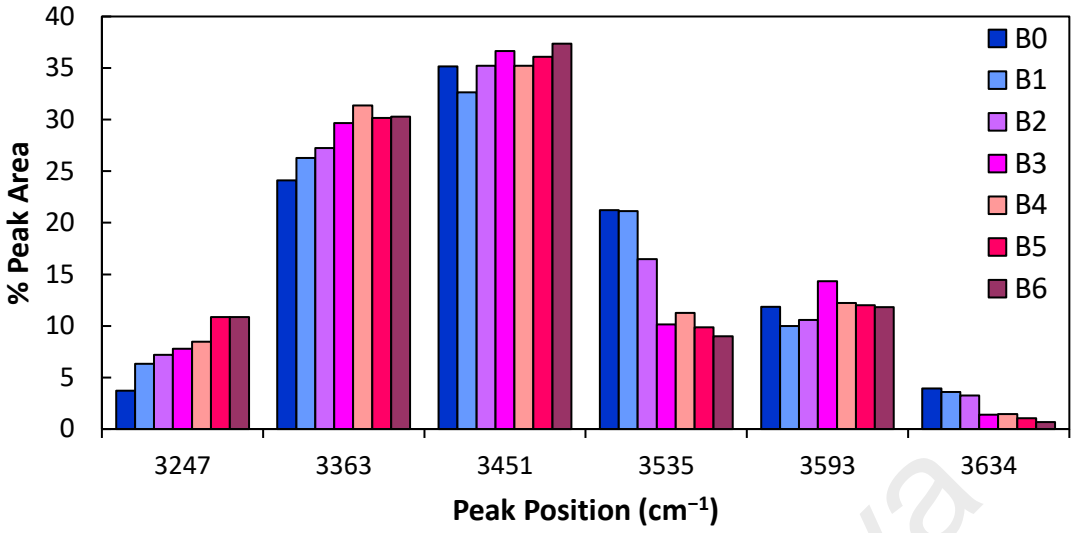

Figure 4.27: Relative FTIR band percentage area in the range of 3130-3700 cm^{-1}.

4.3.3. XRD Analysis

XRD patterns for each sample of the GPE is shown in Figure 4.28 (and detailed data is given in Appendix C). The total weight concentration of the Li/TPAI was held constant for all the samples, however the XRD results clearly show a decremental change in the area and height of the peaks at $2\theta \approx 22°$ as the ratio of LiI is raised. This concurs with the EIS and FTIR analyses whereby LiI plays a strong role in reducing the amorphousness of the GPE samples. Since Li^+ has a higher charge density as well as a smaller cationic size compared to TPA^+, it would have had greater steric accessibility to form coordination complexes with electron rich sites and thus is better able to disrupt the crystalline network in the GPE matrix. The X-rays will be scattered in many directions since the periodicity of the matrix structure decreases, thus lead to a formation of a broad peak of lower intensity. In the case of this PhCh–EC–DMF–TPAI-Li based gel electrolyte system, the peak area was reduced from 22727 a.u. to 11987 a.u. corresponding to samples with salt systems that consists entirely of TPAI (B0) and LiI (B6) respectively.

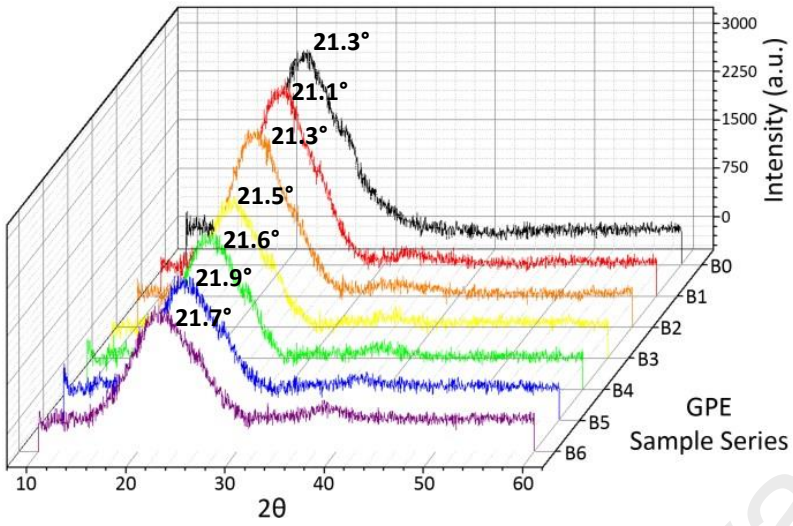

Figure 4.28: XRD patterns of PhCh based gel polymer electrolytes with various ratio of TPAI:LiI content.

4.3.4. DSSC Analysis

The DSSC parameters for the devices having the binary salt system are shown in Table 4.8. The incorporation of small amount of LiI into the electrolyte has improved the solar cell performance with the maximum efficiency of 6.36 % achieved by the electrolyte with the combination of 0.06 g TPAI and 0.06 g LiI. It is also interesting to note that the efficiencies for all the electrolytes with mixed iodide salts were higher than the two end members which consists only one of them. This increase in efficiency can be attributed to the mixed cation effect (having smaller and larger cations) as observed with many binary salt electrolytes (Ileperuma et al., 2004; Yu et al., 2010). The impact of the mixed salt system on the overall efficiency can be further comprehended by analysing the trend in photocurrent density, J_{SC} and open circuit voltage, V_{OC} with the addition of LiI.

The interactions experienced by the cations at the electrolyte-TiO_2 interface are very crucial in determining the V_{OC} parameter. In a typical DSSC, after illumination, the electrons will be injected from the dye accumulate at the conduction band (CB), causing the cations of the electrolyte to be adsorbed for charge compensation (Kalyanasundaram, 2010). Naturally, smaller cations such as Li^+ could adsorb on the nano TiO_2 grains more

easily compared to bulky cations like TPA^+. The adsorption of the small cation induces upward shift of the CB edge, thus reducing the V_{OC} value of the solar cell (Dissanayake et al., 2012; Shi et al., 2011). This behaviour is well observed in our system, in which the V_{OC} value showed gradual decrease upon increment in LiI, reaching the lowest value in B6.

However, as shown in Table 4.8, the efficiency of DSSC in this study is mainly influenced by the changes in J_{SC}, it can be approximated by the following expression:

$$J_{SC} = q\eta_{lh}\eta_{inj}\eta_{cl}I_o \quad (4.3)$$

where q is the elementary charge, η_{lh} is the light-harvesting efficiency, η_{inj} is the charge injection efficiency, η_{cl} is the charge collecting efficiency and I_o is the light intensity. According to (Shi et al., 2011), the charge collecting efficiency of the cell is independent of cations in the electrolyte and in a system with different cations, the J_{SC} value is mainly influenced by the charge injection efficiency. As mentioned earlier, the adsorption of Li^+ on the TiO_2 surface causes a large potential drop as a result of the CB shift. This will enhance the driving force for the electron injection process from the LUMO level of the dye into the CB of TiO_2, resulting in faster electron dynamics at the semiconductor/electrolyte interface and generating a larger photocurrent (Kou et al., 2013). This mechanism explains the increase in the J_{SC} value from B0 to B3.

On the other hand, high TPAI concentrations favour better iodide conductivity which serves as another salient factor in improving the J_{SC} value (Bandara et al., 2014a; Dissanayake et al., 2014). Ozawa et al. (2013) had also shown that the inclusion of tetraalkylammonium iodide salt aids in the retardation of the backward electron transfer from TiO_2 to I_3^- causing an effective improvement in the J_{SC} value. Thus, the increase of LiI at the expense of TPAI, justifies the drop in J_{SC} value from B3 to B6. In total, the two competing mechanisms imposed by the small and large cations, work synergistically in this binary iodide system to produce an optimum J_{SC} and hence efficiency at B3. Figure

4.30 shows that the efficiency of the solar cell for the binary salt is not dependent on the ionic conductivity as the previous system (Table 4.6). This is because the conductivity only depends on free mobile ions. Meanwhile, the efficiency of a solar cell is influenced by many factors including conductivity and activity of iodide ions in the dye sensitized TiO_2 semiconductor electrode/electrolyte interface redox.

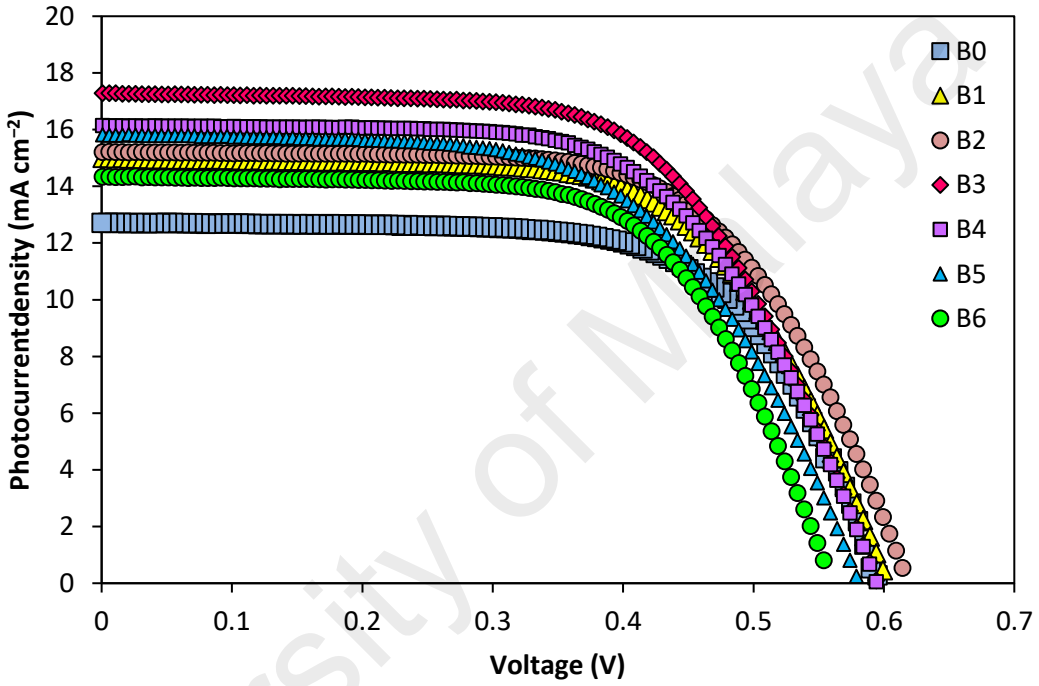

Figure 4.29: Current-Voltage curve of PhCh-EC-DMF electrolytes with various ratio of TPAI:LiI.

Table 4.8: DSSC parameters of PhCh-EC-DMF-TPAI-LiI electrolytes

Designations	J_{SC}/ **mA cm^{-2}**	V_{OC}/ **V**	***FF***	η/ **%**
B0	12.72	0.60	0.66	5.00
B1	15.01	0.60	0.63	5.70
B2	15.22	0.61	0.64	6.00
B3	**17.29**	**0.59**	**0.62**	**6.36**
B4	16.15	0.59	0.62	5.94
B5	15.82	0.58	0.59	5.44
B6	14.34	0.55	0.65	5.16

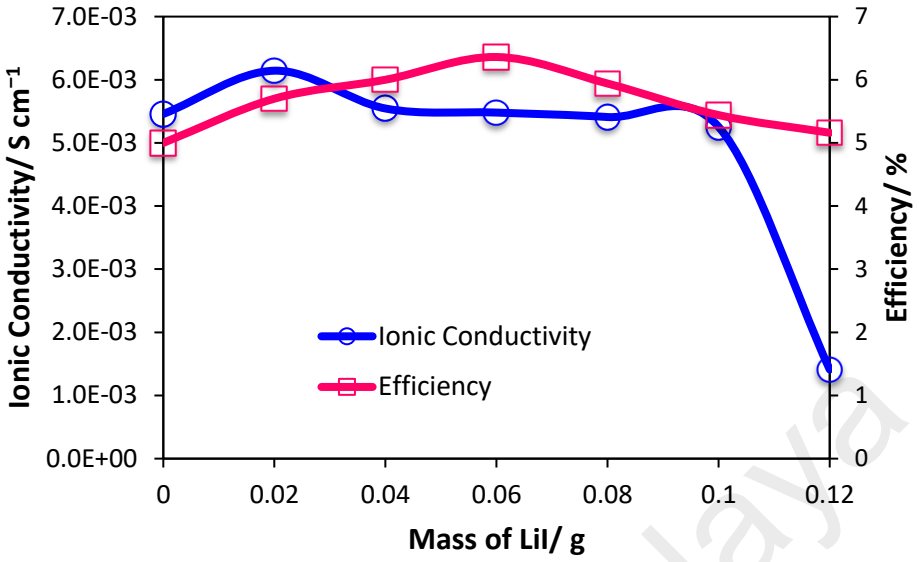

Figure 4.30: Effects of ionic conductivity and efficiency to the different ratio of TPAI:LiI in double salt system.

A brief summary of some recent work in the literature for the parameters of mixed iodide salt studies in polymer electrolyte based DSSC is shown in Table 4.5. In all cases, it was observed that the mixed salt systems were always superior in performance compared against systems consisting of only single salts. To the best of our knowledge, GPE systems utilizing biopolymers are still scarce, and yet from Table 2.5, it is evident that this work has shown that the solar cell efficiency attained is comparable or in some cases, even better than synthetic polymer based DSSCs.

4.4. GEL POLYMER ELECTROLYTE WITH ADDITION OF IONIC LIQUID

A long list of additives has been proposed over the years and it has often been observed that an additive acts favourably only on a specific photovoltaic cell parameter, but not on others. Thus, there is the need to adopt mixtures of two or more additives in order to maximize each of the cell parameters (Bella et al., 2014). In this subtopic, we have introduced ionic liquid (IL) to the binary salt system GPEs with the goal to improve the efficiency of the DSSC as IL is a green solvent (Hulsbosch et al., 2016; Thomas & Marvey, 2016). According to Bidikoudi et al. (2015), ILs possess good solubility with polysaccharides and biomacromolecules, thus it is suitable with chitosan.

IL is a molten salt at room temperature. IL comprises of a large asymmetrical cation and a weakly coordinating inorganic or organic anion (Sim et al., 2014). IL gives advantages (Abate et al., 2012; Jayaweera et al., 2015; Suzuki et al., 2013) such as

- Low volatility
- Tunable miscibility,
- High thermal stability,
- Wide electrochemical window
- High ionic conductivity.

Imidazolium cation (Im^+) based ILs has been frequently chosen by researchers to be applied in DSSCs. According to Huo et al. (2015), in the electrolyte with Li^+ and Im^+ cations, due to the electrostatic effect, Im^+ can adsorb onto the TiO_2 surfaces to form Im^+ multilayer and further influence the adsorption and function of Li^+. Shi et al. (2008) have fabricated a DSSC using electrolyte consist of *1*-methyl-*3*-propylimidazolium iodide (MPII)/LiI/I_2/*t*-BP/*3*-methoxypropionitrile. The cell exhibited efficiency of 6.73% with J_{SC} of 14.82 mA cm^{-2}, V_{OC} of 0.69 V, and *FF* of 0.66.

Suzuki et al. (2006) have developed a new ionic gel electrolytes by gelation of IL electrolyte (mixture was stirred at 150 °C for 10 min) in order to improve the durability of DSSCs. The semi-solid state electrolytes that consist of 1.0-1.5 wt% of agarose, *1*-methyl-*3*-propylimidazolium iodide, I_2, LiI, *t*-BP exhibited a DSSC efficiency of 2.93 % with a light intensity of 100 mW cm^{-2} at 310 h. Without agarose, the efficiency value was just slightly higher, which is 2.95 %.

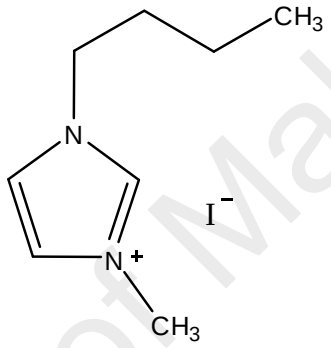

Figure 4.31: Chemical structure of BMII ionic liquid.

1-butyl-*3*-methylimidazolium iodide (BMII) can give rise to a constant efficiency at a high level in a wide range of illumination and to the largest efficiency at 1 sun among the various tested imidazolium iodide with short alkyl chains (Otaka et al., 2004). One unique characteristic of BMII compared to the BMICl and BMIBr is that BMII is coloured while the rest is colourless. This is due to the charge transfer transition occurring from HOMO (the non-bonding orbital localized on iodide ion (due to presence of lone pair electron)) to LUMO (mainly localized on imidazolium ring and is antibonding in nature (π^*). Besides, since the main stabilization energy between BMI^+ and I^- (11.00 kcal/mol) is lower compared to the BMI^+ with Cl^- and Br^- (37.28 and 29.28 kcal/mol, respectively), thus BMII exists as liquid at room temperature while the other two are solid (Shukla et al., 2010).

In this work, various percentages of BMII from 1 to 5 wt.% were introduced into the most efficient PhCh based GPEs with binary salts system.

4.4.1. EIS Analysis

Relationship between ionic conductivity with various weight percentages of BMII of PhCh-EC-DMF-TPAI-LiI based GPE is exhibited in Figure 4.32. After 1 wt. % of BMII was added to the GPE, the conductivity value has slightly decreased from 6.089×10^{-3} to 5.464×10^{-3} S cm^{-1}. As the ionic conductivity was further dropped, the E_a values were observed to increase with more BMII added, from 0.120 to 0.148 eV for samples C0 and C3, respectively. The opposite effects of these two parameters on different wt. % of BMII show that as BMII content is increased, the energy barrier gets higher and consequently the ionic conductivity value will decrease.

By adding BMII, the ionic conductivity is expected to increase as the number of charge carriers available for conduction will increase and at the same time the low viscosity of the IL will reduce the crystallinity of the matrix thereby increases the mobility of the charge carriers (Singh et al., 2008, Singh et al., 2009). However, as weight percentage of BMII increases, the efficiency is observed to decrease. This phenomenon can be observed previously in mixed cations system. The conductivity drop can be attributed to the reduction of polymer flexibility due to its high charge density. Thus, the reduction of polymer flexibility can increase the local viscosity of electrolyte medium hindering mobility of charge carriers (Stepniak et al., 2014).

The values of the transport parameters, n, μ and D have also been tabulated in Table 4.9 in order to explain the ionic conductivity trend. The values of diffusion coefficient, D decrease from 1.522×10^{-4} to 8.608×10^{-5} with increasing of BMII content, consequently, reducing the conductivity. Effect of BMII on the other two parameters, n and μ is shown

in Figure 4.33. As the number density of mobile ions, *n*, increases, the mass of charge carrier, μ, decreases. *n* values rise up to 9.500×10^{-18} cm^{-3} with 3 wt. % of BMII content and fall after additional of BMII. However, value of μ is observed to follow the ionic conductivity pattern which decreases with the wt.% of BMII. This shows that conductivity is heavily influenced by the mobility of the charge carriers.

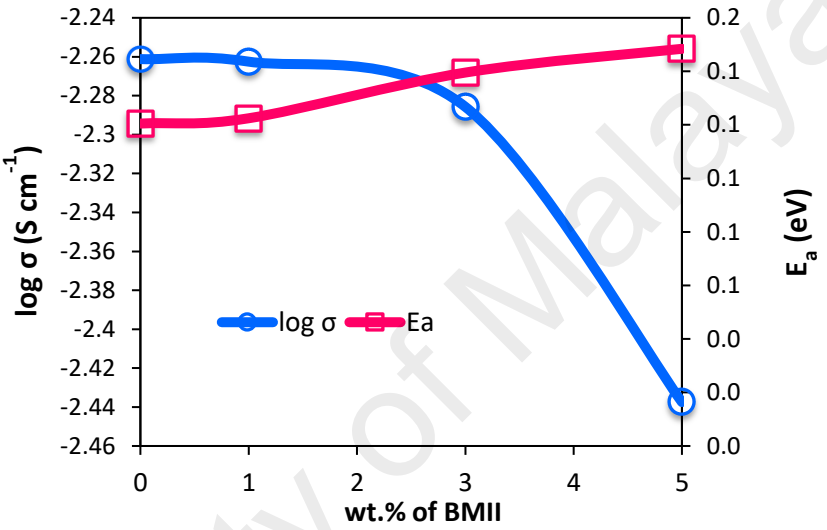

Figure 4.32: Effects of BMII on the PhCh-EC-DMF-TPAI-LiI based GPE.

Table 4.9: Ionic conductivity values of PhCh-EC-DMF-TPAI-LiI based gel polymer electrolyte with various weight percentage of BMII

Samples	σ/ S cm^{-1}	*Ea*/ eV	*n*/ cm^{-3}	μ/ cm^2 V^{-1} *S*	*D*
C0	6.089×10^{-3}	0.120	6.519×10^{-18}	5.830×10^{-3}	1.522×10^{-4}
C1	5.464×10^{-3}	0.122	9.298×10^{-18}	3.668×10^{-3}	9.574×10^{-5}
C2	5.179×10^{-3}	0.140	9.500×10^{-18}	3.403×10^{-3}	8.883×10^{-5}
C3	3.652×10^{-3}	0.148	6.913×10^{-18}	3.298×10^{-3}	8.608×10^{-5}

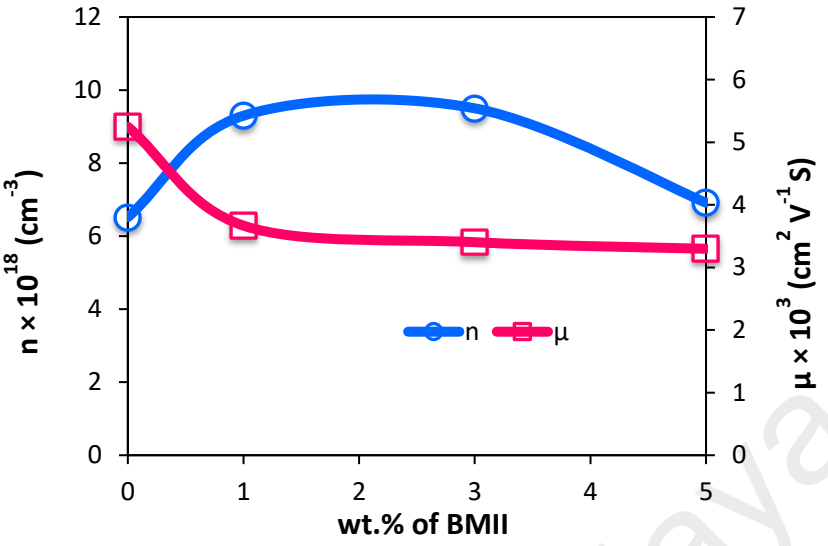

Figure 4.33: Relationship between ***n*** and ***μ*** of the PhCh-EC-DMF-TPAI-LiI based gel polymer electrolyte with various weight percentage of BMII.

4.4.2. FTIR Analysis

FTIR spectra of the pure BMII is shown in Figure 4.34 and all the peaks assigned to the spectra are tabulated in Table 4.10. The peak assigned to the C-H vibration mode for cyclic BMI^+ appears at wavenumber 748 cm^{-1}. Characteristic peak at 1560 cm^{-1} observed is due to the presence of C-N bending mode. A sharp and strong peak at 1170 cm^{-1} is attributed to the stretching mode of CH_3-N. The doublet peaks at 1330 and 1380 cm^{-1} are due to the CH_2 deformation of cyclic BMI^+ and CH_3 asymmetric stretching mode, respectively. However, the CH_3 symmetric stretching mode peak arises at 1460 cm^{-1}. Another sharp peak present at 1560 cm^{-1} is assigned to C-C and C-N bending mode. Other peaks at 2870, 2930 and 2960 cm^{-1} are attributed to υ(C-H) attached to the BMI^+ ring. The two peaks at 3070 and 3140 cm^{-1} are assigned to the υ(=C-H) mode.

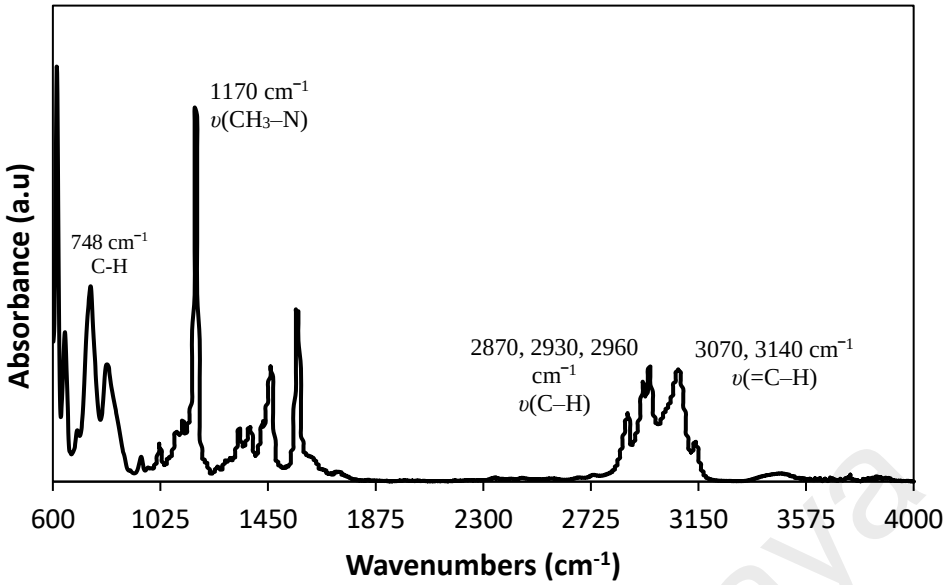

Figure 4.34: FTIR spectra of pure BMII ionic liquid.

Table 4.10: Peak assignments of pure ionic liquid BMII

Vibrational mode	Wavenumbers/ cm^{-1}		References
	Current study	**Literature review**	
C-H vibration mode for cyclic BMI^+	748	740	Ramesh et al. (2011)
$\upsilon(CH_3–N)$	1170	1162	Sim et al. (2014)
			Sim et al. (2016)
		1170	Moumene et al. (2014)
CH_2 deformation of cyclic BMI^+	1330	1332	Ramesh et al. (2011)
CH_3 asymmetric stretching mode	1380	1388	Ramesh et al. (2011)
CH_3 symmetric stretching mode	1460	1465	Ramesh et al. (2011)
C-C and C-N bending mode	1560	1576	Ramesh et al. (2011)
υ(C–H) attached to the BMI^+ ring	2870, 2930, 2960	2879, 2938, 2965	Sim et al. (2014)
		2960, 2931, 2871	Sim et al. (2016)
		2968, 3119, 3168	Ramesh et al. (2011)
υ(=C–H)	3070, 3140	3072, 3138	Sim et al. (2016)
		3116, 3152	Sim et al. (2014)
		3132	Moumene et al. (2014)

The FTIR spectrum of the PhCh-EC-DMF-TPAI-LiI with various wt.% of BMII are presented in Figure 4.35. The interaction behaviour of the IL with the other components in the GPE can be observed by the changes in the FTIR peaks in terms of intensity, bandwidth and position (Huang et al., 2013). Deconvolution was conducted to certain significant regions in order to study the interaction within the GPEs. Similar to the previous single and double salts systems, four deconvolution regions from the FTIR spectrum were identified for possible coordination environment. The four areas which undergo deconvolution are depicted in Figure 4.35 which are (i) ether, (ii) amide, (iii) carbonyl and (iv) amine/hydroxyl region.

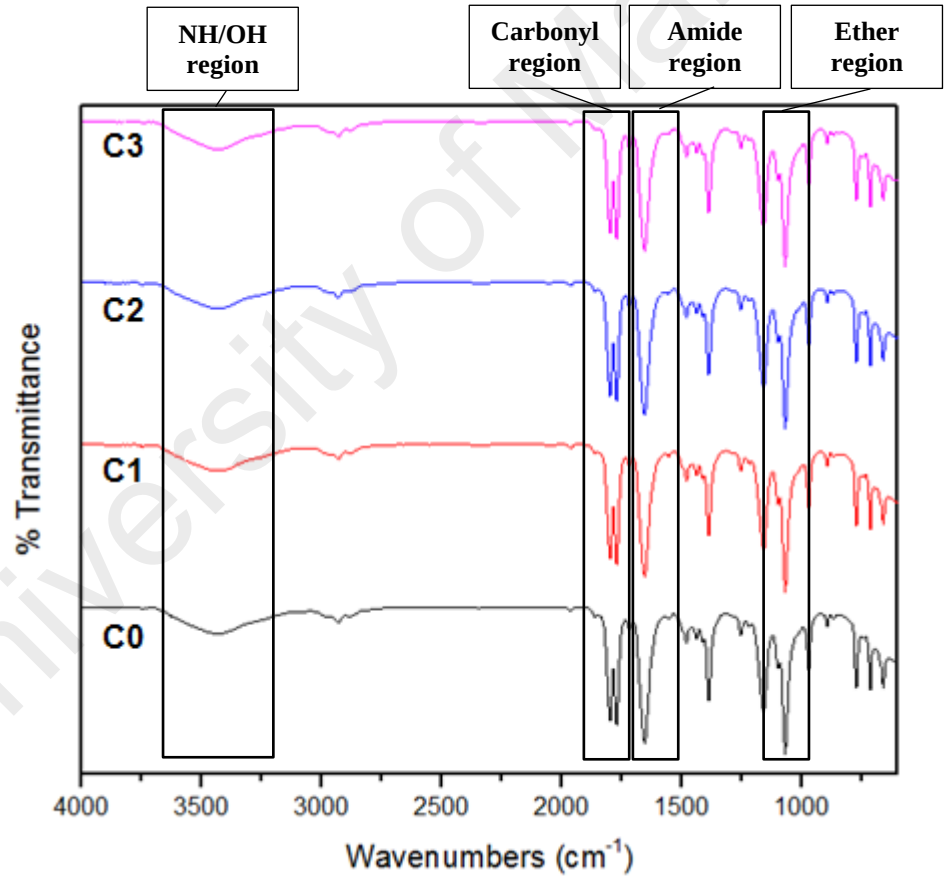

Figure 4.35: FTIR spectra for PhCh based gel polymer electrolytes containing various wt.% of BMII.

FTIR spectra of ether group in the range from 1000 to 1200 cm^{-1}

There are eight deconvoluted peaks obtained from the ether region from wavenumber 1000 to 1200 cm^{-1}. Relative areas of each of the peaks are presented in Figure 4.36. The first deconvoluted peak at 1047 cm^{-1} is dedicated to the H-bonded C-O-C stretching mode. Similar behaviour is observed to this highly sensitive peak, i.e. the intensity increases with increasing BMII content. The peak intensity at 1069 cm^{-1} which is attributed to the CH_3 rocking mode decreases as the BMII content increases. The highest intensity peak at 1079 cm^{-1} is assigned to cations complexing to the C-O-C site. The peak at 1095 cm^{-1} is dedicated to the crystalline complexes. The intensity of the peaks decrease as the BMII content increases. Another peak at 1104 cm^{-1} dedicated to the coordination of cations with C-O-C site appears after BMII is added to the gel electrolytes suggesting the coordination between BMI^+ with the ether site which in turn stifles the crystallinity of the GPE matrix. In the discussion of FTIR of double salts (*Section* 4.3.2), the two peaks at 1156 and 1171 cm^{-1} did not show much change with different salt ratios. However, significant changes can be seen to the peak intensity after the BMII is introduced to the GPE system. Changes in intensity of peak 1156 cm^{-1} which is attributed to the stretching vibration of C-O from EC might be due to the coordination between EC and with BMII. Peak 1171 cm^{-1} increases with increasing BMII content might be due to the contribution of CH_3-N stretching mode which can be seen from the FTIR spectra of pure BMII.

FTIR spectra of amide/carbonyl group in the range from 1580 to 1840 cm^{-1}

The presence of the C=O group in most of the components in the PhCh based GPEs allows possible coordination with the other species. Deconvolution has been done to the first part of this region, amide region, in the range between 1580 and 1700 cm^{-1}. The contributions of each resolved peak is presented in histogram in Figure 4.37. The

first two peaks in this region attributed to the ordered and disordered interfacial domains from polymer arise at 1637 and 1649 cm^{-1}, respectively. Unlike in double salt system, no significant changes can be seen to the peak intensity of these peaks with variation of BMII content. The most intense peak at 1660 cm^{-1} is dedicated to carboxamide group from chitosan. Low intensity peak at 1668 cm^{-1} is detected in the double salt system. The peak diminished as soon as the BMII is added to the system. The peak attributed to the DMF arised at 1674 cm^{-1}. Overall, the peaks in this first half of the C=O region shows not much difference with the increasing of BMII wt. %.

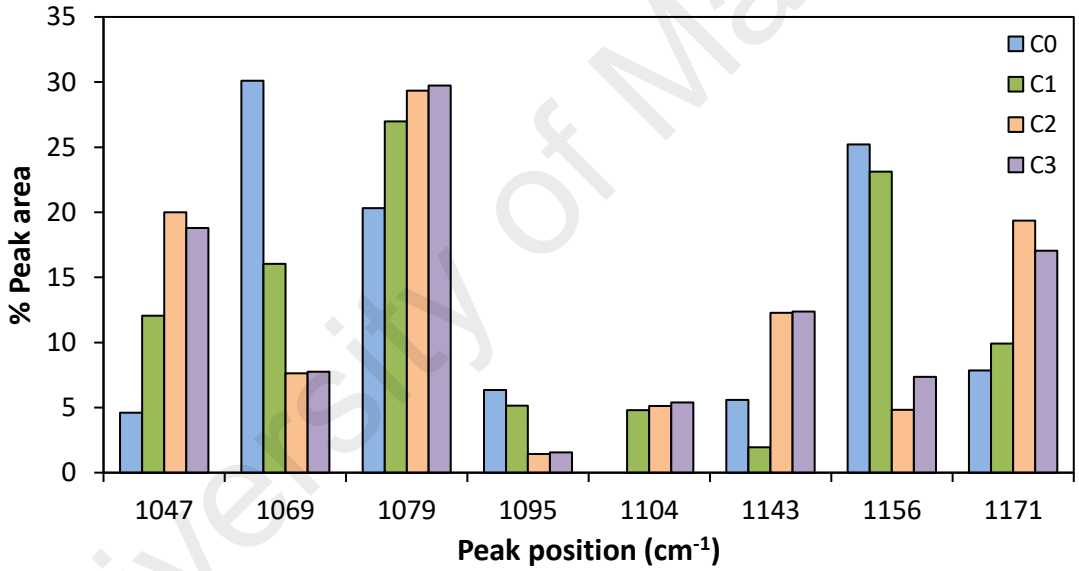

Figure 4.36: Relative FTIR percentage area in the region of 1000-1200 cm^{-1}.

The second part of the C=O region is located between 1700 and 1840 cm^{-1}. This region corresponds to the presence of amide $R(C=O)NR_2$ group. The relative areas of each of the resolved peaks are shown in Figure 4.38. Similar observation with the previous two systems, the intensity of the peak at 1718 cm^{-1} which is due to the coordination of cations to the phthalimido group in PhCh is seen to be independent of the BMII content. The intensity of the peaks attributed to the EC at 1773 and 1805 cm^{-1}

showed increment after addition of BMII, but then no changes are observed as the content of BMII is increased. The peak associated to the non-bonded C=O at 1788 cm^{-1} dramatically dropped in intensity after BMII is added.

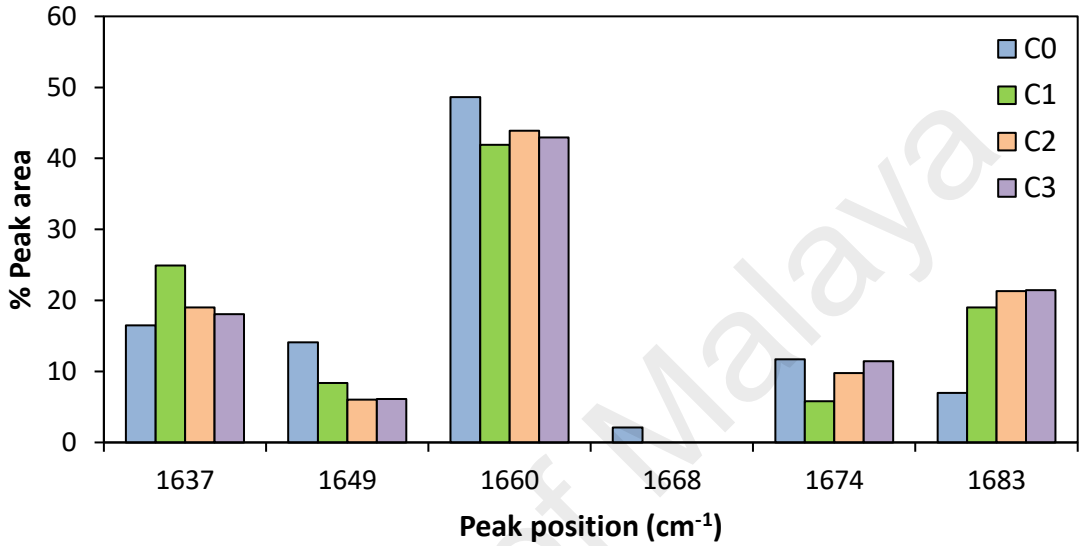

Figure 4.37: Relative FTIR percentage area in the region of 1580-1700 cm^{-1}.

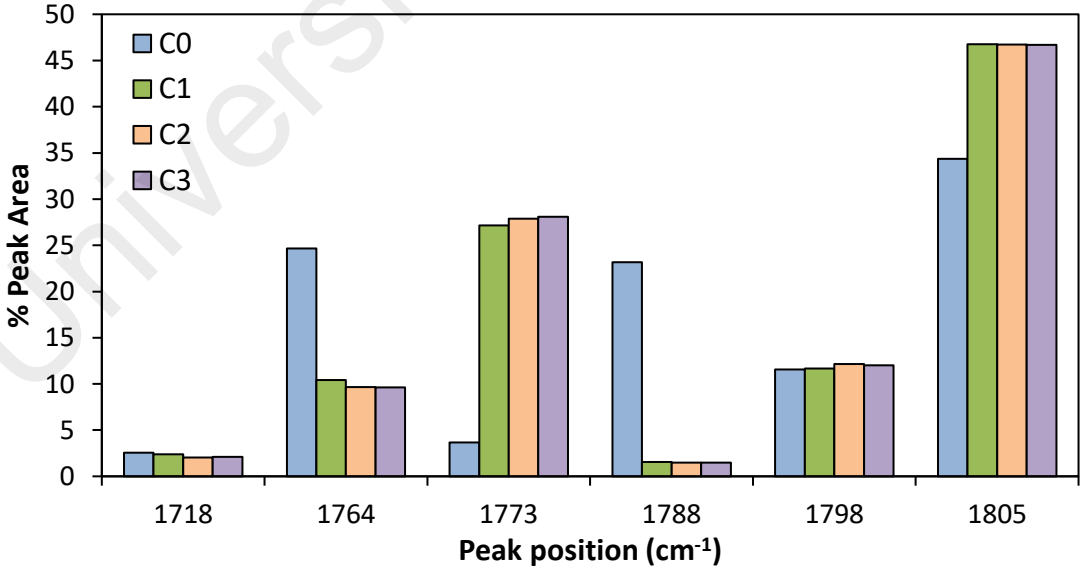

Figure 4.38: Relative FTIR percentage area in the region of 1700-1840 cm^{-1}.

FTIR spectra of amine/hydroxyl group in the range from 3130 to 3700 cm^{-1}

Figure 4.39 presents the contribution of the deconvoluted peaks from the region of 3130 to 3700 cm^{-1} involving amine and hydroxyl groups of the GPEs. The peak at 3247 cm^{-1} assigned to the coordination of N-H to C-O-C is observed to increase with BMII content. However, the small peaks at 3363, 3535 and 3593 cm^{-1} which attributed to coordination of N-H to C=O, N-H band with cations and O-H with cations, respectively, show no significant changes as the BMII content is increased. Lower intensity of these three significant peaks compared to the other two previous system might likely be the reason for the decreasing in conductivity. The most intense peak at 3451 cm^{-1} due to the O-H shifted the band of PhCh from the original position of 3442 cm^{-1}. The intensity of the peak is seen to be decreasing with increasing wt.% of BMII. In single salts system, the peak at 3634 cm^{-1} which is assigned to the coordination of cation slightly increase with increasing salt content. After the introduction of second iodide salt, the peak intensity started to decrease due to the competition between the two existing cations. Then, after addition of BMII ionic liquid, the peak disappeared suggesting no more of cations coordination occurred at this band.

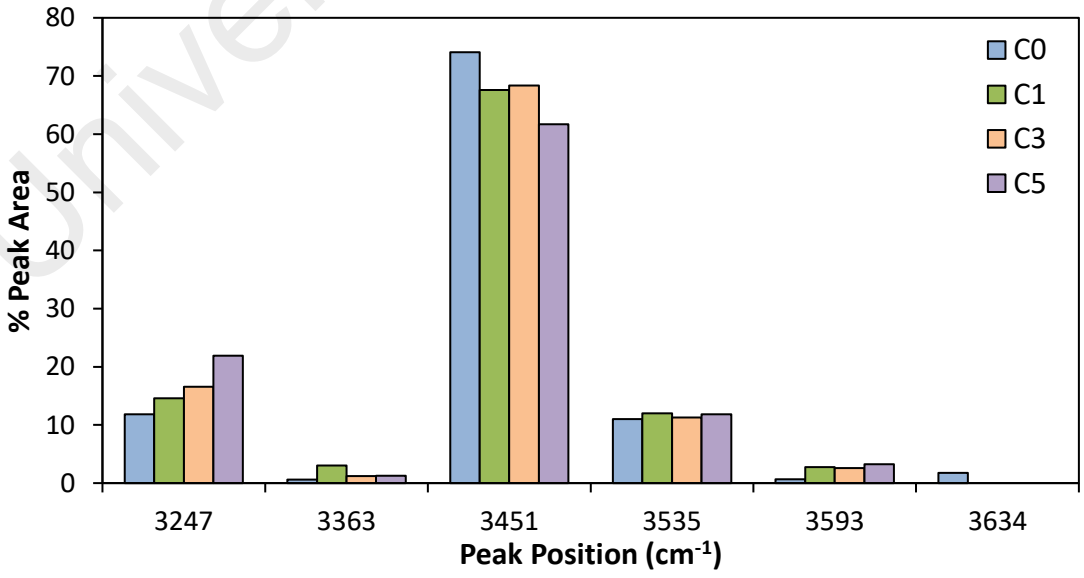

Figure 4.39: Relative FTIR percentage area in the region of 3130-3700 cm^{-1}.

4.4.3. XRD Analysis

XRD pattern of the GPEs containing various weight percentages of BMII ionic liquid are presented in Figure 4.40. There is no obvious trend shown by the intensity of the peaks as the content of BMII is increased. Different observation was obtained to this series compared to the previous systems where the peak intensity will decrease parallel to the increasing of ionic conductivity values. This might be due increasing interaction among the molecules of BMII with the gel components including polymer, salts and plasticizers as the BMII content increases, thus the gel network becomes more compact (Huo et al., 2015). Consequently, the viscosity of the GPE increases leading to the decreases in ionic conductivity (Shalu et al., 2013).

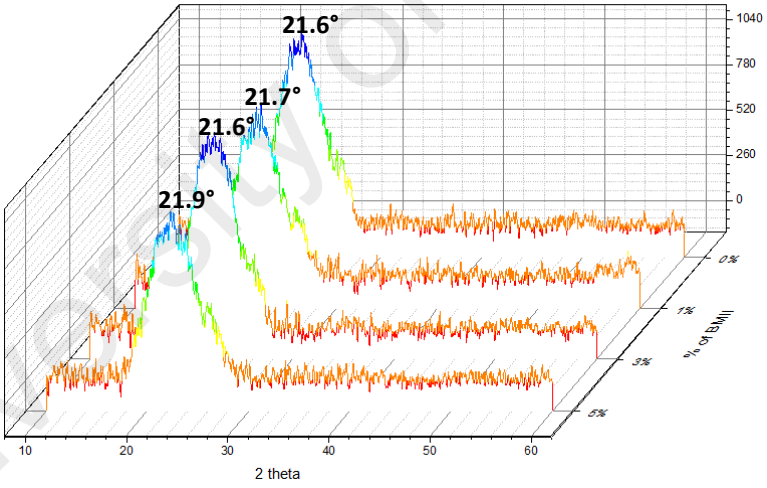

Figure 4.40: XRD pattern of the PhCh-EC-DMF-TPAI-LiI based GPE with different wt. % of BMII

4.4.4. DSSC Analysis

In order to enhance the efficiency of the dye-sensitized solar cells, IL is added into the polymer electrolyte system (Bandara et al., 2010c; Singh et al., 2011; Singh et al., 2009). In this work, *1*-butyl-*3*-methylimidazolium iodide (BMII) was introduced into the

most efficient PhCh-EC-DMF-TPAI-LiI GPE, B3, also designed as C0 in this system. The effect of BMII on the mixed iodide electrolytes in photovoltaic aspect can be observed in the I-V curve as shown in Figure 4.41.

The DSSC parameters have been tabulated in Table 4.11. The efficiency of the DSSC increases after 1 wt.% of BMII is added to the gel polymer electrolyte with the value of 6.69 %. The J_{SC}, V_{OC} and *FF* obtained are 16.53 mA cm^{-2}, 0.62 *V* and 0.65, respectively. The addition of IL into the polymer electrolyte matrix has enhanced the overall solar cell efficiency. It shows that the dispersal of IL having low viscosity has increased the homogeneity, reduced the crystallinity of polymer electrolyte and provided more amorphous regions which may assist in the contact of working electrode and electrolyte (Singh et al., 2011). The J_{SC} value is decreased after the increment of the DSSC efficiency, meanwhile the V_{OC} value was seen to increase. This might correlates to the upward shift of the conduction band edge induced by the adsorption of low-charge-density cations on the surface of TiO_2 nanocrystals. According to Shi et al. (2008), V_{OC} value increase as the equilibrium potentials of I^-/I_3^- and V_{OC} of DSSCs increased with the decrease of total concentrations of I^- and I_3^- in the IL mixtures. At higher BMII content, the DSSC performance drops until the efficiency value reached 5.97 % with 5 wt. % of IL. The J_{SC}, V_{OC} and *FF* are 14.82 mA cm^{-2}, 0.61 *V* and 0.66, respectively.

Table 4.11: DSSC parameters of the GPEs with various content of BMII

Designations	J_{SC}**/ mA cm^{-2}**	V_{OC}**/ V**	***FF***	***η*/ %**
C0	17.29	0.59	0.62	6.36
C1	**16.53**	**0.62**	**0.65**	**6.69**
C2	14.98	0.63	0.68	6.41
C3	14.82	0.61	0.66	5.97

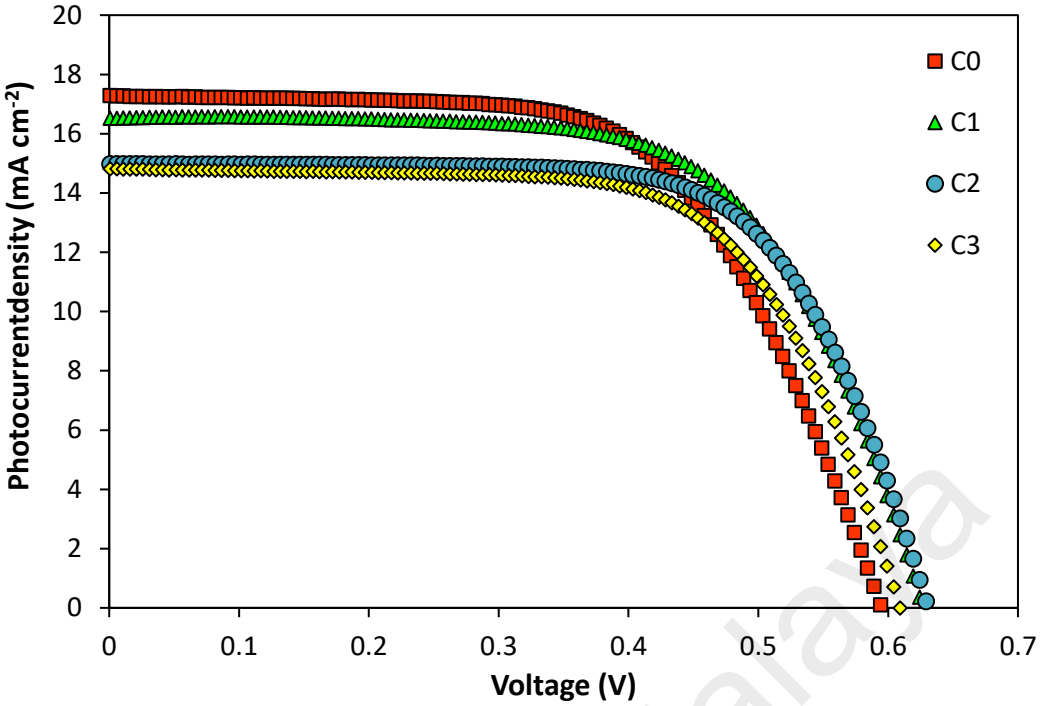

Figure 4.41: *J-V* curve of the GPEs with various content of BMII.

CHAPTER 5 : CONCLUSIONS

5.1. Conclusions

N-Phthaloylchitosan (PhCh) has been prepared by reacting chitosan with phthalic anhydride; success of the phthaloylation procedure was confirmed by ^{1}H NMR, FTIR and XRD characterizations. This modified chitosan, PhCh, showed a great potential as a gel polymer electrolyte host. The chemical structure of N-phthaloylchitosansynthesized was confirmed by FTIR and ^{1}H NMR while its amorphousness by XRD. In the solubility test, PhCh was observed to be completely soluble in DMF, DMSO, DMAc and pyridine. Thus, DMF was used as the solvent and also plasticizer in the preparation of PhCh based gel polymer electrolytes.

A gel polymer electrolyte was successfully prepared with *N*-phthaloylchitosan as the polymer host matrix with variation in EC and DMF as the entrapped solvents. The entrapment of TPA^{+} in these interactions enabled more mobility for I^{-} ions as TPAI content increases, which in turn lead to higher conductivities and solar cell efficiencies. The optimum conditions was obtained for the gel polymer electrolyte which showed the highest conductivity of 5.46×10^{-3} S cm^{-1} at room temperature and exhibited the best performance in DSSC with efficiency of 5.0%. XRD analyses revealed that addition of tetrapropylammonium iodide (TPAI) in GPE further reduced the amorphousness of the PhCh. FTIR analyses indicated significant occurrence of both inter- and intra hydrogen bonded interactions and evidence of ion complexation between polymer–plasticizer–salt.

Introduction of smaller cations, Li^{+}, to the gel polymer electrolytes along with the bulky cations was shown to improve the photogeneration of electrons at the dye with optimum condition found to increase the efficiency to 6.36% though its conductivity was not the highest. This results also showed that the conductivity parameter was not necessarily a direct indicator of the optimum efficiency for this GPE system since various other transport processes also occur in the DSSC. Nonetheless the synergistic salt-matrix

interactions have shown that properties of the binary salt system were superior to that of either single salt system.

Ionic liquid was introduced to the binary salt system gel polymer electrolytes with the goal to improve the efficiency of the dye sensitized solar cell. The ionic conductivity was further dropped with more BMII added from 6.089×10^{-3} to 3.652×10^{-3} S cm^{-1}. However, the performance of the DSSC slightly increased after 1 wt.% of BMII was added to the GPE with the value of 6.69 %.

5.2. Suggestions for future studies

Further work should be carried out to improve the performance of PhCh based polymer electrolytes in the devices. Interesting approaches are:

1. To characterize these electrolytes using rheology in order to determine the elastic and viscous properties.
2. To improve the ionic conductivity and efficiency of DSSC by substituting EC/DMF with succinonitrile as it has high dielectric constant which shows the ability of succinonitrile to dissociate the salts for high ionic conductivity to the larger extent.
3. To improve the efficiency of the DSSC by adding *4*-tertbutyl pyridine (TBP). By introducing TBP in the gel polymer electrolytes, V_{OC} of the DSSC is expected to increase, thus may lead to increasing in value of efficiency.

REFERENCES

Abate, A., Petrozza, A., Roiati, V., Guarnera, S., Snaith, H., Matteucci, F., Lanzani, G., Metrangolo, P., and Resnati, G. (2012). A polyfluoroalkyl imidazolium ionic liquid as iodide ion source in dye sensitized solar cells. *Organic Electronics, 13*(11), 2474-2478.

Alves, N. M., and Mano, J. F. (2008). Chitosan derivatives obtained by chemical modifications for biomedical and environmental applications. *International Journal of Biological Macromolecules, 43*(5), 401-414.

Aranaz, I., Mengíbar, M., Harris, R., Paños, I., Miralles, B., Acosta, N., Galed, G., and Heras, A. (2009). Functional characterization of chitin and chitosan. *Current Chemical Biology, 3*, 203-230.

Arof, A. K., Aziz, M. F., Noor, M. M., Careem, M. A., Bandara, L. R. A. K., Thotawatthage, C. A., Rupasinghe, W. N. S., and Dissanayake, M. A. K. L. (2014a). Efficiency enhancement by mixed cation effect in dye-sensitized solar cells with a PVdF based gel polymer electrolyte. *International Journal of Hydrogen Energy, 39*(6), 2929-2935.

Arof, A. K., Jun, H. K., Sim, L. N., Kufian, M. Z., and Sahraoui, B. (2013). Gel polymer electrolyte based on LiBOB and PAN for the application in dye-sensitized solar cells. *Optical Materials, 36*(1), 135-139.

Arof, A. K., Naeem, M., Hameed, F., Jayasundara, W. J. M. J. S. R., Careem, M. A., Teo, L. P., and Buraidah, M. H. (2014b). Quasi solid state dye-sensitized solar cells based on polyvinyl alcohol (PVA) electrolytes containing I^-/I^{-3} redox couple. *Optical and Quantum Electronics, 46*, 143-154.

Aziz, M. F., Buraidah, M. H., Careem, M. A., and Arof, A. K. (2015). PVA based gel polymer electrolytes with mixed iodide salts (K^+I^- and $Bu_4N^+I^-$) for dye-sensitized solar cell application. *Electrochimica Acta, 182*, 217-223.

Aziz, M. F., Noor, I. M., Sahraoui, B., and Arof, A. K. (2014). Dye-sensitized solar cells with PVA–KI–EC–PC gel electrolytes. *Optical and Quantum Electronics, 46*(1), 133-141.

Aziz, N. A., Majid, S. R., and Arof, A. K. (2012). Synthesis and characterizations of phthaloyl chitosan-based polymer electrolytes. *Journal of Non-Crystalline Solids, 358*(12–13), 1581-1590.

Badawy, M. E. I., Rabea, E. I., Rogge, T. M., Stevens, C. V., Smagghe, G., Steurbaut, W., and Höfte, M. (2004). Synthesis and fungicidal activity of new N,O-Acyl chitosan derivatives. *Biomacromolecules, 5*(2), 589-595.

Bandara, T. M. W. J., Aziz, M. F., Fernando, H. D. N. S., Careem, M. A., Arof, A. K., and Mellander, B.-E. (2015). Efficiency enhancement in dye-sensitized solar cells with a novel PAN-based gel polymer electrolyte with ternary iodides. *Journal of Solid State Electrochemistry, 19*, 2353–2359.

Bandara, T. M. W. J., Dissanayake, M. A. K. L., Albinsson, I., and Mellander, B. E. (2010a). Dye-sensitized, nano-porous TiO_2 solar cell with poly(acrylonitrile): MgI_2 plasticized electrolyte. *Journal of Power Sources, 195*(11), 3730-3734.

Bandara, T. M. W. J., Dissanayake, M. A. K. L., and Mellander, B. E. (2010b). Dye sensitized solar cells with poly(acrylonitrile) based plasticized electrolyte containing MgI_2. *Electrochimica Acta, 55*(6), 2044-2047.

Bandara, T. M. W. J., Ekanayake, P., Dissanayake, M. A. K. L., Albinsson, I., and Mellander, B. E. (2010c). A polymer electrolyte containing ionic liquid for possible applications in photoelectrochemical solar cells. *Journal of Solid State Electrochemistry, 14*, 1221–1226.

Bandara, T. M. W. J., Jayasundara, W. J. M. J. S. R., Dissanayake, M. A. K. L., Fernando, H. D. N. S., Furlani, M., Albinsson, I., and Mellander, B. E. (2014a). Quasi solid state polymer electrolyte with binary iodide salts for photo-electrochemical solar cells. *International Journal of Hydrogen Energy, 39*(6), 2997–3004.

Bandara, T. M. W. J., Jayasundara, W. J. M. J. S. R., Dissanayake, M. A. K. L., Furlani, M., Albinsson, I., and Mellander, B. E. (2013). Effect of cation size on the performance of dye sensitized nanocrystalline TiO_2 solar cells based on quasi-solid state PAN electrolytes containing quaternary ammonium iodides. *Electrochimica Acta, 109*, 609-616.

Bandara, T. M. W. J., Jayasundara, W. J. M. J. S. R., Fernado, H. D. N. S., Dissanayake, M. A. K. L., De Silva, L. A. A., Fernando, P. S. L., Furlani, M., and Mellander, B.-E. (2014b). Efficiency enhancement of dye-sensitized solar cells with PAN:CsI:LiI quasi-solid state (gel) electrolytes. *Journal of Applied Electrochemistry, 44*(8), 917-926.

Bandara, T. M. W. J., Mellander, B. E., Albinsson, I., and Dissanayake, M. A. K. L. (2009). Effect of thermal history and characterization of plasticized, composite polymer electrolyte based on PEO and tetrapropylammonium iodide salt ($Pr_4N^+I^-$). *Solid State Ionics, 180*(4–5), 362-367.

Bandara, T. M. W. J., Svensson, T., Dissanayake, M. A. K. L., Furlani, M., Jayasundara, W. J. M. J. S. R., and Mellander, B. E. (2012). Tetrahexylammonium iodide containing solid and gel polymer electrolytes for dye sensitized solar cells. *Energy Procedia, 14*(0), 1607-1612.

Bar, N., and Basak, P. (2014). Quasi-solid semi-interpenetrating polymer networks as electrolytes: Part II. Assessing the modes of ion–ion and ion–polymer interactions employing mid-fourier transform infrared vibrational spectroscopy. *The Journal of Physical Chemistry C, 118*(20), 10640-10650.

Bar, N., Ramanjaneyulu, K., and Basak, P. (2014). Quasi-solid semi-interpenetrating polymer networks as electrolytes: Part I. Dependence of physicochemical characteristics and ion conduction behavior on matrix composition, cross-link density, chain length between cross-links, molecular entanglements, charge carrier concentration, and nature of anion. *The Journal of Physical Chemistry C, 118*(1), 159-174.

Barea, E. M., and Bisquert, J. (2013). Properties of chromophores determining recombination at the TiO_2–dye–electrolyte interface. *Langmuir, 29*(28), 8773-8781.

Baril, D., Michot, C., and Armand, M. (1997). Electrochemistry of liquids vs. solids: Polymer electrolytes *Solid State Ionics*, *94*, 35-47.

Barth, A. (2000). The infrared absorption of amino acid side chains. *Progress in Biophysics and Molecular Biology, 74*(3–5), 141-173.

Bella, F., Mobarak, N. N., Jumaah, F. N., and Ahmad, A. (2015). From seaweeds to biopolymeric electrolytes for third generation solar cells: An intriguing approach. *Electrochimica Acta, 151*, 306-311.

Bella, F., Naira, J. R., and Gerbaldi, C. (2013). Towards green, efficient and durable quasi-solid dyesensitized solar cells integrated with a cellulose-based gel-polymer electrolyte optimized by a chemometric DoE approach. *RSC Advances, 3*, 15993–16001.

Bella, F., Sacco, A., Pugliese, D., Laurenti, M., and Bianco, S. (2014). Additives and salts for dye-sensitized solar cells electrolytes: What is the best choice? *Journal of Power Sources, 264*(0), 333-343.

Bian, F., Jia, L., Yu, W., and Liu, M. (2009). Self-assembled micelles of N-phthaloylchitosan-g-polyvinylpyrrolidone for drug delivery. *Carbohydrate Polymers, 76*, 454–459.

Bicak, N. (2005). A new ionic liquid: 2-hydroxy ethylammonium formate. *Journal of Molecular Liquids, 116*, 15– 18.

Bidikoudi, M., Perganti, D., Karagianni, C.-S., and Falaras, P. (2015). Solidification of ionic liquid redox electrolytes using agarose biopolymer for highly performing dye-sensitized solar cells. *Electrochimica Acta, 179*, 228-236.

Binette, A., and Gagnon, J. (2007). Regioselective silylation of N-phthaloylchitosan with TBDMS and TBDPS groups. *Biomacromolecules, 8*(6), 1812-1815.

Bodnar, M., Hartmann, J. F., and Borbely, J. (2006). Synthesis and study of cross-linked chitosan-N-poly(ethylene glycol) nanoparticles. *Biomacromolecules, 7*(11), 3030-3036.

Bond, W. L. (1965). Measurement of the refractive indices of several crystals. *Journal of Applied Physics, 36*(5), 1674-1677.

Bordenave, N., Grelier, S., and Coma, V. (2008). Advances on selective C-6 oxidation of chitosan by TEMPO. *Biomacromolecules, 9*(9), 2377-2382.

Bruice, P. Y. (2004). *Organic Chemistry*. United States: Pearson Education, Inc.

Bu, I. Y. Y., and Zheng, J. (2015). A new type of counter electrode for dye sensitized solar cells based on solution processed SnO_2 and activated carbon. *Materials Science in Semiconductor Processing, 39*, 223-228.

Buraidah, M. H., Teo, L. P., Majid, S. R., Yahya, R., Taha, R. M., and Arof, A. K. (2010). Characterizations of chitosan-based polymer electrolyte photovoltaic cells. *International Journal of Photoenergy, 2010*, 805836, 7 pages.

Buraidah, M. H., Teo, L. P., Yusuf, S. N. F., Noor, M. M., Kufian, M. Z., Careem, M. A., Majid, S. R., Taha, R. M., and Arof, A. K. (2011). TiO_2/chitosan-NH_4I(+I_2)-BMII-based dye-sensitized solar cells with anthocyanin dyes extracted from black rice and red cabbage. *International Journal of Photoenergy, 2011*, 273683, 11 pages.

Calogero, G., and Marco, G. D. (2008). Red Sicilian orange and purple eggplant fruits as natural sensitizers for dye-sensitized solar cells. *Solar Energy Materials and Solar Cells, 92*(11), 1341-1346.

Cameron, P. J., and Peter, L. M. (2003). Characterization of titanium dioxide blocking layers in dye-sensitized nanocrystalline solar cells. *The Journal of Physical Chemistry B, 107*(51), 14394-14400.

Casettari, L., Vllasaliu, D., Castagnino, E., Stolnik, S., Howdle, S., and Illum, L. (2012). PEGylated chitosan derivatives: Synthesis, characterizations and pharmaceutical applications. *Progress in Polymer Science, 37*(5), 659-685.

Cha, S. Y., Lee, Y.-G., Kang, M.-S., and Kang, Y. S. (2010). Correlation between ionic conductivity and cell performance in solid-state dye-sensitized solar cells employing polymer electrolyte. *Journal of Photochemistry and Photobiology A: Chemistry, 211*(2–3), 193-196.

Chaisorn, W., Prasertsan, P., O-Thong, S., and Methacanon, P. (2016). Production and characterization of biopolymer as bioflocculant from thermotolerant Bacillus subtilis WD161 in palm oil mill effluent. *International Journal of Hydrogen Energy, 41*(46), 21657-21664.

Chang, H., and Lo, Y.-J. (2010). Pomegranate leaves and mulberry fruit as natural sensitizers for dye-sensitized solar cells. *Solar Energy, 84*, 1833–1837.

Chang, H., Wu, H. M., Chen, T. L., Huang, K. D., Jwo, C. S., and Lo, Y. J. (2010). Dye-sensitized solar cell using natural dyes extracted from spinach and ipomoea. *Journal of Alloys and Compounds, 495*(2), 606-610.

Chatzivasiloglou, E., Stergiopoulos, T., Kontos, A. G., Alexis, N., Prodromidis, M., and Falaras, P. (2007). The influence of the metal cation and the filler on the performance of dye-sensitized solar cells using polymer-gel redox electrolytes. *Journal of Photochemistry and Photobiology A: Chemistry, 192*(1), 49–55.

Cui, H., Zhu, G., Liu, X., Liu, F., Xie, Y., Yang, C., Lin, T., Gu, H., and Huang, F. (2015). Niobium nitride Nb_4N_5 as a new high-performance electrode material for supercapacitors. *Advanced Science, 2*(12), 1500126.

Das, S., and Ghosh, A. (2015). Effect of plasticizers on ionic conductivity and dielectric relaxation of PEO-$LiClO_4$ polymer electrolyte. *Electrochimica Acta, 171*, 59-65.

de la Torre, P. M., Torrado, S., and Torrado, S. (2003). Interpolymer complexes of poly(acrylic acid) and chitosan: Influence of the ionic hydrogel-forming medium. *Biomaterials, 24*(8), 1459–1468.

de Léis, C. M., Nogueira, A. R., Kulay, L., and Tadini, C. C. (2017). Environmental and energy analysis of biopolymer film based on cassava starch in Brazil. *Journal of Cleaner Production, 143*, 76-89.

Denuziere, A., Ferrier, D., Damour, O., and Domard, A. (1998). Chitosan-chondroitin sulfate and chitosan-hyaluronate polyelectrolyte complexes: Biological properties. *Biomaterials, 19*(14), 1275-1285.

Devore, J. R. (1951). Refractive indices of rutile and sphalerite. *Journal of the Optical Society of America, 41*(6), 416-417.

Dissanayake, M. A. K. L., Bandara, L. R. A. K., Bokalawala, R. S. P., Jayathilaka, P. A. R. D., Ileperuma, O. A., and Somasundaram, S. (2002). A novel gel polymer electrolyte based on polyacrylonitrile (PAN) and its application in a solar cell. *Materials Research Bulletin, 37*(5), 867-874.

Dissanayake, M. A. K. L., Jayathissa, R., Seneviratne, V. A., Thotawatthage, C. A., Senadeera, G. K. R., and Mellander, B. E. (2014). Polymethylmethacrylate (PMMA) based quasi-solid electrolyte with binary iodide salt for efficiency enhancement in TiO_2 based dye sensitized solar cells. *Solid State Ionics, 265*(0), 85-91.

Dissanayake, M. A. K. L., Thotawatthage, C. A., Senadeera, G. K. R., Bandara, T. M. W. J., Jayasundera, W. J. M. J. S. R., and Mellander, B. E. (2012). Efficiency enhancement by mixed cation effect in dye-sensitized solar cells with PAN based gel polymer electrolyte. *Journal of Photochemistry and Photobiology A: Chemistry, 246*(0), 29-35.

Divakaran, R., and Pillai, V. N. S. (2004). Mechanism of kaolinite and titanium dioxide flocculation usingchitosan—assistance by fulvic acids? *Water Research, 38*, 2135–2143.

Dodane , V., and Vilivalam, V. D. (1998). Pharmaceutical applications of chitosan. *Pharmaceutical Science & Technology Today, 1*(6), 246-253.

Dodge, M. J. (1986). Refractive Index. In M. J. Weber (Ed.), *Handbook of Laser Science and Technology* (Vol. 4). CRC Press: Boca Raton.

El-Sawy, N. M., El-Rehim, H. A. A., Elbarbary, A. M., and Hegazy, E. S. A. (2010). Radiation-induced degradation of chitosan for possible use as a growth promoter in agricultural purposes. *Carbohydrate Polymers, 79*, 555–562.

Ellis-Gibbings, L., Johansson, V., Walsh, R. B., Kloo, L., Quinton, J. S., and Andersson, G. G. (2012). Formation of N719 dye multilayers on dye sensitized solar cell photoelectrode surfaces investigated by direct determination of element concentration depth profiles. *Langmuir, 28*(25), 9431-9439.

Felicio, S. G. F., Sierakowski, M. R., Petkowicz, C., Silveira, J., Lubambo, A., and de Freitas, R. (2008). Spherical aggregates obtained from N-carboxymethylation and acetylation of chitosan. *Colloid and Polymer Science, 286*(12), 1387-1394.

Fernandez-Saiz, P., Lagaron, J. M., Hernandez-Muñoz, P., and Ocio, M. J. (2008). Characterization of antimicrobial properties on the growth of S. aureus of novel

renewable blends of gliadins and chitosan of interest in food packaging and coating applications. *International Journal of Food Microbiology, 124*, 13–20.

Finkenstadt, V. L. (2005). Natural polysaccharides as electroactive polymers. *Applied Microbiology and Biotechnology, 67*(6), 735–745.

Fredheim, G. E., and Christensen, B. E. (2003). Polyelectrolyte Complexes: Interactions between Lignosulfonate and Chitosan. *Biomacromolecules, 4*(2), 232-239.

Gao, L., Lemarchand, F., and Lequime, M. (2012). Exploitation of multiple incidences spectrometric measurements for thin film reverse engineering. *Optics Express, 20*(14), 15734-15751.

Gao, Y., Zhang, Z., Chen, L., Gu, W., and Li, Y. (2009). Synthesis of 6-N,N,N-trimethyltriazole chitosan via "click chemistry" and evaluation for gene delivery. *Biomacromolecules, 10*(8), 2175-2182.

Ghosh, R., Brennaman, M. K., Uher, T., Ok, M.-R., Samulski, E. T., McNeil, L. E., Meyer, T. J., and Lopez, R. (2011). Nanoforest Nb_2O_5 photoanodes for dye-sensitized solar cells by pulsed laser deposition. *ACS Applied Materials & Interfaces, 3*(10), 3929-3935.

Gokilamani, N., Muthukumarasamy, N., Thambidurai, M., Ranjitha, A., and Velauthapillai, D. (2014). Grape pigment (malvidin-3-fructoside) as natural sensitizer for dye-sensitized solar cells. *Materials for Renewable and Sustainable Energy, 3*(3), 33, 1-7.

Göktepe, F., Bozkurt, A., and Günday, Ş. T. (2008). Synthesis and protonconductivity of poly(styrene sulfonicacid)/heterocycle-based membranes. *Polymer International, 57*, 133–138.

Gómez-Ortíz, N. M., Vázquez-Maldonado, I. A., Pérez-Espadas, A. R., Mena-Rejón, G. J., Azamar-Barrios, J. A., and Oskam, G. (2010). Dye-sensitized solar cells with natural dyes extracted from achiote seeds. *Solar Energy Materials and Solar Cells, 94*(1), 40-44.

Grätzel, M. (2005). Solar energy conversion by dye-sensitized photovoltaic cells. *Inorganic Chemistry, 44*(20), 6841-6851.

Gregor, H. P. (1968). Ion-exchange membranes-Correlation between structure and function. *Pure and Applied Chemistry, 16*(2-3), 329-350.

Hassan, H. C., Abidin, Z. H. Z., Careem, M. A., and Arof, A. K. (2014). Chlorophyll as sensitizer in I^-/I_3^--based solar cells with quasi-solid-state electrolytes. *High Performance Polymers, 26*(6), 647-652.

Hassan, H. C., Abidin, Z. H. Z., Chowdhury, F. I., and Arof, A. K. (2016). A high efficiency chlorophyll sensitized solar cell with quasi solid PVA based electrolyte. *International Journal of Photoenergy, 2016*, 3685210, 9 pages.

He, B., Liu, S.-Q., Chen, Q., Li, H.-H., Ding, W.-J., and Deng, M. (2011). Carboxymethylated chitosan stimulates proliferation of Schwann cells in vitro via the activation of the ERK and Akt signaling pathways. *European Journal of Pharmacology, 667*(1–3), 195-201.

Holappa, J., Nevalainen, T., Savolainen, J., Soininen, P., Elomaa, M., Safin, R., Suvanto, S., Pakkanen, T., Másson, M., Loftsson, T., and Järvinen, T. (2004). Synthesis and characterization of chitosan n-betainates having various degrees of substitution. *Macromolecules, 37*(8), 2784-2789.

Hsu, H.-L., Tien, C.-F., Yang, Y.-T., and Leu, J. (2013). Dye-sensitized solar cells based on agarose gel electrolytes using allylimidazolium iodides and environmentally benign solvents. *Electrochimica Acta, 91,* 208–213.

Hu, C., Li, B., Guo, R., Wu, H., and Jiang, Z. (2007). Pervaporation performance of chitosan–poly(acrylic acid) polyelectrolyte complex membranes for dehydration of ethylene glycol aqueous solution. *Separation and Purification Technology, 55*, 327–334.

Huang, Y., Ma, X., Wang, X., and Liang, X. (2013). Determination of the interaction using FTIR within the composite gel polymer electrolyte. *Journal of Molecular Structure, 1031*, 30-37.

Hulsbosch, J., De Vos, D. E., Binnemans, K., and Ameloot, R. (2016). Biobased ionic liquids: Solvents for a green processing industry? *ACS Sustainable Chemistry & Engineering, 4*(6), 2917-2931.

Huo, Z., Dai, S., Zhang, C., Kong, F., Fang, X., Guo, L., Liu, W., Hu, L., Pan, X., and Wang, K. (2008). Low molecular mass organogelator based gel electrolyte with effective charge transport property for long-term stable quasi-solid-state dye-sensitized solar cells. *The Journal of Physical Chemistry B, 112*(41), 12927-12933.

Huo, Z., Tao, L., Wang, L., Zhu, J., Chen, S., Zhang, C., Dai, S., and Zhang, B. (2015). Effect of alkyl chain length of imidazolium cations on the electron transport and recombination kinetics in ionic gel electrolytes based quasi-solid-state dye-sensitized solar cells. *Electrochimica Acta, 168*, 313-319.

Ikezawa, Y., and Nishi, H. (2008). In situ FTIR study of the Cu electrode/ethylene carbonate + dimethyl carbonate solution interface. *Electrochimica Acta, 53*(10), 3663-3669.

Ileperuma, O. A., Dissanayake, M. A. K. L., Somasunderam, S., and Bandara, L. R. A. K. (2004). Photoelectrochemical solar cells with polyacrylonitrile-based and polyethylene oxide-based polymer electrolytes. *Solar Energy Materials and Solar Cells, 84*(1–4), 117-124.

Inta, O., Yoksan, R., and Limtrakul, J. (2014). Hydrophobically modified chitosan: A bio-based material for antimicrobial active film. *Materials Science and Engineering: C, 42*(0), 569-577.

Issa, M. M., Köping-Höggård, M., and Artursson, P. (2005). Chitosan and the mucosal delivery of biotechnology drugs. *Drug Discovery Today: Technologies, 2*(1), 1-6.

Jacob, M. M. E., and Arof, A. K. (2000). FTIR studies of DMF plasticized polyvinyledene fluoride based polymer electrolytes. *Electrochimica Acta, 45*(10), 1701-1706.

Jančiauskaitė, U., and Makuška, R. (2008). Polyelectrolytes from natural building blocks: Synthesis and properties of chitosan-*O*-dextran graft copolymers. *Chemija, 19*(2), 35–42.

Jayaweera, E. N., Ranasinghe, C. S. K., Kumara, G. R. A., Wanninayake, W. M. N. M. B., Senarathne, K. G. C., Tennakone, K., Rajapakse, R. M. G., and Ileperuma, O. A. (2015). Novel method to improve performance of dye-sensitized solar cells based on quasi-solid gel-polymer electrolytes. *Electrochimica Acta, 152*(0), 360-367.

Jeon, C., and Höll, W. H. (2003). Chemical modification of chitosan and equilibrium study for mercury ion removal. *Water Research, 37*(19), 4770-4780.

Jeong, G., Kim, M., Han, J., Kim, H.-J., Shul, Y.-G., and Cho, E. (2016). High-performance membrane-electrode assembly with an optimal polytetrafluoroethylene content for high-temperature polymer electrolyte membrane fuel cells. *Journal of Power Sources, 323*, 142-146.

Jin, H. M., Seo, D. W., Lee, S. H., Lim, Y. D., Islam, M. M., and Kim, W. G. (2012). Synthesis and characterization of urea-containing imidazolium iodide electrolyte for dye-sensitized solar cells. *Journal of Industrial and Engineering Chemistry, 18*(4), 1499-1503.

Kalyanasundaram, K. (1998). Application of functionalized transition metal complexes in photonic and optoelectronic devices. *Coordination Chemistry Reviews, 177*, 347-414.

Kalyanasundaram, K. (2010). *Dye-sensitized Solar Cells*. Lausanne, Switzerland: EFPL Press.

Karan, N. K., Pradhan, D. K., Thomas, R., Natesan, B., and Katiyar, R. S. (2008). Solid polymer electrolytes based on polyethylene oxide and lithium trifluoro- methane sulfonate (PEO–$LiCF_3SO_3$): Ionic conductivity and dielectric relaxation. *Solid State Ionics, 179*(19–20), 689-696.

Karmakar, A., and Ghosh, A. (2012). Dielectric permittivity and electric modulus of polyethylene oxide (PEO)–$LiClO_4$ composite electrolytes. *Current Applied Physics, 12*(2), 539-543.

Katoh, R., and Furube, A. (2014). Electron injection efficiency in dye-sensitized solar cells. *Journal of Photochemistry and Photobiology C: Photochemistry Reviews, 20 (2014)* 1–16.

Khanmirzaei, M. H., Ramesh, S., and Ramesh, K. (2015). Polymer electrolyte based dye-sensitized solar cell with rice starch and 1-methyl-3-propylimidazolium iodide ionic liquid. *Materials & Design, 85*, 833-837.

Khiar, A. S. A., Puteh, R., and Arof, A. K. (2006). Conductivity studies of a chitosan-based polymer electrolyte. *Physica B: Condensed Matter, 373*(1), 23-27.

Kim, B., Park, S. W., Kim, J. Y., Yoo, K., Lee, J. A., Lee, M. W., Lee, D. K., Kim, J. Y., Kim, B., Kim, H., Han, S., Son, H. J., and Ko, M. J. (2013). Rapid dye adsorption via surface modification of TiO_2 photoanodes for dye-sensitized solar cells. *ACS Applied Materials and Interfaces, 5*(11), 5201-5207.

Kim, J., Hwang, J., Seo, Y., Jo, Y., Son, J., and Choi, J. (2017). Engineered chitosan–xanthan gum biopolymers effectively adhere to cells and readily release incorporated antiseptic molecules in a sustained manner. *Journal of Industrial and Engineering Chemistry, 46*, 68-79.

Klotzbach, T., Watt, M., Ansari, Y., and Minteer, S. D. (2006). Effects of hydrophobic modification of chitosan and Nafion on transport properties, ion-exchange capacities, and enzyme immobilization. *Journal of Membrane Science, 282*(1–2), 276-283.

Kou, D., Liu, W., Hu, L., and Dai, S. (2013). Cooperative effect of adsorbed cations on electron transport and recombination behavior in dye-sensitized solar cells. *Electrochimica Acta, 100*, 197-202.

Koyama, H., Fujimoto, M., Ohno, T., Suzuki, H., and Tanaka, J. (2006). Effects of thermal annealing on formation of micro porous titanium oxide by the sol–gel method. *Journal of the American Ceramic Society, 89*(11), 3536-3540.

Kurita, K. (2006). Chitin and chitosan: Functional biopolymers from marine crustaceans. *Marine Biotechnology, 8*, 203–226.

Kurita, K., Akao, H., Yang, J., and Shimojoh, M. (2003). Nonnatural branched polysaccharides: Synthesis and properties of chitin and chitosan having disaccharide maltose branches. *Biomacromolecules, 4*(5), 1264-1268.

Kurita, K., Ikeda, H., Shimojoh, M., and Yang, J. (2007). N-phthaloylated chitosan as an essential precursor for controlled chemical modifications of chitosan: Synthesis and evaluation. *Polymer Journal, 39*(9), 945–952.

Kurita, K., Ikeda, H., Yoshida, Y., Shimojoh, M., and Harata, M. (2001). Chemoselective protection of the amino groups of chitosan by controlled phthaloylation: Facile preparation of a precursor useful for chemical modifications. *Biomacromolecules, 3*(1), 1-4.

Kurita, K., Kojima, T., Nishiyama, Y., and Shimojoh, M. (2000). Synthesis and some properties of nonnatural amino polysaccharides: Branched chitin and chitosan. *Macromolecules, 33*(13), 4711-4716.

Kurita, K., Shimada, K., Nishiyama, Y., Shimojoh, M., and Nishimura, S.-I. (1998). Nonnatural branched polysaccharides: Synthesis and properties of chitin and chitosan having *α*-mannoside branches. *Macromolecules, 31*(15), 4764-4769.

Kurita, K., Sugita, K., Kodaira, N., Hirakawa, M., and Yang, J. (2005). Preparation and evaluation of trimethylsilylated chitin as a versatile precursor for facile chemical modifications. *Biomacromolecules, 6*(3), 1414-1418.

Kurita, K., Tomita, K., Tada, T., Nishimura, S.-l., and Ishii, S. (1993). Reactivity characteristics of a new form of chitosan Facile N-phthaloylation of chitosan prepared from squid/3-chitin for effective solubilization. *Polymer Bulletin, 30*, 429-433.

Lee, J.-H., Park, N.-G., and Shin, Y.-J. (2011). Nano-grain SnO_2 electrodes for high conversion efficiency SnO_2–DSSC. *Solar Energy Materials and Solar Cells, 95*(1), 179-183.

Lertsutthiwong, P., Sutti, S., and Powtongsook, S. (2009). Optimization of chitosan flocculation for phytoplankton removal in shrimp culture ponds. *Aquacultural Engineering, 41*, 188–193.

Li, G. R., Wang, F., Jiang, Q. W., Gao, X. P., and Shen, P. W. (2010). Carbon nanotubes with titanium nitride as a low-cost counter-electrode material for dye-sensitized solar cells. *Angewandte Chemie International Edition, 49*(21), 3653-3656.

Li, L., Xu, C., Zhao, Y., Chen, S., and Ziegler, K. J. (2015). Improving performance via blocking layers in dye-sensitized solar cells based on nanowire photoanodes. *ACS Applied Materials & Interfaces, 7*(23), 12824-12831.

Li, W., Kang, J., Li, X., Fang, S., Lin, Y., Wang, G., and Xiao, X. (2005). A novel polymer quaternary ammonium iodide and application in quasi-solid-state dye-sensitized solar cells. *Journal of Photochemistry and Photobiology A: Chemistry, 170*, 1–6.

Lin, W.-J., and Chen, M. H. (2007). Synthesis of multifunctional chitosan with galactose as a targeting ligand for glycoprotein receptor. *Carbohydrate Polymers, 67*(4), 474-480.

Liu, J., Yang, H., Tan, W., Zhou, X., and Lin, Y. (2010). Photovoltaic performance improvement of dye-sensitized solar cells based on tantalum-doped TiO_2 thin films. *Electrochimica Acta, 56*(1), 396-400.

Liu, L., Li, Y., Fang, Y.-e., and Chen, L. (2005). Microwave-assisted graft copolymerization of ε-caprolactone onto chitosan via the phthaloyl protection method. *Carbohydrate Polymers, 60*(3), 351-356.

Liu, L., Li, Y., Li, Y., and Fang, Y.-E. (2004). Rapid N-phthaloylation of chitosan by microwave irradiation. *Carbohydrate Polymers, 57*, 97–100.

Liu, X., Zhi, X., Liu, Y., Wu, B., Sun, Z., and Shen, J. (2012). Effect of chitosan, O-carboxymethyl chitosan, and N-[(2-hydroxy-3-N,N-dimethylhexadecyl ammonium)propyl] chitosan chloride on overweight and insulin resistance in a murine diet-induced obesity. *Journal of Agricultural and Food Chemistry, 60*(13), 3471-3476.

Luo, P., Niu, H., Zheng, G., Bai, X., Zhang, M., and Wang, W. (2009). From salmon pink to blue natural sensitizers for solar cells: Canna indica L., Salvia splendens, cowberry and Solanum nigrum L. *Spectrochimica Acta Part A: Molecular and Biomolecular Spectroscopy, 74*, 936–942.

Lv, S., Liu, J., Zhou, Q., Huang, L., and Sun, T. (2014). Synthesis of modified chitosan superplasticizer by amidation and sulfonation and its application performance and working mechanism. *Industrial & Engineering Chemistry Research, 53*(10), 3908-3916.

Ma, L., Li, G., Li, L., and Liu, P. (2010). Synthesis and characterization of diethoxy phosphoryl chitosan. *International Journal of Biological Macromolecules, 47*(4), 578-581.

Maçaira, J., Andrade, L., and Mendes, A. (2013). Review on nanostructured photoelectrodes for next generation dye-sensitized solar cells. *Renewable and Sustainable Energy Reviews, 27*, 334-349.

Mack, F., Morawietz, T., Hiesgen, R., Kramer, D., Gogel, V., and Zeis, R. (2016). Influence of the polytetrafluoroethylene content on the performance of high-temperature polymer electrolyte membrane fuel cell electrodes. *International Journal of Hydrogen Energy, 41*(18), 7475-7483.

Macquarrie, D. J., and Hardy, J. J. E. (2005). Applications of functionalized chitosan in catalysis. *Industrial & Engineering Chemistry Research, 44*(23), 8499-8520.

Majid, S. R., and Arof, A. K. (2005). Proton-conducting polymer electrolyte films based on chitosan acetate complexed with NH_4NO_3 salt. *Physica B: Condensed Matter, 355*(1–4), 78-82.

Majid, S. R., and Arof, A. K. (2007). Electrical behavior of proton-conducting chitosan-phosphoric acid-based electrolytes. *Physica B: Condensed Matter, 390*, 209–215.

Makuška, R., and Gorochovceva, N. (2006). Regioselective grafting of poly(ethylene glycol) onto chitosan through C-6 position of glucosamine units. *Carbohydrate Polymers, 64*, 319-327.

Matsuda, Y., Fukushima, T., Katoh, Y., Ishiko, E., Nishiura, M., Kikuta, M., and Kono, M. (2003). Characteristics of gel alkylene oxide polymer electrolytes containing γ-butyrolactone. *Journal of Power Sources, 119–121*, 473-477.

Maya, S., Sarmento, B., Lakshmanan, V.-K., Menon, D., Seabra, V., and Jayakumar, R. (2014). Chitosan cross-linked docetaxel loaded EGF receptor targeted nanoparticles for lung cancer cells. *International Journal of Biological Macromolecules, 69*, 532-541.

Miretzky, P., and Cirelli, A. F. (2009). Hg(II) removal fromwater by chitosan and chitosan derivatives: A review. *Journal of Hazardous Materials, 167*, 10–23.

Mohamad, S. A., Yahya, R., Ibrahim, Z. A., and Arof, A. K. (2007). Photovoltaic activity in a ZnTe/PEO–chitosan blend electrolyte junction. *Solar Energy Materials and Solar Cells, 91*(13), 1194-1198.

Morni, N. M., and Arof, A. K. (1999). Chitosan–lithium triflate electrolyte in secondary lithium cells. *Journal of Power Sources, 77*, 42–48.

Moumene, T., Belarbi, E. H., Haddad, B., Villemin, D., Abbas, O., Khelifa, B., and Bresson, S. (2014). Vibrational spectroscopic study of ionic liquids: Comparison between monocationic and dicationic imidazolium ionic liquids. *Journal of Molecular Structure, 1065–1066*, 86-92.

Mourya, V. K., and Inamdar, N. N. (2008). Chitosan-modifications and applications: Opportunities galore. *Reactive and Functional Polymers, 68*(6), 1013-1051.

Mu, Q., and Fang, Y. (2008). Preparation of thermosensitive chitosan with poly(N-isopropylacrylamide) side at hydroxyl group via O-maleoyl-N-phthaloyl-chitosan (MPCS). *Carbohydrate Polymers, 72*(2), 308-314.

Muchakayala, R., Song, S., Gao, S., Wang, X., and Fan, Y. (2017). Structure and ion transport in an ethylene carbonate-modified biodegradable gel polymer electrolyte. *Polymer Testing, 58*, 116-125.

Mustafa, M. F., Ridwan, N. I. M., Hatta, F. F., and Yahya, M. Z. A. (2012). Effect of dimethyl carbonate plasticizer on ionic conductivity of methyl cellulose-based polymer electrolytes. *The Malaysian Journal of Analytical Sciences, 16*(3), 283-289.

Nazeeruddin, M. K., Zakeeruddin, S. M., Lagref, J. J., Liska, P., Comte, P., Barolo, C., Viscardi, G., Schenk, K., and Graetzel, M. (2004). Stepwise assembly of amphiphilc ruthenim sensitizers and their aplications in dye-sensitized solar cell. *Coordination Chemistry Reviews, 248*, 1317–1328.

Ng, L. S., and Mohamad, A. A. (2006). Protonic battery based on a plasticized chitosan-NH_4NO_3 solid polymer electrolyte. *Journal of Power Sources, 163*(1), 382-385.

Nguyen, C. A., Xiong, S., Ma, J., Lu, X., and Lee, P. S. (2009). Toward electrochromic device using solid electrolyte with polar polymer host. *The Journal of Physical Chemistry B, 113*(23), 8006-8010.

Nicotera, I., Coppola, L., Oliviero, C., Castriota, M., and Cazzanelli, E. (2006). Investigation of ionic conduction and mechanical properties of PMMA–PVdF blend-based polymer electrolytes. *Solid State Ionics, 177*(5–6), 581-588.

Nishimura, S., Kohgo, O., Kurita, K., and Kuzuhara, H. (1991). Chemospecific manipulations of a rigid polysaccharide: Syntheses of novel chitosan derivatives with excellent solubility in common organic solvents by regioselective chemical modifications. *Macromolecules, 24*(17), 4745-4748.

Noor, M. M., Buraidah, M. H., Careem, M. A., Majid, S. R., and Arof, A. K. (2014). An optimized poly(vinylidene fluoride-hexafluoropropylene)–NaI gel polymer electrolyte and its application in natural dye sensitized solar cells. *Electrochimica Acta, 121*(0), 159-167.

Noor, M. M., Buraidah, M. H., Yusuf, S. N. F., Careem, M. A., Majid, S. R., and Arof, A. K. (2011). Performance of dye-sensitized solar cells with (PVDF-HFP)-KI-EC-PC electrolyte and different dyematerials. *International Journal of Photoenergy, 2011*, 960487, 5 pages.

Nosheen, E., Shah, S. M., Hussain, H., and Murtaza, G. (2016). Photo-sensitization of ZnS nanoparticles with renowned ruthenium dyes N3, N719 and Z907 for application in solid state dye sensitized solar cells: A comparative study. *Journal of Photochemistry and Photobiology B: Biology, 162*, 583-591.

O'Regan, B., and Gratzel, M. (1991). A low-cost, high-efficiency solar cell based on dye-sensitized colloidal TiO_2 films. *Nature, 353*(6346), 737-740.

Opanasopit, P., Ngawhirunpat, T., Chaidedgumjorn, A., Rojanarata, T., Apirakaramwong, A., Phongying, S., Choochottiros, C., and Chirachanchai, S. (2006). Incorporation of camptothecin into N-phthaloyl chitosan-g-mPEG self-assembly micellar system. *European Journal of Pharmaceutics and Biopharmaceutics, 64*(3), 269-276.

Osman, Z., and Arof, A. K. (2003). FTIR studies of chitosan acetate based polymer electrolytes. *Electrochimica Acta, 48*, 993-999.

Otaka, H., Kira, M., Yano, K., Ito, S., Mitekura, H., Kawata, T., and Matsui, F. (2004). Multi-colored dye-sensitized solar cells. *Journal of Photochemistry and Photobiology A: Chemistry, 164*(1), 67-73.

Ozawa, H., Okuyama, Y., and Arakawa, H. (2013). Effects of cation composition in the electrolyte on the efficiency improvement of black dye-based dye-sensitized solar cells. *RSC Advances, 3*(24), 9175-9177.

Pan, S. S., Zhang, Y. X., Teng, X. M., Li, G. H., and Li, L. (2008). Optical properties of nitrogen-doped SnO_2 films: Effect of the electronegativity on refractive index and band gap. *Journal of Applied Physics, 103*(9), 093103.

Parisi, M. L., Maranghi, S., and Basosi, R. (2014). The evolution of the dye sensitized solar cells from Grätzel prototype to up-scaled solar applications: A life cycle assessment approach. *Renewable and Sustainable Energy Reviews, 39*(0), 124-138.

Park, N.-G. (2010). Light management in dye-sensitized solar cell. *Korean Journal of Chemical Engineering, 27*(2), 375-384.

Parussulo, A. L. A., Huila, M. F. G., Araki, K., and Toma, H. E. (2011). N3-Dye-Induced Visible Laser Anatase-to-Rutile Phase Transition on Mesoporous TiO2 Films. *Langmuir, 27*(15), 9094-9099.

Patel, M. N., Williams, R. D., May, R. A., Uchida, H., Stevenson, K. J., and Johnston, K. P. (2008). Electrophoretic deposition of Au nanocrystals inside perpendicular mesochannels of TiO_2. *Chemistry of Materials, 20*(19), 6029-6040.

Payne, G. F., and Raghavan, S. R. (2007). Chitosan: A soft interconnect for hierarchical assembly of nano-scale components. *Soft Matter, 3*(5), 521-527.

Peesan, M., Sirivat, A., Supaphol, P., and Rujiravanit, R. (2006). Dilute solution properties of hexanoyl chitosan in chloroform, dichloromethane, and tetrahydrofuran. *Carbohydrate Polymers, 64*(2), 175-183.

Peesan, M., Supaphol, P., and Rujiravanit, R. (2005). Preparation and characterization of hexanoyl chitosan/polylactide blend films. *Carbohydrate Polymers, 60*(3), 343-350.

Peng, X., and Zhang, L. (2007). Formation and Morphologies of Novel Self-Assembled Micelles from Chitosan Derivatives. *Langmuir, 23*(21), 10493-10498.

Petibon, R., Harlow, J., Le, D. B., and Dahn, J. R. (2015). The use of ethyl acetate and methyl propanoate in combination with vinylene carbonate as ethylene carbonate-free solvent blends for electrolytes in Li-ion batteries. *Electrochimica Acta, 154*, 227-234.

Petrowsky, M., and Frech, R. (2010). Salt concentration dependence of the compensated Arrhenius equation for alcohol-based electrolytes. *Electrochimica Acta, 55*(4), 1285-1288.

Pillai, C. K. S., Paul, W., and Sharma, C. P. (2009). Chitin and chitosan polymers: Chemistry, solubility and fiber formation. *Progress in Polymer Science, 34*(7), 641-678.

Pradeepa, P., and Prabhu, M. R. (2015). Investigations on the addition of different plasticizers in poly(ethylmethacrylate)/poly(vinylidene fluoride-co-hexafluro propylene) based polymer blend electrolyte system. *International Journal of ChemTech Research, 7*(4), 2077-2084.

Pradhan, D. K., Choudhary, R. N. P., and Samantaray, B. K. (2008). Studies of dielectric relaxation and AC conductivity behavior of plasticized polymer nanocomposite electrolytes. *International Journal of Electrochemical Science, 3*, 597 - 608.

Prashanth, K. V. H., and Tharanathan, R. N. (2007). Chitin/chitosan: Modifications and their unlimited application potential - An overview. *Trends in Food Science & Technology, 18*(3), 117-131.

Qi, B., and Wang, J. (2013). Fill factor in organic solar cells. *Physical Chemistry Chemical Physics, 15*(23), 8972-8982.

Qin, C., Li, H., Xiao, Q., Liu, Y., Zhu, J., and Du, Y. (2006). Water-solubility of chitosan and its antimicrobial activity. *Carbohydrate Polymers, 63*, 367–374.

Qin, Y., and Peng, Q. (2012). Ruthenium Sensitizers and Their Applications in Dye-Sensitized Solar Cells. *International Journal of Photoenergy, 2012*, 291579, 21.

Ramesh, S., and Arof, A. K. (2000). Electrical conductivity studies of polyvinyl chloride-based electrolytes with double salt system. *Solid State Ionics, 136–137*(0), 1197-1200.

Ramesh, S., and Arof, A. K. (2001). Structural, thermal and electrochemical cell characteristics of poly(vinyl chloride)-based polymer electrolytes. *Journal of Power Sources, 99*(1–2), 41-47.

Ramesh, S., Liew, C.-W., and Arof, A. K. (2011). Ion conducting corn starch biopolymer electrolytes doped with ionic liquid 1-butyl-3-methylimidazolium hexafluorophosphate. *Journal of Non-Crystalline Solids, 357*(21), 3654-3660.

Ramesh, S., Winie, T., and Arof, A. K. (2007). Investigation of mechanical properties of polyvinyl chloride–polyethylene oxide (PVC–PEO) based polymer electrolytes for lithium polymer cells. *European Polymer Journal, 43*(5), 1963-1968.

Ramesh, S., Yahaya, A. H., and Arof, A. K. (2002a). Dielectric behaviour of PVC-based polymer electrolytes. *Solid State Ionics, 152–153*(0), 291-294.

Ramesh, S., Yahaya, A. H., and Arof, A. K. (2002b). Miscibility studies of PVC blends (PVC/PMMA and PVC/PEO) based polymer electrolytes. *Solid State Ionics, 148*(3–4), 483-486.

Rapsomanikis, A., Sygkridou, D., Voutsinas, E., and Stathatos, E. (2016). Transparent quasi-solid state dye-sensitized solar cells sensitized with naturally derived pigment extracted from red seaweed. *Current Applied Physics, 16*(6), 651-657.

Rice, M. J., and Roth, W. L. (1972). Ionic transport in super ionic conductors: A theoretical model. *Journal of Solid State Chemistry, 4*(2), 294-310.

Richardson, P. M., Voice, A. M., and Ward, I. M. (2016). NMR self diffusion and relaxation time measurements for poly (vinylidene fluoride) (PVDF) based polymer gel electrolytes containing $LiBF_4$ and propylene carbonate. *Polymer, 97*, 69-79.

Rinaudo, M. (2006). Chitin and chitosan: Properties and applications. *Progress in Polymer Science, 31,* 603–632.

Roberts, G. A. F., and Wood, F. A. (2001). A study of the influence of structure on the effectiveness of chitosan as an anti-felting treatment for wool. *Journal of Biotechnology, 89,* 297–304.

Rocco, A. M., da Fonseca, C. P., and Pereira, R. P. (2002). A polymeric solid electrolyte based on a binary blend of poly(ethylene oxide), poly(methyl vinyl ether-maleic acid) and $LiClO_4$. *Polymer, 43*(13), 3601-3609.

Rofaiel, A., Ellis, J. S., Challa, P. R., and Bazylak, A. (2012). Heterogeneous through-plane distributions of polytetrafluoroethylene in polymer electrolyte membrane fuel cell gas diffusion layers. *Journal of Power Sources, 201*, 219-225.

Rohan, R., Sun, Y., Cai, W., Zhang, Y., Pareek, K., Xu, G., and Cheng, H. (2014). Functionalized polystyrene based single ion conducting gel polymer electrolyte for lithium batteries. *Solid State Ionics, 268, Part B,* 294-299.

Rosli, N. H. A., Chan, C. H., Subban, R. H. Y., and Winie, T. (2012). Studies on the structural and electrical properties of hexanoyl chitosan/polystyrene-based polymer electrolytes. *Physics Procedia, 25*(0), 215-220.

Rout, D. K., Pulapura, S. K., and Gross, R. A. (1993). Liquid-crystalline characteristics of site-selectively-modified chitosan. *Macromolecules, 26*(22), 5999-6006.

Rudhziah, S., Ahmad, A., Ahmad, I., and Mohamed, N. S. (2015). Biopolymer electrolytes based on blend of kappa-carrageenan and cellulose derivatives for potential application in dye sensitized solar cell. *Electrochimica Acta, 175,* 162-168.

Sæther, H. V., Holme, H. K., Maurstad, G., Smidsrød, O., and Stokke, B. T. (2008). Polyelectrolyte complex formation using alginate and chitosan. *Carbohydrate Polymers, 74*(4), 813-821.

Saito, Y., Kataoka, H., Capiglia, C., and Yamamoto, H. (2000). Ionic conduction properties of PVDF−HFP type gel polymer electrolytes with lithium imide salts. *The Journal of Physical Chemistry B, 104*(9), 2189-2192.

Salvador, G. P., Pugliese, D., Bella, F., Chiappone, A., Sacco, A., Bianco, S., and Quaglio, M. (2014). New insights in long-term photovoltaic performance characterization of cellulose-based gel electrolytes for stable dye-sensitized solar cells. *Electrochimica Acta, 146*(0), 44-51.

Sankararamakrishnan, N., Dixit, A., Iyengar, L., and Sanghi, R. (2006). Removal of hexavalent chromium using a novel cross linked xanthated chitosan. *Bioresource Technology, 97*(18), 2377-2382.

Sankararamakrishnan, N., and Sanghi, R. (2006). Preparation and characterization of a novel xanthated chitosan. *Carbohydrate Polymers, 66*(2), 160-167.

Sashiwa, H., Kawasaki, N., Nakayama, A., Muraki, E., Yamamoto, N., Zhu, H., Nagano, H., Omura, Y., Saimoto, H., Shigemasa, Y., and Aiba, S.-i. (2002). Chemical modification of chitosan. 13. synthesis of organosoluble, palladium adsorbable, and biodegradable chitosan derivatives toward the chemical plating on plastics. *Biomacromolecules, 3*(5), 1120-1125.

Shalu, Chaurasia, S. K., Singh, R. K., and Chandra, S. (2013). Thermal stability, complexing behavior, and ionic transport of polymeric gel membranes based on polymer PVdF-HFP and ionic liquid, [BMIM][BF_4]. *The Journal of Physical Chemistry B, 117*(3), 897-906.

Shannon, R. (1976). Revised effective ionic radii and systematic studies of interatomic distances in halides and chalcogenides. *Acta Crystallographica Section A, 32*(5), 751-767.

Shen, X., Xu, W., Xu, J., Liang, G., Yang, H., and Yao, M. (2008). Quasi-solid-state dye-sensitized solar cells based on gel electrolytes containing different alkali metal iodide salts. *Solid State Ionics, 179*(35–36), 2027-2030.

Shi, C., Ge, Q., Han, S., Cai, M., Dai, S., Fang, X., and Pan, X. (2008). An improved preparation of *1*-methyl-*3*-propylimidazolium iodide and its application in dye-sensitized solar cells. *Solar Energy, 82*(5), 385-388.

Shi, J., Peng, S., Pei, J., Liang, Y., Cheng, F., and Chen, J. (2009). Quasi-solid-state dye-sensitized solar cells with polymer gel electrolyte and triphenylamine-based organic dyes. *ACS Applied Materials & Interfaces, 1*(4), 944-950.

Shi, Y., Wang, Y., Zhang, M., and Dong, X. (2011). Influences of cation charge density on the photovoltaic performance of dye-sensitized solar cells: Lithium, sodium, potassium, and dimethylimidazolium. *Physical Chemistry Chemical Physics, 13*(32), 14590-14597.

Shieh, J. J., and Huang, R. Y. M. (1997). Pervaporation with chitosan membranes II. Blend membranes of chitosan and polyacrylic acid and comparison of homogeneous and composite membrane based on polyelectrolyte complexes of chitosan and polyacrylic acid for the separation of ethanol-water mixtures. *Journal of Membrane Science, 127*, 185-202.

Shukla, M., Srivastava, N., and Saha, S. (2010). Theoretical and spectroscopic studies of 1-butyl-3-methylimidazolium iodide room temperature ionic liquid: Its differences with chloride and bromide derivatives. *Journal of Molecular Structure, 975*(1–3), 349-356.

Silva, M. M., Barros, S. C., Smith, M. J., and MacCallum, J. R. (2002). Study of novel lithium salt-based, plasticized polymer electrolytes. *Journal of Power Sources, 111*, 52–57.

Sim, L. N., Majid, S. R., and Arof, A. K. (2014). Effects of 1–butyl–3–methyl imidazolium trifluoromethanesulfonate ionic liquid in poly(ethyl methacrylate)/poly(vinylidenefluoride–co–hexafluoropropylene) blend based polymer electrolyte system. *Electrochimica Acta, 123*, 190-197.

Sim, L. N., Yahya, R., and Arof, A. K. (2016). Blend polymer electrolyte films based on poly(ethyl methacrylate)/poly(vinylidenefluoride-co-hexafluoropropylene) incorporated with 1-butyl-3-methyl imidazolium iodide ionic liquid. *Solid State Ionics, 291*, 26-32.

Singh, P. K., Bhattacharya, B., M., M. R., and Rhee, H.-W. (2011). Plasticizer doped ionic liquid incorporated solid polymer electrolytes for photovoltaic application. *Current Applied Physics, 11*, 616-619.

Singh, P. K., Kim, K.-W., and Rhee, H.-W. (2008). Electrical, optical and photoelectrochemical studies on a solid PEO-polymer electrolyte doped with low viscosity ionic liquid. *Electrochemistry Communications, 10*, 1769–1772.

Singh, P. K., Kim, K.-W., and Rhee, H.-W. (2009). Development and characterization of ionic liquid doped solid polymer electrolyte membranes for better efficiency. *Synthetic Metals, 159*, 1538–1541.

Singh, R., Jadhav, N. A., Majumder, S., Bhattacharya, B., and Singh, P. K. (2013). Novel biopolymer gel electrolyte for dye-sensitized solar cell application. *Carbohydrate Polymers, 91*(2), 682-685.

Singh, R., Polu, A. R., Bhattacharya, B., Rhee, H.-W., Varlikli, C., and Singh, P. K. (2016). Perspectives for solid biopolymer electrolytes in dye sensitized solar cell and battery application. *Renewable and Sustainable Energy Reviews, 65*, 1098-1117.

Smitha, B., Devi, D. A., and Sridhar, S. (2008). Proton-conducting composite membranes of chitosan and sulfonated polysulfone for fuel cell application. *International Journal of Hydrogen Energy, 33*(15), 4138-4146.

Smitha, B., Sridhar, S., and Khan, A. A. (2005). Chitosan–sodium alginate polyion complexes as fuel cell membranes. *European Polymer Journal, 41*(8), 1859-1866.

Sobahi, T. R. A., Abdelaal, M. Y., and Makki, M. S. I. (2014). Chemical modification of chitosan for metal ion removal. *Arabian Journal of Chemistry, 7*(5), 741–746.

Stepniak, I., Andrzejewska, E., Dembna, A., and Galinski, M. (2014). Characterization and application of N-methyl-N-propylpiperidinium bis(trifluoromethanesulfonyl)imide ionic liquid–based gel polymer electrolyte prepared in situ by photopolymerization method in lithium ion batteries. *Electrochimica Acta, 121*, 27-33.

Suzuki, K., Yamaguchi, M., Kumagai, M., Tanabe, N., and Yanagida, S. (2006). Dye-sensitized solar cells with ionic gel electrolytes prepared from imidazolium salts and agarose. *Comptes Rendus Chimie, 9*(5–6), 611-616.

Suzuki, Y., Wakatsuki, J., Tsubaki, M., and Sato, M. (2013). Imidazolium-based chiral ionic liquids: Synthesis and application. *Tetrahedron, 69*(46), 9690-9700.

Tang, H., Prasad, K., Sanjinbs, R., Schmid, P. E., and Levy, F. (1994). Electrical and optical properties of TiO_2 anatase thin films. *Journal of Applied Physics, 75*(4), 2042-2047.

Tétreault, N., Arsenault, É., Heiniger, L.-P., Soheilnia, N., Brillet, J., Moehl, T., Zakeeruddin, S., Ozin, G. A., and Grätzel, M. (2011). High-efficiency dye-sensitized solar cell with three-dimensional photoanode. *Nano Letters, 11*(11), 4579-4584.

Thomas, P. A., and Marvey, B. B. (2016). Room temperature ionic liquids as green solvent alternatives in the metathesis of oleochemical feedstocks. *Molecules, 21*(2), 184.

Torii, Y., Ikeda, H., Shimojoh, M., and Kurita, K. (2009). Chemoselective protection of chitosan by dichlorophthaloylation: Preparation of a key intermediate for chemical modifications. *Polymer Bulletin, 62*, 749–759.

Vijayakumar, P., Senthil Pandian, M., Lim, S. P., Pandikumar, A., Huang, N. M., Mukhopadhyay, S., and Ramasamy, P. (2015). Investigations of tungsten carbide nanostructures treated with different temperatures as counter electrodes for dye sensitized solar cells (DSSC) applications. *Journal of Materials Science: Materials in Electronics, 26*(10), 7977–7986.

Wan, Y., Creber, K. A. M., Peppley, B., and T., B. V. (2003). Ionic conductivity of chitosan membranes. *Polymer, 44*, 1057–1065.

Wang, H., Wei, W., and Hu, Y. H. (2013). Efficient ZnO-based counter electrodes for dye-sensitized solar cells. *Journal of Materials Chemistry A, 1*(22), 6622-6628.

Wang, X., Ma, J., Wang, Y., and He, B. (2001). Structural characterization of phosphorylated chitosan and their applications as effective additives of calcium phosphate cements. *Biomaterials, 22*(16), 2247-2255.

Wang, X. L., Huang, Y., Zhu, J., Pan, Y. B., He, R., and Wang, Y. Z. (2009). Chitosan-graft poly(*p*-dioxanone) copolymers: Preparation, characterization, and properties. *Carbohydrate Research, 344*(6), 801-807.

Wanninayake, W. M. N. M. B., Premaratne, K., Kumara, G. R. A., and Rajapakse, R. M. G. (2016). Use of lithium iodide and tetrapropylammonium iodide in gel electrolytes for improved performance of quasi-solid-state dye-sensitized solar cells: Recording an efficiency of 6.40%. *Electrochimica Acta, 191*, 1037-1043.

Warnan, J., Guerin, V.-M., Anne, F. B., Pellegrin, Y., Blart, E., Jacquemin, D., Pauporté, T., and Odobel, F. (2013). Ruthenium sensitizer functionalized by acetylacetone anchoring groups for dye-sensitized solar cells. *The Journal of Physical Chemistry C, 117*(17), 8652-8660.

Winie, T., and Arof, A. K. (2006). FT-IR studies on interactions among components in hexanoyl chitosan-based polymer electrolytes. *Spectrochimica Acta Part A: Molecular and Biomolecular Spectroscopy, 63*(3), 677-684.

Winie, T., Ramesh, S., and Arof, A. K. (2009). Studies on the structure and transport properties of hexanoyl chitosan-based polymer electrolytes. *Physica B: Condensed Matter, 404*(21), 4308-4311.

Wolfrom, M. L., and Han, T. M. S. (1959). The Sulfonation of Chitosan1,2. *Journal of the American Chemical Society, 81*(7), 1764-1766.

Wu, M., Lin, X., Wang, Y., Wang, L., Guo, W., Qi, D., Peng, X., Hagfeldt, A., Grätzel, M., and Ma, T. (2012). Economical Pt-free catalysts for counter electrodes of dye-sensitized solar cells. *Journal of the American Chemical Society, 134*(7), 3419-3428.

Wu, M., Wang, Y., Lin, X., Guo, W., Wu, K., Lin, Y.-n., Guo, H., and Ma, T. (2013). TiC/Pt composite catalyst as counter electrode for dye-sensitized solar cells with long-term stability and high efficiency. *Journal of Materials Chemistry A, 1*(34), 9672-9679.

Wu, Y., Seo, T., Maeda, S., Sasaki, T., Irie, S., and Sakurai, K. (2004). Preparation of benzoylchitosans and their chiroptical properties in dilute solutions. *Journal of Polymer Science: Part B: Polymer Physics, 42*(22), 4107-4115.

Yahya, M. Z. A., and Arof, A. K. (2002). Studies on lithium acetate doped chitosan conducting polymer system. *European Polymer Journal, 38*(6), 1191–1197.

Yang, L. N., Sun, Z. Z., Chen, S. L., and Li, Z. S. (2013). The effects of various anchoring groups on optical and electronic properties of dyes in dye-sensitized solar cells. *Dyes and Pigments, 99*(1), 29-35.

Yang, S., Kou, H., Wang, J., Xue, H., and Han, H. (2010). Tunability of the band energetics of nanostructured $SrTiO_3$ electrodes for dye-sensitized solar cells. *The Journal of Physical Chemistry C, 114*(9), 4245-4249.

Yella, A., Lee, H. W., Tsao, H. N., Yi, C., Chandiran, A. K., Nazeeruddin, M. K., Diau, E. W.-G., Yeh, C. Y., Zakeeruddin, S. M., and Grätzel, M. (2011). Porphyrin-sensitized solar cells with cobalt (II/III)–based redox electrolyte exceed 12 percent efficiency. *Science, 334*, 629-634.

Yoksan, R., Akashi, M., Biramontri, S., and Chirachanchai, S. (2001). Hydrophobic chain conjugation at hydroxyl group onto γ-ray irradiated chitosan. *Biomacromolecules, 2*(3), 1038-1044.

Yoksan, R., Matsusaki, M., Akashi, M., and Chirachanchai, S. (2004). Controlled hydrophobic/hydrophilic chitosan: Colloidal phenomena and nanosphere formation. *Colloid and Polymer Science, 282*, 337–342.

Yu, Q., Wang, Y., Yi, Z., Zu, N., Zhang, J., Zhang, M., and Wang, P. (2010). High-efficiency dye-sensitized solar cells: The influence of lithium ions on exciton dissociation, charge recombination, and surface states. *ACS Nano, 4*(10), 6032-6038.

Yusuf, S. N. F., Aziz, M. F., Hassan, H. C., Bandara, T. M. W. J., Mellander, B. E., Careem, M. A., and Arof, A. K. (2014). Phthaloylchitosan-based gel polymer electrolytes for efficient dye-sensitized solar cells. *Journal of Chemistry, 2014*, 783023, 8 pages.

Yusuf, S. N. F., Azzahari, A. D., Yahya, R., Majid, S. R., Careem, M. A., and Arof, A. K. (2016). From crab shell to solar cell: a gel polymer electrolyte based on N-

phthaloylchitosan and its application in dye-sensitized solar cells. *RSC Advances, 6*, 27714 - 27724.

Zallen, R., and Moret, M. P. (2006). The optical absorption edge of brookite TiO_2. *Solid State Communications, 137*, 154–157.

Zhang, B., Zhou, Y., Li, X., Wang, J., Li, G., Yun, Q., and Wang, X. (2014). Li^+-molecule interactions of lithium tetrafluoroborate in propylene carbonate + N,N-dimethylformamide mixtures: An FTIR spectroscopic study. *Spectrochimica Acta Part A: Molecular and Biomolecular Spectroscopy, 124*(0), 40-45.

Zhang, C., Ren, Z., Yin, Z., Jiang, L., and Fang, S. (2011). Experimental FTIR and simulation studies on H-bonds of model polyurethane in solutions. I: In dimethylformamide (DMF). *Spectrochimica Acta Part A: Molecular and Biomolecular Spectroscopy, 81*(1), 598-603.

Zhang, L., and Cole, J. M. (2015). Anchoring groups for dye-sensitized solar cells. *ACS Applied Materials & Interfaces, 7*(6), 3427-3455.

Zhang, S., Dong, G.-Y., Lin, B., Qu, J., Yuan, N.-Y., and Ding, J.-N. (2015). A polymer gel electrolyte with an inverse opal structure and its effects on the performance of quasi-solid-state dye-sensitized solar cells. *Journal of Power Sources, 277*(0), 52-58.

Zohuriaan-Mehr, M. J. (2005). Advances in chitin and chitosan modification through graft copolymerization: A comprehensive review. *Iranian Polymer Journal, 14*, 235-265.

Zong, Z., Kimura, Y., Takahashi, M., and Yamane, H. (2000). Characterization of chemical and solid state structures of acylated chitosans. *Polymer, 41*, 899–906.

LIST OF PUBLICATIONS AND PAPERS PRESENTED

1. Yusuf, S. N. F., Azzahari, A. D., Yahya, R., Majid, S. R., Careem, M. A., and Arof, A. K. (2016). From crab shell to solar cell: a gel polymer electrolyte based on N-phthaloylchitosan and its application in dye-sensitized solar cells. *RSC Advances*, *6*, 27714 - 27724.

2. Yusuf, S. N. F., Azzahari, A. D., Yahya, R., Majid, S. R., Careem, M. A., and Arof, A. K. (2017). Improvement of N-phthaloylchitosan based gel polymer electrolyte in dye-sensitized solar cells using a binary salt system. *Carbohydrate Polymers, 157*, 938–944.